Koopman Operator-based System Identification & Prediction in Vehicular Applications with Nonlinear Dynamics

by

Waqas A. Manzoor

A dissertation submitted in partial fulfillment
of the requirements for the degree of
Doctor of Engineering
(Automotive Systems and Mobility)
in the University of Michigan-Dearborn
2023

Doctoral Committee:

Assistant Professor Alireza Mohammadi, Chair
Professor Hafiz Malik
Associate Professor Samir Rawashdeh
Mario Santillo, Ford Motor Company

Robotic Motion Intelligence Lab

University of Michigan - Dearborn

Waqas A. Manzoor
wmanzoor@umich.edu
ORCID iD: 0000-0002-7080-3998

DEDICATION

Praise be to God, the source of all glory and success, for providing me with the capacity to realize all achievements. After Him, I dedicate this dissertation to the most important people in my life, who have supported and encouraged me throughout my personal and academic journey.

To my parents, Manzoor Raja and Nasim Manzoor, you have instilled in me a zeal for success and have provided me with the foundation upon which I have become who I am today. If policy did not bar me from doing so, I would have opted to be identified only as Ibn Manzoor on the cover of this work, in line with ancient practices from which we derive the academic tradition of referring to authors by their last [father's] name, for I do not deserve any name of my own to be ascribed with recognition for any achievements above that of those who raised me.

Also to my in-laws, Abdul Qayyum and Nazia Qayyum, you have welcomed me with open arms and have supported me through rough tides. The assistance you have provided in looking after my household affairs was above and beyond expectations and has undoubtedly made this reality possible. I am also in diffidence of the guidance you have provided to ensure our genuine success in all aspects.

To my wife, Hibah Qayyum, for her encouragement and belief in me to undertake this endeavor in the first place. Your unwavering love and support have been fundamental to my success. Through long days and sleepless nights, you have stood by my side, with understanding and tolerance of me even through the toughest of times. As we celebrate ten years of marriage, I am reminded of just how much of a treasure you are in my life. You have shared in my accomplishments and have been a source of comfort and support through my failures.

And finally, to my daughter, Haniya Waqas, you are the light of my life. Thank you for reminding me every day of the importance of this work and for giving me the motivation to work hard to create a better future for you and for all those to come after you. Your upcoming start of Kindergarten makes the timing of this terminus extra emotional, as you take off in your own quest of seeking knowledge. I hope I have set for you a standard of strength, curiosity and relentlessness.

ACKNOWLEDGEMENTS

Completing this dissertation would not have been possible without the support and guidance of my academic adviser, Alireza Mohammadi, to whom I would like to express my deepest gratitude. The invaluable support and personal responsibility you have taken for my success has driven me to the final round and victory by knock-out. I thank you greatly for your belief in me and your patience with me. I would also like to thank my co-advisor, Samir Rewashdeh, for his encouragement to pursue this program. I remember your warning, "Motivation is fragile"; thank you for helping me keep it together.

I am also grateful to the faculty and staff of the department, whose guidance has been invaluable. Your dedication to teaching and research have created a supportive and intellectually stimulating environment that has allowed me to grow and thrive as a student. It has been an absolute honor to have chosen this university to undertake doctoral studies and I commit to supporting its reputation throughout my career as an exemplar of competence, confidence and relentlessness in the pursuit of a stronger future for humanity.

Finally, I would like to express my gratitude to all of my friends and colleagues, who have supported me and shared in my excitement throughout this process. And to my supervisors at Ford Motor Company, Yan Wang, Clay Maranville, Joe Thomas, Mike Goebelbecker and Bill Olsen, who endorsed my enrollment, tuition assistance applications and guided my overall professional development. Thank you all for your support and encouragement. This work would not have been possible without you.

PREFACE

This dissertation is a collection of works undertaken and published in peer-reviewed scientific literature over the course of the degree program, i.e., a dissertation-by-publications. A brief explanation of each chapter or its correspondence to the published works is given as follows:

Chapter 1 - This introduces the motivation of Koopman operator theory and alternatives to its goal in the sense of global linearization and identification of general [nonlinear] dynamical systems.

Chapter 2 - WA Manzoor, S Rawashdeh, and A Mohammadi. "Vehicular Applications of Koopman Operator Theory – A Survey". In: IEEE Access, vol. 11 (2023), pp. 25917–25931. DOI: 10.1109/ACCESS.2023.3257109.

Chapter 3 - This is a dedicated segment that factors out the common mathematical background from the other chapters for minimizing repetition and improved readability. It is mainly the Appendix section from the paper presented in Chapter 4.

Chapter 4 - WA Manzoor, S Rawashdeh, and A Mohammadi. "Real-Time Prediction of Pre-ignition and Super-Knock in Internal Combustion Engines". In: SAE International Journal of Engines, vol. 16, no. 3 (2022), pp. 363–375. DOI: 10.4271/03-16-03-0021.

Chapter 5 - WA Manzoor, S Rawashdeh, and A Mohammadi. "Koopman Operator- Based Data-Driven Identification of Tethered Subsatellite Deployment Dynamics". In: Journal of Aerospace Engineering, vol. 36, no. 4 (2023). DOI: 10.1061/JAEEEZ/ASENG-4836.

Chapter 6 - This provides concluding remarks and presents potentially valuable future research directions which have become evident over the course of the presented research. These include adaptive control for a robot undergoing peristaltic locomotion, and a method for seismic hazard threat assessment for railway and mine safety. Preliminary results are also included for the latter.

Special acknowledgment is given to Professor Igor Mezić from the University of California - Santa Barbara for reaching out to provide personal guidance on the historical developments associated with Koopman operator theory and its applications.

This work was partially funded by the Michigan Space Grant Consortium, NASA Award #NNX15AJ20H.

TABLE OF CONTENTS

LIST OF FIGURES

FIGURE

LIST OF TABLES

TABLE

ABSTRACT

This dissertation presents the development and applications of Koopman operator theory for solving system identification and prediction problems in the domain of vehicular systems and mobility from a data-driven perspective. The research is organized into three thrusts, whose results have been published in three peer-reviewed journal articles published over the past two years. The first article provides a comprehensive survey of Koopman operator theory from over 100 research papers and its applications to vehicular systems (aerospace, automotive, marine, rail, robotic, mining/construction, traffic management, and others), highlighting the potential for reduced-order modeling and control in this domain and gaps in the literature. The second article proposes a data-driven algorithm, i.e., the Hankel Alternative View of Koopman analytic approach, for predicting pre-ignition, a dynamically chaotic phenomenon, and resulting super-knock events in an internal combustion engine without the need for physics-based modeling. This is done within a framework designed for real-time implementation on an engine controller. This application has the potential to improve the operational adaptability of a vehicle, improving safety, performance and cost, by dealing with combustion instability through a 'perdition and avoidance' approach rather than the current 'detection and mitigation' approach. Simulation results from real engine data show the generation of a learned model in linear form capable of commanding one or more of several provided mitigating actions approximately 2.27 seconds prior to an event. Further validation results use data from low, medium, and high engine speeds within the envelope of low-speed pre-ignition. Finally, the third article discusses the use of Koopman operator theory for model generation of a tethered satellite system subject to unknown disturbances from several exogenous [nonlinear] environmental sources. The resulting state-space model shows excellent matching between the actual and simulated motion in simulation of the mission-critical maneuver of subsatellite deployment from its mothership. Overall, this research demonstrates the potential of the modern data-driven implementations of Koopman operator theory for system identification and control in various vehicular systems, with two specific case studies that illustrate this potential in a novel way.

CHAPTER 1

Introduction

A *vehicle* is generally anything that can carry a payload, including occupants, equipment, sensors or any other items. In some contexts, the item may be its own presence. Colloquially, this definition is often abstracted into the realm of thoughts and ideas, such as a poem being a "vehicle" to express one's love. Most generally, it has also been defined as any mobile mechanized equipment. All these ideas have been captured in Merriam-Webster's formal definitions [1]. In this dissertation, only the former, physical type of vehicle is considered. This includes systems and processes associated with automotive, aerospace, marine, rail, robotic, and subterranean classes of vehicles, along with some interfacing or noteworthy classes such as biolocomotion, communication and traffic management, amongst others. Advancement in the study of vehicular systems and mobility is critical due to its enablement of modern life and the success of civilization. Transportation is a fundamental property of vehicles that facilitates economic growth, ensures access to basic needs, sustains social interaction, and provides numerous other benefits. Most vehicles today are mechanized in some way and increasingly rely on or are limited by natural forces whose endeavor to harness continues as humanity pushes the boundary of engineering. As such, control systems in progressively novel and generalized contexts has become a flourishing research area in its own right. To this end, global linearization and modeling of unforced trajectories in nonlinear and chaotic systems (system identification) is necessary for reliable control of nonlinear vehicle systems, which explored through Koopman operator theory forms the topic of this dissertation.

Global linearization is an endeavor used in the field of control theory to simplify the analysis and design of nonlinear control systems. A nonlinear system is one in which the time rate of change of a state variable is not directly proportional to the input. These systems are generally difficult to analyze and design, and often require complex mathematical techniques to understand. In contrast, linear systems are much easier to analyze and design, and their behavior can be predicted with a high degree of accuracy. The advantage of global linearization is that it allows for the use of powerful linear control theory and algebraic tools to analyze and design nonlinear systems. Control system techniques have developed in several contexts, from those which aim to

model purely electro-mechanical, hydraulic, pneumatic, gravitational or subatomic processes, to industrial automation and biological systems. In this dissertation, the interest is to focus on a few problems specific to vehicular applications which can be solved using a specific approach to global linearization. Particularly, these applications include the prediction of abnormal combustion in an automotive engine, and the deployment of a tethered subsatellite in orbit about a celestial body subjected to unknown environmental forces, although a comprehensive survey of other problems is also presented. The mathematical approaches discussed herein are the recently emergent expressions of Koopman operator theory.

Real systems can be represented by dynamical models of varying levels of fidelity. On the upper end, there may exist nonlinear state dynamics. These may include processes that act over a wide range of timescales, the required resolution of which may not be justifiable in the trade-off between computational efficiency and meaningful impact on macroscopic properties seen in the output. Further, the nonlinear dynamics may demonstrate chaotic behaviors, bifurcation and sensitivity to initial conditions that are not observable in systems with linear dynamics. The concept of "meaningfulness" may be subjective and is usually quantified in terms of tolerable sensitivity that may be regarded as negligible given the application, where the magnitude of output variation, propagation of measurement errors and imperfect parameter definitions are factors. By sacrificing the required level of output precision or being unable to acquire such, one may choose to simplify a system's description at the expense of losing model fidelity. The neglected dynamics may be considered as disturbance to the system, along with all other processes unknown or unmodelled. Doing this results in an incomplete accountability of mass and energy processes needed to truly isolate the system described. However, it is usually required in order to mold the system description into a mathematically linear form, the advantage of which is the availability of state-space dependent control methods (e.g., linear quadratic regulator/state-dependent Riccati equation, or model predictive control, to name a few), estimation techniques or analyses (e.g., controllability). Thus, when not inherently linear (a rare care), conventional linearization of nonlinear dynamics typically involves negligence or lower fidelity approximations of higher-order dynamics, state-input dependence and disturbances.

The most conventional method of linearization involves approximating a system's behavior at a particular state, usually an equilibrium or operating point. The behavior of a system as described by the solution of differential equations of the state may represent a curve (within a given plane), whose range approaches a linear form as the domain about the point of linearization is limited. Consequently, the model is then only or approximately valid at or near the point of linearization, respectively. Such linear models are typically obtained by way of

small perturbation theory [2] which utilizes small angle approximations and vanishing terms containing products of differentials. Here, all state and input values, along with their derivatives are perturbed with a delta term and the equation is expanded to expose negligible terms. Alternatively, these terms also readily arise in error dynamics, as have previously been derived in terms of equations of motion for a solar sail [3]. Another common approach is the use of a truncated Taylor series expansion about the desired point [4]. These conventional methods of linearization are generally introduced in undergraduate control systems and mathematics courses.

The first three, and most significant, terms of the Laurent series expansion also happen to correspond to the form of impedances of an RLC circuit in the Laplace domain. This can be useful in approximating component values in an unknown branch of a bridge circuit by simply expanding the balance equation where the unknown branch's impedance is rearranged as a function of the Laplace variable. Another approach to linearize affine equations of motion was applied for spacecraft formation control using vectored thrust [3]. The procedure there was to take the triple derivative of the state yielding the jolt dynamics, where small angle approximation was then useful to decouple the state variables and control angles. The result was integrated in the feedback loop successively to feed into the original (acceleration) and jolt equations, for the plant model and cost function optimization, respectively, in the following time steps of a control scheme.

Changing state variables is also a traditional method for global linearization, e.g., [5], [6]. According to the latter, this can be accomplished using either the General or Heuristic methods to find a system of linear equations in an intermediate variable which is itself a function of the original state variable. In the Heuristic method, one equates the nonlinear equation to the general state space equation in controller canonical-like Frobenius form and unknowns are selected to comply with the Routh-Hurwitz stability criteria. The disadvantages of this approach are that a stable solution may not be easy to find, and it is computationally complex for automation. In the General method, the approach is a matter of collecting like terms containing state variables from the expanded nonlinear equation and grouping them into convenient definitions for intermediate variables. A potential pitfall of these methods, in some cases, arises in cases where the system of equations is time-varying and linearization does not necessarily isolate the effect of state from control inputs. Thus, the result is not generally in true state space form which is problematic for the implementation of some control methods and analyses.

Additional classifications of global linearization methods exist for affine and bilinear systems, including state linearization, feedback linearization and restricted feedback linearization. In studies such as [7] and others, a formal definition is provided as an overarching condition for global

linearizability with respect to that which may be achievable via a change of state variables as previously described. However, there are examples of some systems given in [7] that do not fulfill the definition yet are linearizable within some range, at some point(s), at all but some point(s), or at "every point locally". While appreciating the topological formality with which such literature is produced, it sometimes tends to lack consideration for the practicality of engineering application for real systems wherein, for example, proving smoothness of a vector field for all possible solutions of a system's description is not of concern beyond its intended operating range, or even at all with the realities of noise and disturbance. Hence, guarantees from formal proofs are usually unachievable, especially in the case of system descriptions purposefully modeled empirically whether by design, for simplicity, or due to limitations in understanding of the physical processes involved. However, such methods continue to be invaluable and definitely yield superior results over model-based controllers relying on locally linearized dynamics. For example, feedback linearization has been used for coupled attitude and orbital control of a spacecraft [8].

Other global linearization methods involve alternative ways of representing nonlinear systems descriptions to forms which may be linear (i.e., with decoupled input/output, endogenous feedback and disturbance) including as difference fields, 1-forms, Kähler differentials, Carleman linearization (using polynomials), generalized transfer functions, using output feedback, and as time-delay systems (see [9] for details on each these approaches). These methods are least common and continue to be studied as open areas of research in the field of pure mathematics. Lying obscurely in the middle remains the class of global linearization methods relating to regression methods, among which include those based on the Koopman operator [10].

Generally, global linearization of nonlinear systems was a research area that experienced its first boom in the 1970s (e.g., Krener, 1973 and Brockett, 1978, as cited in [7]). This followed a period around the 1930s, during which it was shown that linear transformations of nonlinear dynamical systems exist when represented in Hilbert [function] space. This high dimensional space is framed upon a coordinate system consisting of up to infinite orthonormal bases of functions rather than unit vectors, wherein the properties of spatial completeness are preserved, i.e., integration, Hausdorff, etc. While working with Hamiltonian equations, David Hilbert's contemporary, Bernard Koopman presented an approach [11], built in turn off of the work of John von Neumann, to resolve this operator to an explicit combination of spectral modes related to a system's observed motion. Hence, this transformation matrix is expressed as the Koopman operator, now commonly denoted as K. Research activity around this idea resurged around 2010 by some notable researchers including Igor Mezić [12], Peter Schmid [13], Steven Brunton [14] and others [15]–[19], whose cited research has been very thoroughly reviewed.

In the remainder of this dissertation, the following notations will be used with respect to letters and symbols. Vectors are generally represented with an overbar ($\vec{}$) in the form of a rightwards harpoon. Vectors and matrices are generally boldface. A shifted matrix is followed by a prime. The transpose is indicated by the superscript T, whereas the complex-conjugate transpose is indicated with a superscripted asterisk ($*$); the former and latter are interchangeable in the case of real numbers. The pseudo-inverse of a matrix is indicated by a superscripted dagger ($\dagger$), whereas the regular inverse is indicated by a superscripted -1. Estimated and truncated quantities are represented by a tilde ($\tilde{}$). Derivatives with respect to time are represented by an overdot ($\dot{}$), with the number of overdots corresponding to the order of the derivative. The forward slash (/) indicates division, or in the context of matrices indicates regular matrix multiplication of the first matrix with the inverse of the subsequent matrix (i.e., right matrix division). Finally, R.H.S. and L.H.S. are used as acronyms for right- and left-hand side, respectively, in relation to the equality symbol in an equation.

Chapter 2 presents a detailed literature review of the various vehicular applications utilizing the Koopman operator, along with the various implementations of Koopman operator theory that have arisen since the popularization of the dynamic mode decomposition (DMD) algorithm [20]. Specifically, the types of applications span the realms of aerospace, automotive, rail, marine, mining, traffic, and robotic systems and subsystems. Chapter 3 provides a mathematical background on the Koopman operator with some major forms of its solutions (e.g., DMD, HAVOK) which are implemented in the proceeding novel case studies. These include the prediction of pre-ignition and superknock in an internal combustion engine (ICE), in Chapter 4, and in the deployment of a subsatellite from its mothership in a tethered satellite system (TSS), in Chapter 5. Superknock is a combustion instability seeded by pre-ignition which is highly detrimental to the structural integrity, performance and harshness of an engine's operation. Its reliable prediction in a computationally efficient manner (i.e., that which is suitable for real-time application) is a significant contribution given that the dynamics involved are highly sensitive, or chaotic, and its avoidance directly translates to efficiency, safety, user satisfaction and cost savings. Similarly, tethered satellite deployment is a highly sensitive and mission-critical operation dependent on numerous environmental factors which cannot be modeled practically. This requires a system identification technique also suitable for real-time implementation that captures all dynamical effects, over all relevant time-scales, imposed upon the TSS for effective control. Ineffective control has in past missions led to expensive loss, rendering this research a valuable contribution from that perspective as well.

CHAPTER 2

Literature Review

2.1 Abstract

Koopman operator theory has proven to be a promising approach to nonlinear system identification and global linearization. For nearly a century, there had been no efficient means of calculating the Koopman operator for applied engineering purposes. The introduction of a recent computationally efficient method in the context of fluid dynamics, which is based on the system dynamics decomposition to a set of normal modes in descending order, has overcome this long-lasting computational obstacle. The purely data-driven nature of Koopman operators holds the promise of capturing unknown and complex dynamics for reduced-order model generation and system identification, through which the rich machinery of linear control techniques can be utilized. Given the ongoing development of this research area and the many existing open problems in the fields of smart mobility and vehicle engineering, a survey of techniques and open challenges of applying Koopman operator theory to this vibrant area is warranted. This review focuses on the various solutions of the Koopman operator which have emerged in recent years, particularly those focusing on mobility applications, ranging from characterization and component-level control operations to vehicle performance and fleet management. Moreover, this comprehensive review of over 100 research papers highlights the breadth of ways Koopman operator theory has been applied to various vehicular applications with a detailed categorization of the applied Koopman operator-based algorithm type. Furthermore, this literature review discusses theoretical aspects of Koopman operator theory that have been largely neglected by the smart mobility and vehicle engineering community and yet have large potential for contributing to solving open problems in these areas.

2.2 Introduction

Koopman operator theory is named after Bernard Koopman, who in the 1930s proved the premise that linear transformations of nonlinear dynamical systems exist when represented in Hilbert [function] space [11]. Historically, determining a Koopman-invariant subspace was accomplished by trial and error despite being unsuccessful for most dynamical systems. The enabling engine for modern-day data-driven applications of the Koopman operator theory are due to the profound insights on geometrical and statistical properties of dynamical systems in the Ph.D. dissertation [21] and the foundational line of work [22], [23] on harmonic analysis of the Koopman operator. Mezić's pioneering work [21]–[23] along with the computational breakthroughs based on singular value decomposition (SVD) enabled approximation of the Koopman operator from large amounts of data without relying on the pseudo-inversion of large non-square matrices. It is remarked that *the first modern-day engineering application* of Koopman operator theory has been due to Mezić and Banaszuk [23] for model parameter identification in combustion rigs.

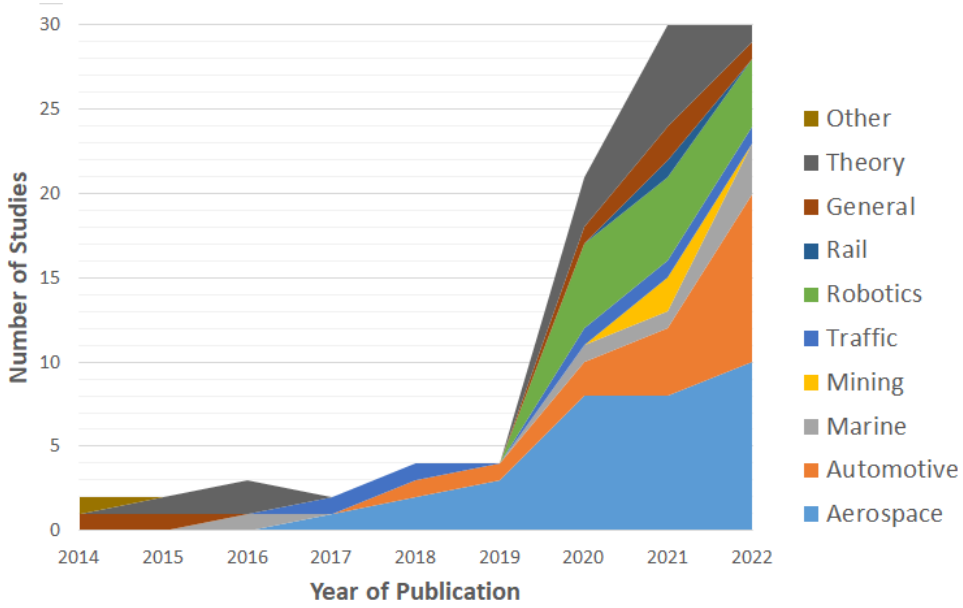

Fig. 2.1. Publication timeline of the surveyed literature. The number of studies incorporating Koopman operator-based methods in smart mobility and vehicle engineering applications has been increasing nearly exponentially over an eight-year span thus far.

As demonstrated in Figure 2.1, *the first vehicular applications* started to emerge only six years after the computational breakthrough due to the Dynamic Mode Decomposition (DMD) technique was achieved in 2008 [20]. Among vehicular applications alone, it is evident from Figure 2.1 that the number of studies incorporating Koopman operator-based methods has been increasing nearly

exponentially over an eight-year time span since 2014. However, with a mere maximum of 30 such studies published so far in a given year, the likely trend is further exponential growth as more researchers become aware of the associated algorithms, and as the applicability of such algorithms simultaneously evolves.

Features of the Current Survey. The purely data-driven nature of Koopman operators holds the promise of capturing unknown and complex dynamics for reduced-order model generation and system identification, through which the rich machinery of linear control techniques can be utilized. The emergent nature of the smart mobility and vehicular-related applications, where the Koopman operator in each particular application needs to be approximated, implies that the development of various Koopman operator approximation algorithms is expected to grow along with the vehicular problems they aim to solve. Given the ongoing development of this research area and the many existing open problems in the fields of smart mobility and vehicle engineering, a survey of techniques and open challenges of applying Koopman operator theory to this vibrant area is warranted. To the best of the author's knowledge, this survey is the *first of its kind* reviewing the applications of Koopman operator theory within a focused research area, namely, smart mobility and vehicle engineering applications. A *notable feature* of this survey is reviewing and categorizing the results of over 100 research papers based on both application and algorithm type (see Table 2.1 and Section 2.5) that are concerned with the applications of Koopman operator theory to the field of smart mobility and vehicular engineering. Such a *comprehensive and detailed categorization* will be beneficial to the research practitioners working in the field. Furthermore, this review chapter discusses theoretical aspects of Koopman operator theory that have been largely neglected by the smart mobility and vehicle engineering community and yet have large potential for contributing to solving open problems in these areas. Additionally, this chapter seeks to *identify gaps* in the smart mobility and vehicle engineering research where new and existing Koopman operator-based methods have the potential to further develop and address unsolved problems potentially benefiting from the perspectives of nonlinear system identification, control, global linearization, and the predictive powers that Koopman operator theory has to offer (see, e.g., Remarks 4–9).

The rest of this chapter is organized as follows. After presenting the relevant taxonomy in Section 2.3, a brief overview of the basic underpinnings of the Koopman operator theory is provided in Section 2.4. The literature review with categorized vehicular applications is presented in Section 2.5, where each subsection concludes with a list of open research questions for the application of Koopman operator-based methods in terms of vehicle types not encountered in the literature. Other relevant applications, which are not explicitly vehicular in nature, and

theoretical/algorithmic variations are reviewed in Section 2.6.

Remark 1 *A survey paper on variants of DMD authored by Chen* et al. *[24] had been published in 2012. However, being conducted a decade ago, it was well before the emergence of Koopman operator vehicular applications in the literature. Nevertheless, a very interesting discussion on the optimal application of DMD can be found in that paper. Another influential review in the field of Koopman operator theory is due to Budišić* et al. *[25]. Over the course of developing this chapter, Schmid [26], who is the pioneer of the original mode decomposition method, has also published his own survey on the variants of his method found in the literature. However, Schmid's survey is not focused on the specific topic of smart mobility and vehicle engineering applications. Finally, it is remarked that while Schmid's survey paper is focused on DMD and its variants, a complete review on Koopman operator methods in fluid mechanics due to Mezić has been presented in [27].*

2.3 General Taxonomy and Vehicle Type Categorization

For the purposes of this survey, a *vehicle* is generally considered to be any man-made instrument that can carry a payload, including occupants, equipment, sensors or any other items. In some contexts, the item may be its own presence. Most generally, vehicle has also been defined as any mechanized equipment. All these ideas have been captured in Merriam-Webster's formal definitions [1]. In this chapter, the physical type of vehicle according to Merriam-Webster is considered. This physical type includes systems and processes associated with automotive, aerospace, marine, rail, robotic, and subterranean classes of vehicles, along with some interfacing or noteworthy classes such as biolocomotion, communication, and traffic management, amongst others.

The *motivation* to focus on vehicular applications stems from the fact that many processes and subsystems are not easily modeled to a sufficient level of fidelity and/or are subject to a significant level of noise/disturbances. Such conditions pose limitations on the performance, control and overall utilization of the processes and subsystems that transduce energy into motion. Vehicles of different types, such as aircraft and automobiles, may further share common subsystems (e.g., combustion chamber or pump) or types of maneuvers (e.g., braking or collision avoidance). Consequently, from a dynamics and controls standpoint, it is sufficient to maintain the scope of this study to include all major vehicle categories.

Of all the studies found in this survey, Figure 2.2 (the pie chart on the top) illustrates their proportions in terms of the type of vehicles represented. These include aerospace, automotive,

marine, mining, traffic, robotics and rail vehicles. Also included are some studies that are theoretical only in terms of presenting a novel Koopman operator-based algorithm or those of general relevance (e.g., pertaining to a generic subsystem or component of multiple possible vehicles) without substantially demonstrating it on any vehicle, whether in simulation, in-vehicle, or on a hardware-in-the-loop test bench.

Figure 2.2 (the pie chart on the bottom) further breaks down the proportions of studies that pertain to specific types of functions, rather than vehicle platforms. These include traverse, maneuver, subsystem and guidance, as defined in what follows.

- **Traverse:** refers to the macro-scale function of a vehicle moving from one point to another (e.g., orbiting).
- **Maneuver:** refers to a specific mission, operation, reconfiguration or change in situation a vehicle may undertake within its journey (e.g., docking).
- **Subsystem:** refers to the subject of the study focusing on a component or set of components and their specific operation (e.g., a battery).
- **Guidance:** refers to the navigational aspect of vehicle path-finding and maintenance, correction or modification of trajectory (e.g., obstacle avoidance).

Finally, “Traffic Management" is concerned with the coordinated motion of multiple vehicles. Given the uniqueness of certain problems arising in traffic management, it was decided to segregate such studies into their own category.

Remark 2 (Machine Learning Community Taxonomy) *With the mainstreaming of Koopman operator-based methods, there also seems to be a linguistic generalization in that the term “Koopman" or “Koopman model" is increasingly used to describe any finite state transition matrix approximated for an unmodeled or nonlinear system. This is especially true in the artificial intelligence and machine learning community (see, e.g., [28]). Such use may continue to uphold validity since Koopman operator theory remains one of the main formal justifications for utilizing linear state transition matrices for closely capturing the behavior of nonlinear dynamical systems by means of proper linearization.*

Remark 3 (A Brief Note on CFD studies) *The inclusion of computational fluid dynamics (CFD) studies has generally been avoided in this review. The only exceptions are the studies containing an explicit vehicular application or proposing a new type of Koopman operator-based system*

identification method/variant. This is because the DMD solution to the Koopman operator was itself first derived in the very context of CFD (see the seminal work by Schmid [13]) and has since had the most time to mature in the CFD literature. Many such CFD-centric studies involve a generic case study of flow past a cylinder or airfoil, which may have relevance to, e.g., lifting surfaces, screw propellers, or more generically, pumps and turbines. Thus, the inclusion of literature from the CFD domain poses a vast grey area, often with speculative applicability. For example, residual DMD (resDMD) was used in a CFD-focused study [29] for supersonic plasma discharge but has significant relevancy to satellite propulsion systems. To narrow the scope of the search, all literature pertaining to the fluid dynamics realm has been excluded, other than those with explicit vehicular applications, or those which identify a novel algorithm (in which case the corresponding study was grouped into the 'Theory' category). This takes away a major source of ambiguity, given that much of the pure fluid dynamics literature is generalized (e.g., flow past a cylinder) such that it may or may not be relevant to vehicle motion.

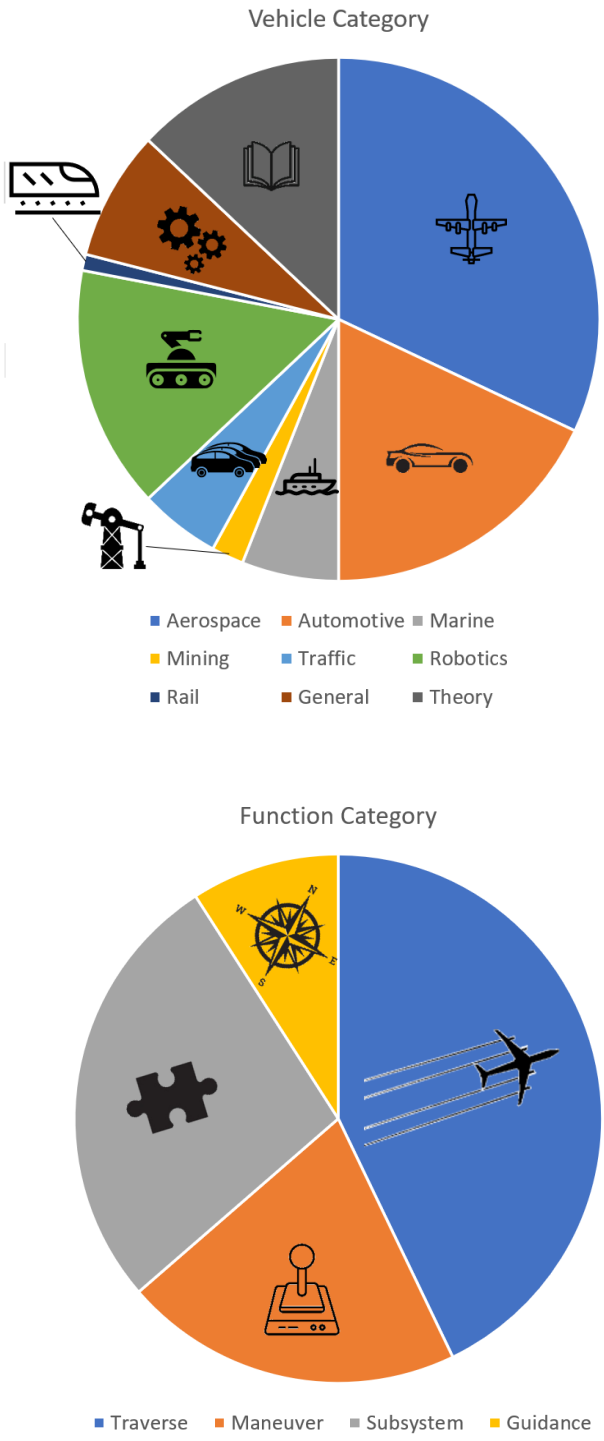

Fig. 2.2. Vehicle categories (top) and function categories (bottom) of the surveyed smart mobility and vehicular engineering literature. The area of each piece in the pie charts is proportional to the ratio of the number of the conducted studies within each particular area to the number of total studies.

Table 2.1. Summary of studies organized by employed method.

Algorithm	Studies‡
Direct Method of Selecting Koopman Observables (**DMa**)	[30][31]
Direct Methods using Frobenius–Perron Method or [Factorization of PDEs for] Adjoint Koopman Operator, Method of Characteristics, Legendre polynomials or Schur Decomposition (**DMb**)	[32][26][33][34][35] [36][37][38]
Direct Methods including Error Minimization (e.g., using Taylor Series Error Bounds), Minimization of Frobenius Norm through Pseudo-inversion of Data Matrix or other Optimization (**DMc**)	[39][40][41]
Duel Faceted Linearization (**DFL**)	[42]
Bilinear Koopman Realization	[43]
Robust Koopman MPC (**RK-MPC**) or Robust Tube-based MPC with Koopman (**r-KMPC**)	[44][45]
Koopman Mode Decomposition (**KMD**) and/or determination of Koopman modes only (not Koopman operator), including through Arnoldi iteration (Note: KMD was first discovered in [22].)	[46][47][48]
Koopman Map Inversion (**KMI**)	[49]
Projection Methods onto Selected/Derived/Required Basis, including use of Principle Orthogonal Decomposition (**POD**)	[50][51][52][53]
Dynamic Mode Decomposition (**DMD**), excluding where DMD is compared against modified methods	[54][26][55][56][57] [58][59][60][61] [62][63][64][65] [66]
Extended DMD (**EDMD**) or slightly modified EDMD, e.g., Naturally Structured DMD (**NSDMD**)	[67][68][26][69][70] [71][72][73][74] [75][76][77][78] [79][80][81][82] [83][84][85][86] [87]
Weighted Online EDMD (**WOEDMD**)	[88]
Koopman Eigenfunction Extended Dynamic Mode Decomposition (**KEEDMD**) or modified KEEDMD	[89][90]
DMD with Control (**DMDc**)	[91][66]
Rescaled DMD (rDMD)	[54]
Exact DMD, ANN-based Exact DMD (**ANN-EDMD**)	[26][77]

‡ Detail descriptions are provided in the text.

Table 2.1. (continued) Summary of studies organized by employed method.

Algorithm	Studies[‡]
Debiased DMD, Forward/Backward DMD (**FB-DMD**)	[26]
Multi-resolution DMD (**mrDMD**)	[26][92]
Hankel Alternative View of Koopman (**HAVOK**), Hankel DMD (**HDMD**) (partial or full-predictive) (Note: Hankel DMD was first introduced by Arbabi and Mezić[93].)	[26][94][95][96][97]
Higher-order DMD (**HODMD**)	[26][98]
Physics-based Higher-order EDMD (**PhysEDMD**)	[99]
Physics-informed DMD (**PiDMD**)	[100]
Residual DMD (**rDMD**)	[29]
Bilinear EDMD (**bEDMD**)	[101]
Constant Energy Multiscale DMD (**CEM-DMD**)	[77]
Iterative learning of Koopman invariant subspace (**LIR-DMD**)	[77]
Time Delay DMD (**TD-DMD**)	[87]
Kernel DMD (**KDMD**)	[87]
Sparcity Promoting DMD (**spDMD**)	[87]
Deep Koopman, Deep Direct Koopman, or other general Artificial Neural Network (**DDK-ANN**) Scheme	[102][103][104][105] [106][107][108][109] [91]
Neural Koopman Lyapunov Control (**nKLC**)	[110]
Deterministic/Convolutional Koopman Network (**DCKNet**, **CK-Net**), Deep Convolutional Koopman Network (**DKN**)	[111][112]
Deep Learning-based EDMD (**DL-EDMD**)	[103]
Deep Learning with Recurrent Neural Network (**DL-RNN**)	[113]
Direct Koopman Reinforcement Learning (**DKRL**)	[114]
Split Koopman Autoencoder (**SKA**)	[115]
EDMD with Autodidact Stiffness Learning (**ASL-EDMD**)	[116]
Sparse Identification of Nonlinear Dynamics (**SINDy**)	[117][118]
Stepwise Akaike Information Criteria (**SAIC**)	[118]
Stochastic Koopman Operator (**SKO**), or Stochastic Adversarial Koopman Operator (**SAK**) with Auxillary Neural Network, Gaussian Process-based Koopman Operator (**GPK**), or other Stochastic Methods	[28][119][120][83]

[‡] Detail descriptions are provided in the text.

2.4 A Brief Overview of Koopman Operator Theory

Koopman operator theory is founded on the premise that linear transformations of nonlinear dynamical systems exist when represented in Hilbert [function] space [11]. This high dimensional space is framed upon a coordinate system consisting of [up to] an infinite number of orthonormal bases (i.e., a linear combination of functions rather than unit vectors), wherein the properties of spatial completeness are preserved. The composition operator (i.e., the “Koopman" operator) mapping “observables" between these two spaces could be resolved explicitly as a combination of spectral modes that are related to a dynamical system’s observed trajectories. Observables can be selected as the system’s state and/or some functions thereof. If a set of observables could be found such that the resultant Koopman operator is finite, then those observables form the basis of a “Koopman-invariant subspace".

Consider a nonlinear system where the state $\mathbf{x}$ is propagated in time according to

$$\mathbf{x}_{k+1} = \mathcal{F}\mathbf{x}_k, \tag{2.1}$$

where $\mathbf{x}_k = \mathbf{x}(t_k)$ is the state at time at sample number k and $\mathcal{F}$ is a proper dynamical mapping. The premise of the theory is that there exists a Koopman operator, $\mathcal{K}$, which has the property of linearly propagating the observables, $\mathbf{y} \in \mathbb{R}^m$, of any system (including nonlinear and chaotic systems) through Hilbert space [11]. In other words, the operator $\mathcal{K}$ acts according to

$$\mathbf{y}_{k+1} = \mathcal{K}\mathbf{y}_k, \tag{2.2}$$

where $\mathbf{y}_k = \mathbf{y}(t_k)$ is a vector of observables (the state and/or functions thereof) at time k, and can be decomposed to a set of observables, $\mathbf{g}$, which may or may not be finite, such that (for brevity of exposition, let us work with the finite presentation with p functions)

$$\mathbf{y}_k = \mathbf{g}(\mathbf{x}_k) = [g_1(\mathbf{x}_k), g_2(\mathbf{x}_k), \ldots, g_p(\mathbf{x}_k)]^\top. \tag{2.3}$$

Additionally, under the property of function composition given by

$$\mathcal{K}(\mathbf{g}) = \mathbf{g} \circ \mathcal{F}, \tag{2.4}$$

ensures that the state transition rule

$$\mathbf{x}_{k+1} = \mathcal{K}(\mathbf{g}(\mathbf{x}_k)) = \mathbf{A}(\mathbf{x}_k), \tag{2.5}$$

where $\mathbf{A} := \mathcal{K} \circ \mathbf{g}$ governs the state propagation through time.

Historically, determining a Koopman-invariant subspace and computing the matrix A given by (2.5) was accomplished by trial and error despite being unsuccessful for most dynamical systems [10]. The enabling engine for modern-day data-driven applications of the Koopman operator theory are due to the profound insights on geometrical and statistical properties of dynamical systems in the Ph.D. dissertation [21] and the foundational line of work [22], [23] on harmonic analysis of the Koopman operator. Mezić's pioneering work [21]–[23] along with the computational breakthroughs based on singular value decomposition (SVD) enabled approximation of the Koopman operator from large amounts of data without relying on the pseudo-inversion of large non-square matrices. It is remarked that *the first modern-day engineering application* of Koopman operator theory has been due to Mezić and Banaszuk [23] for model parameter identification in combustion rigs. In what follows, a brief exposition is provided for the main DMD technique that has been the main driving force behind the proliferation of various applications of Koopman operator theory to a plethora of disciplines including geology, epidemiology, finance, and neurology, to name a few (see, e.g., [121] and the references therein). Additionally, Figure 2.3 provides an intuitive overview of the explained DMD process for the generation of a linearized and reduced-order model of an example nonlinear dynamical system (i.e., a tethered satellite system subject to unknown disturbances [122]).

From a practical perspective, the matrix $\mathbf{A}$ in (2.5) is the approximation of the Koopman operator acting upon the function space. Since $\mathbf{A}$ is constant in a Koopman-invariant subspace, it may be applied to an entire collection of m measurements, propagating the data matrix $\mathbf{X}$ to the time-shifted data matrix $\mathbf{X}'$, in which the set of observables are arranged column-wise. Specifically, these data matrices are represented as

$$\begin{aligned} \mathbf{X} &= [\mathbf{x}_0, \cdots, \mathbf{x}_{m-1}], \\ \mathbf{X}' &= [\mathbf{x}_1, \cdots, \mathbf{x}_m]\,. \end{aligned} \tag{2.6}$$

A straightforward and yet computationally inefficient method for computing an approximation of the Koopman operator can be achieved by multiplying both sides of Eq. 2.5 by the inverse of the data matrix, $\mathrm{inv}(\mathbf{X})$. However, this matrix may be too large to invert or non-square. Rather, a more practical solution relies on solving the following optimization problem

$$\mathbf{A} = \mathrm{argmin}_{\mathbf{A}} \|\mathbf{X}' - \mathbf{A}\mathbf{X}\|_F, \tag{2.7}$$

where $\|\cdot\|_F$ denotes the Frobenius norm.

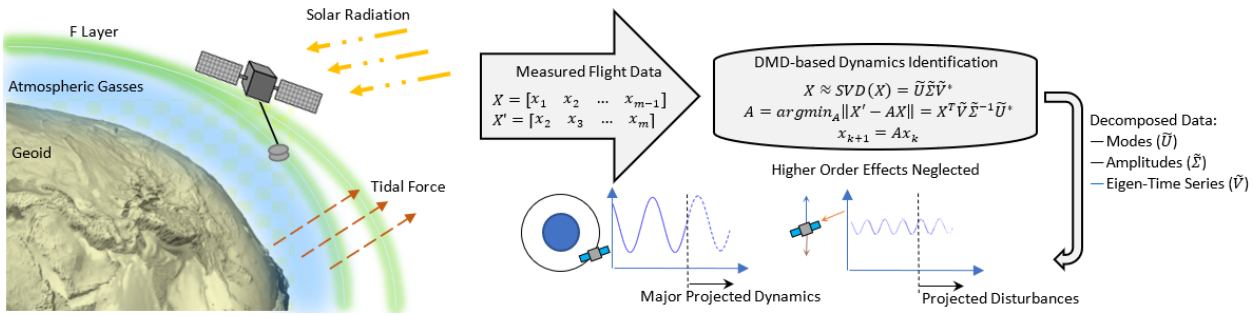

Fig. 2.3. DMD process for linearized, reduced-order model generation of nonlinear Tethered Satellite System subject to unknown disturbances.

To solve the optimization given by (2.7), regression yields the best-fit fixed Koopman operator, which propagates the selected observables, even if not precisely Koopman-invariant, between any two corresponding columns of the original and time-shifted data matrices. Another way of finding an approximate solution to the minimization problem in Equation (2.7) is to compute proper pseudo-inverses. For instance, SVD-based methods rely on computing the Moore-Penrose left pseudo-inverse. If the data matrix is coincidentally square and invertable, yet the observables are not perfectly Koopman-invariant, the attained solution will not act as a reliable Koopman operator between all sets of corresponding observables. Moreover, a *computational roadblock* exists in that observable data over any practical length of time or collected with a reasonably small sampling time quickly accumulates to a data matrix too large to invert using a desktop computer. A typical in-vehicle electronic control unit would likely be even more so limited in terms of available computational capacity.

Methods such as DMD [13] therefore use SVD to obtain a factorization of the transition matrix that is organized by order of modes of decreasing magnitude (see, also, Figure 2.3). This implies that the major components of the dynamics are captured in a manner that dynamical modes of higher ranks have higher noise-to-signal ratios. Thus, although the dynamics are decomposed into a linear combination of a large set of bases, a reasonable truncation can still be made, which results in a reasonable approximation for engineering purposes. One example of this process is illustrated in Figure 2.3, where DMD is used to obtain a linear, reduced-order model of a tethered subsatellite undergoing deployment [122] while subjected to multiple environmental disturbances which are too complicated to accurately model, yet whose effects are captured in the observed data. The model truncation capability afforded by the DMD technique and its variants allows for tuning to achieve a tolerable signal-to-noise ratio.

In the DMD method [13], the dynamics are decomposed into a linear combination of a large

set of bases. Nevertheless, a reasonable truncation, which is suitable for engineering purposes, can be achieved. Essentially, the system dynamics, which are represented by a finite set of nonlinear equations, is approximated with an *up to* infinite set of linear state equations. The order of the obtained linear system can be tuned using a proper reduced-order truncation method as described later. Therefore, in the DMD method, an approximated linear system is used such that

$$\mathbf{x}_{k+1} = \mathbf{A}\mathbf{x}_k. \tag{2.8}$$

To obtain the operator $\mathbf{A}$ for a general nonlinear system using the SVD-based approach, the snapshots of measurable quantities are obtained from Equation (2.6). For the data matrix $\mathbf{X}$, the following SVD factorization holds

$$\mathbf{X} = \mathbf{U}\mathbf{\Sigma}\mathbf{V}. \tag{2.9}$$

In the decomposition given by (2.9), $\mathbf{U}$ and $\mathbf{V}$ are unitary matrices and $(\ )^*$ is the complex conjugate transpose operator. Moreover, $\mathbf{\Sigma}$ is a square matrix of singular values arranged by order of decreasing magnitude, with those in the lower rows corresponding to negligible dynamic modes (i.e., lower signal-to-noise ratio). Thus, the three matrices of the right-hand-side in (2.9) can be truncated to rank $r-1$ which maintains the best fit to data. Indeed, r is the optimal hard threshold attained through proper techniques such as the Gavish & Donoho method (see pp. 31 in [14]), to comply with a required truncation size.

Furthermore, it is possible to obtain the eigendecomposition

$$\begin{aligned} \mathbf{X}\mathbf{X}^* &= \mathbf{U}\ \mathrm{diag}(\mathbf{\Sigma}^2, 0)\mathbf{U}^* \\ \mathbf{X}^*\mathbf{X} &= \mathbf{U}\mathbf{\Sigma}^2\mathbf{V}^*, \end{aligned} \tag{2.10}$$

from (2.9). In this eigendecomposition, $\mathbf{U}$ contains the eigenvectors of $\mathbf{X}\mathbf{X}^*$ and its columns are ordered according to how much correlation they capture in the columns of $\mathbf{X}$. A geometric interpretation of the SVD given by (2.10) is that it is a product of rotation matrices scaled by the singular values, which is necessary to project data, $\mathbf{X}$, from the original coordinate system onto a frame wherein the bases of the column-space are defined by $\mathbf{U}$ and the bases of the row-space are defined by $\mathbf{V}$.

Once the data matrix $\mathbf{X}$ from Equation (2.6) has been decomposed, the full state transition matrix can be reconstructed according to

$$\mathbf{A} = \mathbf{X}'\widetilde{\mathbf{V}}\widetilde{\mathbf{\Sigma}}^{-1}\widetilde{\mathbf{U}}^* \tag{2.11}$$

where $\widetilde{U}$ is also interpreted as the modes of principal orthogonal decomposition and the relationship

$$\widetilde{\mathbf{K}} = \widetilde{\mathbf{U}}^{*}\mathbf{K}\widetilde{\mathbf{U}} \tag{2.12}$$

holds for the unitary matrix $\widetilde{\mathbf{U}}$. Finally, the truncated Koopman matrix can be computed according to

$$\widetilde{\mathbf{K}} = \widetilde{\mathbf{U}}^{*}\mathbf{X}'\widetilde{\mathbf{V}}\widetilde{\mathbf{\Sigma}}^{-1}, \tag{2.13}$$

where $(\widetilde{\ })$ denotes the truncated quantities. See the textbook [14] for further details on reverting the obtained truncated states back to the original state space.

Eq. 2.3 provides the most general form for choosing the observables. Alternatively, if a catalog of functions (of the states) were included therein, the algorithm would then be referred to as Extended DMD (EDMD). Similarly, in the Sparse Identification of Nonlinear Dynamics (SINDy) algorithm, the time-shifted data matrix (or time derivative of the state, in the continuous time case) is equated to a matrix of possible coefficients projected onto a candidate library of functions to reproduce a structurally linear equivalent system representation of the nonlinear dynamics.

The Hankel Alternative View of Koopman (HAVOK) is yet another adaptation of DMD which has a characteristically predictive quality, especially for chaotic systems. This approach relies on Takens embedding theorem, which states that the full dynamics of a chaotic attractor can be reconstructed from the time series of a single measurement diffeomorphic to the original dynamics. It is remarked that the first instance of utilization of Takens embedding theorem in data-driven Koopman operator theory is due to Mezić and Banaszuk [23]. This forms a relationship between the Hankel matrix interpretation of all elements propagating through a constant linear transformation of the initial state, and a chaotic system quality of being sensitive to initial conditions. Others have found alternative methods of approximating the Koopman operator (e.g., by use of artificial neural networks), while some have adapted DMD in further creative ways (e.g., Multi-resolution DMD) suited for increased robustness in specific applications. The goal of this chapter is to present the application of the Koopman operator (through DMD and its evolved and alternative forms) on applications in the domain of vehicle engineering and smart mobility. The reader is referred to the textbook [14] for more information on Koopman operator theory, SVD, DMD, optimal truncation and other fundamental methods.

2.5 Literature Review: Vehicular Applications

In this section, a review of the literature is presented and the results of over 100 research papers are categorized based on both application and algorithm type that are concerned with the applications of Koopman operator theory to the field of smart mobility and vehicular engineering. Table 2.1 details the specific Koopman operator-based system identification method/algorithm used by the studies referenced hereafter. Given the vast number of algorithms and variants thereof, the reader is encouraged to refer to the respective studies to obtain their technical details. The following presents the surveyed literature organized by vehicle category.

2.5.1 Aerospace

2.5.1.1 Drones/Quadrotors

Many of the aerospace applications falling under this review are concerned with *unmanned aerial vehicles* (UAVs), usually of the quadcopter variety. Specific studies also focus on particular maneuvers, for example, Koopman Eigenfunction Dynamic Mode Decomposition (KEEDMD) has been used for general quadrotor model generation [90] and, more specifically, to learn the non-linear ground-effect to improve the speed and quality with which a multi-rotor aircraft may land [89].

Optimization of UAV flight has been explored using Dynamic Mode Decomposition (DMD) [61] and DMD with Control (DMDc) [91] in optimal control, and by the adjoint Koopman operator [34] for expected state propagation, with demonstrated advantages over stochastic control schemes. The adjoint Koopman operator in this literature refers to the left adjoint of the Frobenius-Perron operator.

Several methods including DMD, Extended DMD (EDMD), bilinear EDMD (biEDMD) and Koopman Canonical Transform have been compared against each other on a planar quadrotor flight testbed, where the superiority of the Koopman Canonical Transform has been demonstrated in handling affine dynamics for nonlinear model predictive control (NMPC).

Path planning using Robust Koopman Model Predictive Control (RK-MPC) has also been demonstrated in a quadrotor simulation [44]. Optimal control for quadcopter stabilization has been demonstrated with models identified using EDMD [68]. Finally, an artificial neural network (ANN)-based approach called Split Koopman Autoencoder has been used in the context of remote state monitoring of UAVs [115], where the communication aspect of flight pertaining to radio frequency signal processing has been addressed.

2.5.1.2 Missiles/Hypersonic Regime

A few other studies pertaining to the aeronautical domain have also been found to utilize Koopman operator-based methods. This includes the application of *ballistic airdrop*, where the adjoint Koopman operator is used to determine the optimal air release point for ariel delivery to a specified ground target under parametric uncertainty [32]. Modeling of *missile dynamics* from noisy data for model predictive control has also been undertaken using Sparse Identification of Nonlinear Dynamics (SINDy) and Stepwise Akaike Information Criteria (SAIC), where it has been shown to be superior in comparison with state-feedback control [118].

Remaining the theme of *supersonic flight*, model generation for aerodynamic flutter has been performed using Higher Order DMD (HODMD) to extract frequencies and damping from tests with reduced manual interaction and more robust aeroelastic analysis [98]. Further, in this flow regime, *supersonic combustion ramjet* (ScramJet) engines are susceptible to an "unstart condition", which is when the airflow in a duct violently breaks down. This phenomenon occurs when the pre-combustion shock train (PSCT) location translates upstream beyond the front of the inlet, causing flow separation within the engine and resultant shear layer oscillations. The detection and characterization of this condition relies on accurate modeling of flow characteristics which has been the objective of a study through the use of multi-resolution DMD (mrDMD), demonstrating the inadequacy of the regular DMD approach [92].

For *autonomous aircraft* and for *rocket combustion* instability control, principle orthogonal decomposition-based DMD (POD-DMD) was used to simplify equations of motion with a reduced number of variables and selective sensitivity [53]. POD-DMD is also found to have been used in the computational fluid dynamics (CFD) analysis of flow around an *airfoil* in the sub/transonic regime, with the method increasing computational efficiency by three orders of magnitude while accuracy remained within 5% as compared to other methods [52].

Transitioning between air and space flight, upper and trans-atmospheric dynamics have posed a challenge due to the many environmental factors involved as well as vehicle controllability in what is usually the *hypersonic flight regime*. For this situation, EDMD has been employed to identify a system model for optimal attitude control [71]. Similarly, the adjoint Koopman operator has also been used [123] to identify equations of motion through a linearly-constrained quadratic program to model atmospheric reentry.

2.5.1.3 Space Systems

In terms of space system applications, the categories can again be divided into *dynamics-related* (including traversing and maneuvering) and *subsystem-related* (including propulsion). It was found most applications pertained to the minimum-fuel *orbital rendezvous*. One approach employed Koopman Map Inversion to obtain a linearized model for optimal control [49], while another approach demonstrated Neural Koopman Lyapunov Control for linearizing a generalized affine system [110]. Minimization of the Frobenius norm was performed on a similarly affine *thrust-vectoring* application using the pseudo-inverse to directly solve for the Koopman operator [40].

In the study [38], a linear model for *zonal harmonics* around the moon was derived using Schur decomposition, rather than a singular value decomposition (SVD) approach to approximate solutions to perturbed ordinary differential equations. A related problem is *lunar station-keeping*, namely for Lyapunov and Halo orbits in the circular-restricted three-body problem (CR3BP). One study creatively obtained the Koopman operator approximation of the system matrix through direct computation using Legendre polynomials, which are already by their nature a complete and finite set of orthonormal basis in Hilbert space [36]. See [3] for more information on the CR3BP.

Low thrust trajectory optimization in *underactuated orbital flight* was addressed by a projection method onto vector fields defined by the input matrix [50]. The authors of [122] demonstrated the extraction of system equations for a tethered subsatellite deployment maneuver subjected to unmodelled dynamics and disturbances using DMD and DMDc. The same objective was achieved by directly using Koopman-invariant observables [30], but is not always possible or practical for most problems. Further, system equations of a *lander* modeled as an inverted pendulum with stabilization thrusters below its center of gravity were derived using EDMD [76]. EDMD was also used for a lunar lander in the dynamic allocation of control between a human driver and robot [85], [86], referred to as model-based shared control (MbSC).

On the subsystem side of space applications, DMD was used to find resonant frequencies, damping coefficient and mode shapes in a CFD simulation of a rocket engine's *cryogenic swirl injector* [63], the critical flow rate at which vibration occurs, or *"garden hose instability"* (commonly encountered in rocket engines), was investigated using Arnoldi iteration to attain Koopman modes [48].

Remark 4 (Identified Gap in the Literature) *Although the objective of the aforementioned aerospace-related studies has been limited to system identification, the ultimate goal of almost*

37% of the studies within this vehicle category (which is almost 46% above all vehicle categories combined together) was to obtain equations of motion in a linear form for the purposes of control using model predictive control (MPC) or other state-space methods. As it can be seen from Fig. 2.2, Aerospace has been the largest vehicle class employing emerging Koopman operator-based methods as compared to any other vehicle class. Despite this, the variety of aerospace vehicle types was found to be quite limited, mostly being small multi-rotor type UAVs. For this vehicle class, the surveyed literature did not seem to include material pertaining to helicopters and balloons.

2.5.2 Automotive

2.5.2.1 Automobile Engines

In terms of vehicle subsystems for combustion instability in internal combustion engines (ICE), the Hankel Alternative View of Koopman (HAVOK) method was employed for the prediction of *pre-ignition and super-knock* from real-time peak-pressure data [124], while the authors of [96] employed a portion of the same method (although not by name) to describe the thermoacoustic oscillation characterizing the transition between chaotic states and limit cycles. Also for ICE engines, *turbine dynamics* were investigated (e.g., in superchargers) using EDMD to model and predict turbulent and steady-state behavior [73].

2.5.2.2 EV Applications

In terms of *electric vehicles* (EVs), a linear model for motor control was extracted using DMD to actuate a permanent magnet synchronous motor through switching insulated-gate bipolar transistors (IGBTs) [59]. IGBTs are a common means to convert direct current (DC) from a battery to the appropriate coils within a motor to control speed in modern EVs. Similarly, an artificial neural network approach has been used to linearize a *DC-DC converter model* for switching control [109]. Furthermore, linear data-driven predictors afforded by Koopman operator formalism have been utilized to formulate the eco-driving problem for electric vehicles in a constrained quadratic program setting [125], [126]. Additionally, data-driven design methods based on Koopman operator theory have been utilized to design X-in-the-loop environments for electrical vehicle systems [127]. Finally, there is a recent body of literature on Koopman operator-based state estimation/prediction and fault diagnosis for batteries that are widely used in electric vehicles [128], [129].

2.5.2.3 Automotive Model Identification and Control

Model identification for *nonlinear tire dynamics* using EDMD is investigated in both [69] and [70], with the former utilizing a *single-track model* (making it applicable to motorcycles), while the latter

further applies MPC control. Similarly, [31] develops an MPC controller with a single-track model obtained by learning Koopman-invariant observables directly from data to recover the vehicle from a nonlinear state (e.g., skidding), when present. MPC is also used to minimize bounce by means of adjusting propulsive force in [74] while using EDMD for their model generation, thus becoming an alternative method for suspension control. Finally, handling and stability control (with linear time-varying MPC, or LTV-MPC) using *torque vectoring* is explored by [72] using EDMD for model identification.

2.5.2.4 Autonomous Vehicle Motion Control/ADAS Systems

The remaining studies in this vehicle category pertain to motion control in autonomous or *advanced driver-assist systems* (ADAS). In this group, artificial neural network methods were most prevalent. Control for vehicle motion planning was enabled using Deep Direct Koopman (DDK) or variants in [102], [103] and [104], with the latter-most specifically applied to a case study dealing with optimal trajectory prediction in racing. Deep learning-based EDMD was employed in [103], also for system identification in path tracking. For vehicle-to-vehicle related optimized management of traffic comprised of autonomous vehicles, data-driven MPC (DMPC) was employed for coordinated movement [108] (e.g., through a controlled intersection) which they term as "autonomous vehicle platooning"; here their focus is also on the comparison between centralized versus distributed controllers. The final studies in this category all aim to also obtain a linear model for MPC design and have to do with lane-keeping employing Bilinear Koopman Realization [43], Koopman Tracking MPC (KTMPC) [106], and Weighted Online EDMD (WOEDMD) [88] for Operator-AV shared control.

Remark 5 (Identified Gap in the Literature) *For this vehicle class, the surveyed literature did not seem to include studies pertaining to tracked (including tanks) and screw-propelled vehicles, vehicles otherwise specialized for travel over multiple terrains (e.g., snow, sand, grass, or semi-aquatic environments), as well as tractors, emerging e-mobility devices and other specialized vehicles. Relevant information for applications concerning rovers may be found in the robotics literature, presented in an upcoming section.*

2.5.3 Marine

2.5.3.1 Autonomous Marine Vehicles

This vehicle category included some items which could have been categorized instead in the section for robotics, however, where the application dealt specifically with guidance, navigation or propulsion in water, it was considered to be a marine vehicle. This includes a robotic fish, where

an EDMD-like algorithm was employed using high-order derivatives of physics-based functions of the state to linearize affine dynamics [35]. Similarly, the adjoint Koopman operator was used to improve the efficiency of a *swimming robot* in a flow-like environment [37], where it could learn the dynamics of its environment. Finally, a robot was shown to follow a simulated river while avoiding probable locations of unsafe areas (navigation with probabilistic safety constraints) using Naturally Structured DMD (NSDMD) [87], which is actually a modified EDMD algorithm.

2.5.3.2 Oceanic Applications

The next common theme relates to *oceanic applications*. In the context of an oil spill, oceanic flow was modeled using the adjoint Koopman operator to determine the optimal location for ships to release dispersant to control contaminants in a double-gyre fluid flow field [35]. Prediction of wind and oceanic flow patterns was also included in a review that surveyed the use of DMD and its variants [26], including EDMD, Exact DMD, Debiased DMD (also known as forward- and backward-DMD, multiresolution DMD, Hankel DMD (also known as HAVOK), higher-order DMD (which includes derivatives of observable functions) and the adjoint Koopman operator. However, these are not all applied to vehicular applications, yet are a valuable resource for one who seeks to find an appropriate Koopman operator-based method for a potential vehicular application. Finally, a dissertation by [87] presents Time-delay DMD (TD-DMD), EDMD, Kernel DMD (KDMD) and Sparsity Promoting DMD (spDMD), and includes the application of model identification for the 3D turbulent air-wake of a ship.

A unique study has also been found relating to the *measurement of sea ice concentration*, which aims to detect exponentially decaying spatial modes in the Arctic and Antarctic oceans [47]. This study is an example of one explicitly relating to satellite data processing, however, there may be many others using Koopman operator-based methods extending into the area of remote sensing and geographic information systems (GIS) which are not within the scope of this survey.

Remark 6 (Identified Gap in the Literature) *For this vehicle class, the surveyed literature did not seem to include studies pertaining to hovercraft, submarines (including autonomous or remotely piloted underwater vehicles) and offshore platforms. Relevant information for applications concerning hydrofoils may be found in the CFD literature.*

2.5.4 Mining

2.5.4.1 Hydraulic Fracturing

For this category, the most common studies employing Koopman operator-based methods were found for the application of *hydraulic fracturing*, which included [130], [131], [132] and [133]. However, these studies were deemed to fall outside the scope of this review due to their non-vehicular nature. This is due to the fact that they focused largely on the detection of shale deposits with fixed drilling infrastructure. On the other hand, from a subsystem perspective, it may be somewhat appropriate to include processes enabling natural resource extraction through pipelines. In that sense, Hankel-based DMD (HDMD) was used to model the *multiphase flow dynamics* of an oil-gas slug and forecast hold-up time profiles [94]. At the very least, this could have relevance to the operation of inspection/health-monitoring and cleaning vehicles that are typically used in pipelines.

2.5.4.2 Autonomous Excavation

Amongst other studies within this category, an *autonomous excavation* application was found where Koopman operator-based system identification was performed using Duel Faceted Linearization for the selection of Koopman invariant observable variables [42], whereafter an MPC control strategy was applied. Koopman Mode Decomposition (KMD) was used for identifying growing or decaying modes from traffic data and was shown to be superior in performance as compared to artificial intelligence methods [46], [134]. Finally, the aforementioned study on autonomous vehicle platooning [108] can arguably also belong in this category.

Remark 7 (Identified Gap in the Literature) *For this vehicle class, the surveyed literature did not seem to include studies pertaining to subterranean machines, such as those used for tunnel boring or directional drilling, landships, and elevators.*

2.5.5 Traffic

Traffic management was found to be an area of research where Koopman operator-based system identification techniques are being used. Given its distinctness from physical road vehicles, it has been assigned its own category. The majority of applications in this class of vehicle pertained to *traffic signal phase timing*. In the studies by [56] and [57], DMD was utilized for early identification of unstable queue growth, with the latter further proposing an adaptive traffic control system. The same objective was sought by [75], but instead using EDMD to predict pedestrian traffic and an MPC controller for vehicle signaling in response to it.

2.5.6 Robotics

2.5.6.1 Robotic Arms

The operation of *robotic arms* was found to be the most common application in this category and has been treated as a "vehicle" for the purposes of this survey as such devices are usually employed to spatially transport a payload from one point to another. For this purpose, EDMD was used (which they refer to as Koopman-MPC) to actuate the arm under voltage disturbance [67]. An aforementioned study from the Aerospace category [91] also demonstrates DMDc and other approaches including ANN and Reinforcement Learning on a robotic arm.

2.5.6.2 Human-Robot Collaboration

A modified form of EDMD using Autodidact Stiffness Learning was used for detection and adaptivity in applied torque for the human-machine interface of a manipulator (i.e., yoke controller) [116]. Similarly, end-effector motion of industrial robotic arms around humans requires environmental state prediction for safe path planning. This was done in one study where the Koopman operator was directly solved for by taking the pseudo-inverse involved in minimization of the Frobenius norm (a computationally expensive operation) [41]. The same objective of *safe path planning* was also achieved in [33] with the use of the adjoint Koopman operator and in [120] using the Stochastic Koopman Operator. The latter study also cited an interesting application of their method for automated air traffic management but was not selected for inclusion in the Aerospace category given the lack of demonstration (i.e., simulation, physical experiment or substantive formulation).

2.5.6.3 Soft Robotics

Other robotics-related applications found in the literature included a *pneumatically actuated soft manipulator* which used EDMD for pick & place operations for objects of unknown mass [80]. Underactuated control of the same type of robot was explored in [95] using Hankel DMD (HDMD). An aforementioned study from the Aerospace category [68] also involved control of a *robotic ball* (called "Sphero SPRK") rolling in level sand to follow a predetermined trajectory, EDMD was used here. Similarly, another study provides an example of a wheeled robot that uses a modified KEEDMD algorithm to extract unknown mode dynamics with improved computational efficiency [90].

2.5.6.4 Wheeled/Legged/Swimming Robots

A unique study involving a wheeled robot utilized EDMD for increased computational efficiency and real-time implementation [81]. Using *jointed legs* to locomote is another means by which a

robot may traverse; the authors of [55] investigated such crawling and used DMD to expose the method's limitations. Marine robotic applications, as previously mentioned, include the robotic fish [39] and obstacle-avoiding river-traversing robot using NSDMD [84]. The former used an MPC controller to make the fish swim in a line or circle, with the linearized model obtained directly from an adaptive error minimization approach using Taylor series error bounds.

Remark 8 (Identified Gap in the Literature) *For this vehicle class, the surveyed literature did not seem to include studies pertaining to climbing or jumping vehicles, vehicles relying on peristaltic locomotion (see, e.g., [135] for such a robot prototype), attack or surveillance platforms, and robot swarms. Although, a unique biolocomotion study was indeed found to employ DMD to enable mapping between an upper limb and its contra-lateral lower limb while walking forward at constant speed [58]. This may arguably qualify as a mode of transportation (i.e., walking), and may very well apply to bipedal robots which are designed to walk like humans.*

2.5.7 Rail

Only one single study was found pertaining to this vehicle category, which was for an MPC application of a *high-speed train* whose linearized model was obtained via EDMD [82].

Remark 9 (Identified Gap in the Literature) *For this vehicle class, the surveyed literature did not seem to include studies pertaining to trams, cable cars and roller coasters. It is important to note that factors surrounding the operation of vehicles or their subsystems were not discounted in the literature search. For example, the HAVOK algorithm's predictive qualities may have potential in the areas of environmental forecasting (e.g., passenger load, wind and earthquake) and health monitoring (e.g., component mean time between failures), such that vehicles could be operated with appropriate constraints during times of expected adverse conditions.*

2.6 Literature Review: Vehicle-related & Other Relevant Studies

In this section, an overview of other relevant applications was provided which are not explicitly vehicular in nature, and theoretical/algorithmic variations of the Koopman operator framework that might be beneficial for future applications in the area of smart mobility and vehicular engineering.

2.6.1 General Studies Applicable to Vehicles

Studies focused on fluid flow are among the most common vehicle-related research topics where Koopman operator theory has played an integral role. Using DMD, the modeling of nonlinear oscillations due to vortex shedding was investigated in [60] and is highly relevant for aeronautical applications. Also relevant to aeronautical engines that operate in the transonic regime is the use of DMD to model separated and turbulent flow within a convergent-divergent nozzle [112], which manifests as the gas path of gas turbine engines. Most internal and external combustion engines also rely on liquid [fuel] injection, for which [112] is highly relevant as it demonstrates the modeling, prediction and control of nonlinear flow associated with atomization dynamics, enabled by DMD and deep convolutional Koopman network (CKN). Similarly, MPC control of nonlinear fluid flow was demonstrated in [113] using a deep learning approach.

The second most common research area found applicable to this category were studies pertaining to motor control, which is especially relevant to UAVs and robots, but potentially also to other types of vehicles when examining them from a subsystem perspective. This was achieved in [119] using Gaussian process-based Koopman operator in robust controller design, and in [79] using EDMD for current control for the synchronous operation of motors. Finally, a power management study used Stochastic Adversarial Koopman Operator with Auxillary Neural Network for the quick learning of reduced order models that measure the state of charge of Lithium-ion batteries [28]. Potentially applicable to some aircraft and specialized ground vehicles, one study used DMD in the diagnostics of natural gas rotating detonation engines [62].

2.6.2 Theoretical Issues with Potential Applications to Smart Mobility and Vehicular Engineering

This section introduces some studies which are theoretically focused on the derivation of unique Koopman operator-based techniques but have not been utilized in the application-focused literature. They are included in this review due to their potential for any future applications the reader may be motivated towards. Firstly, [54] uses DMD and rescaled DMD (rDMD) for image processing. Also relating to images, [111] used Deterministic and Convolutional Koopman Networks (DCKNet and CKNet, respectively) to predict a suitable trajectory from a provided topography to solve the standard Mountain Car Problem. This may have relevance to energy-limited adaptive cruise control applications in the automotive category. Linearized, reduced order models in [100] are identified using Physics-informed DMD (piDMD), while [51] similarly makes a case for physics preservation but utilizes a projection-based model reduction approach. Examples in the former include channel flow and flow past a cylinder, which may be relevant to Marine

vehicles, but does not explicitly specify such. The inverted pendulum model is generated in [105] using Deep Neural Network-based Koopman (Koopman DNN), with [107] also employing an ANN approach, and [114] combining ANN with accelerated learning using Deep Koopman Reinforcement Learning (DKRL). Finally, an ANN-based Exact DMD approach is also presented in [77] in comparison with EDMD and Iterative Learning of Reconstructed Koopman operator (LIR-DMD) for the development of multi-scale models from coarse data with long-range prediction.

EDMD and Stochastic Koopman Operator (SKO) are used in [83], while [78] presents a modified EDMD. It has been noted that throughout this survey, EDMD was the most used method in a modified form. Sparse Identification of Nonlinear Dynamics with Control (SINDYc) has been developed in [83], and can potentially be applied anywhere DMDc has been used (e.g., in [122] for tethered subsatellite deployment), although the paper demonstrates its application on a predator-prey model and the Lorenz system. An example in [45] applies Robust Tube-based MPC with Koopman (r-KMPC) on the Van der Pol Oscillator, which may have relevance to applications in wireless communication, among other areas. Finally, an interesting application of auto-tuning (i.e., model evaluation) using DMD was presented in [65] in the context of a zero-sum game. This may have potential applications in the balancing of parameters and fuzzy criteria in the realm of AV aggressiveness and wargaming.

2.7 Conclusion

Since its advent in 1931, Koopman operator theory [11] has only recently been actively utilized for solving practical problems, thanks to the introduction of the DMD algorithm in 2008 [20]. Since then, a multitude of DMD algorithm variations have risen to prominence and found utility across various fields. A notable feature of this survey was reviewing and categorizing the results of over 100 research papers based on both application and algorithm type in smart mobility and vehicle engineering (see Table 2.1 and Section 2.5). Additionally, this survey identified potential research gaps in smart mobility and vehicular engineering applications (Remarks 4–9). Finally, this review chapter discussed theoretical aspects of Koopman operator theory that have been largely neglected by the smart mobility and vehicle engineering community and yet have large potential for contributing to solving open problems in these areas (see Section 2.6.2).

Future Research Directions. Given the emergence of cyber-threats against connected and autonomous vehicles as well as robotic systems (see, e.g., [136], [137]), a future research direction might include utilizing Koopman operator-based algorithms for designing cyber-resilient vehicular and smart mobility applications (see, e.g., [138] for a related line of research). Another poten-

tial research direction is using Koopman operator-based algorithms for predicting the motion of vulnerable road users (VRUs), e.g., pedestrians and cyclists (see, e.g., [139], [140]). Finally, rehabilitation robotics and robotic exoskeletons can be the benefactors of the predictive capabilities of Koopman operator-based algorithms for detecting tripping events and/or system identification in various modes of locomotion (see, e.g., [141], [142]).

CHAPTER 3

Mathematical Background

3.1 Introduction

This chapter provides a stand-alone overview of the Koopman operator and its approximation using the Dynamic Mode Decomposition (DMD) algorithm. The Singular Value Decomposition (SVD) approach is used for this, although an iterative approach using the Arnoldi method also exists. As seen in Chapter 2, DMD has been elemental to the recent explosion of research in engineering applications of the Koopman operator, with most other methods being derived therefrom. For example, DMD with Control (DMDc) and the Hankel Alternative View of Koopman (HAVOC) are also utilized in this research but are based fundamentally on the DMD algorithm. This chapter concludes with some comparison with related approaches to nonlinear system identification, namely, the Eigenvalue Realization Algorithm (ERA) and Machine Learning methods in general.

3.2 Koopman Operator Theory

Koopman operator theory is based on the premise that linear transformations of nonlinear dynamical systems exist when represented in the Hilbert (i.e., function) space. This high dimensional space is framed upon a coordinate system consisting of up to infinite orthonormal bases of functions rather than unit vectors, wherein the properties of spatial completeness are preserved, i.e., integration, Hausdorff, etc. The theory aims to resolve this operator to an explicit combination of spectral modes related to a system's observed motion. Hence, this transformation matrix is denoted as the Koopman operator, $\mathcal{K}$.

Nominally, for a nonlinear system of the form

$$\mathbf{x}_{k+1} = F(\mathbf{x}_k) \tag{3.1}$$

where $\mathbf{x}_k = \mathbf{x}(t_k)$, for which there is available data, one could begin by selecting candidate functions of the state, $\mathbf{g}(\mathbf{x}(t))$, termed 'observables' or 'measurables', be they inclusive of the state itself, and/or powers, trigonometric functions, or other nonlinear combinations thereof (e.g., $\mathbf{x}_k^2 sin(\mathbf{x}_k)$), concatenated as

$$\mathbf{y} = [g_1(\mathbf{x}_k), g_2(\mathbf{x}_k), ...g_p(\mathbf{x}_k)]^T \tag{3.2}$$

such that,

$$\mathbf{y}_{k+1} = \mathcal{K}(\mathbf{y}_k). \tag{3.3}$$

These observables are, by definition, linear combinations of eigenfunctions in the Hilbert space which are invariant to linear transformation by the Koopman operator. A deterministic approach to resolving ideal observables remains an open problem in the mathematics literature but approaches such as the Sparse Identification of Nonlinear Dynamics (SINDy) [14] exist wherein a library of candidate functions with arbitrary coefficients is framed as a regression problem upon measured data to yield the best fit. With a sufficiently large coefficient matrix and vector of diverse function terms, it is possible to attain the correct or near-correct form of the solution. This process could then theoretically be repeated until $\hat{\mathbf{K}} = \mathbf{y}_{k+1}/\mathbf{y}_k \rightarrow \mathcal{K}$ iteratively converges to a constant value between all k and $k+1$ observables of the state by way of a regression algorithm. An alternative approach would theoretically be to arrange the collection of m state measurements as a data matrix

$$\mathbf{X} = [\mathbf{x}_k, \mathbf{x}_{k+1}, \mathbf{x}_{k+2}, \ldots, \mathbf{x}_{m-1}] \tag{3.4}$$

and the time-shifted data matrix,

$$\mathbf{X}' = [\mathbf{x}_{k+1}, \mathbf{x}_{k+2}, \mathbf{x}_{k+3}, \ldots, \mathbf{x}_m] \tag{3.5}$$

and solve for $\mathcal{K} = \mathbf{X}'/\mathbf{X}$ from Eq. 3.3 assuming that it is valid to take $\mathbf{y}$ from Eq. 3.2 as the original state vector. However, $\mathbf{y}$ may be too large (or infinite), the selection of observables may be incorrect (i.e., not invariant in the function space, or not "Koopman invariant"), $\mathbf{X}$ may not be square, and/or be practically too large to invert. Thus, it has historically been extremely difficult and impractical to solve for the Koopman operator. If relying on the pseudoinverse to invert the data matrix or using trial-and-error to determine a suitable set of measurables, this approach represents an approximation. However, a globally linear approximation may be sufficiently practical for engineering applications. Fundamentally, the Koopman operator enables a nonlinear system represented in a finite vector space to alternatively be defined in an up to infinite-dimensional function space, yet linear in terms of suitable measurables.

3.3 Dynamic Mode Decomposition

One solution in the construction of a globally linear system representation of a complex system from data is to approximate the Koopman operator and is known as Dynamic Mode Decomposition (DMD) [16]. This involves the application of Singular Value Decomposition (SVD) to factorize the data matrix, whose outputs can be arranged to determine the system's eigenvalues and lower-order approximation. Since the SVD is derived from a correlation matrix, the singular values extracted thereby are conveniently arranged by decreasing magnitudes of dynamic mode, allowing for truncation of negligible dynamics, which may be those with a low signal-to-noise ratio. This in turn is used to propagate some state in time to a future time step. Since the SVD involves a pseudo-inverse, it is regression-based and therefore a best-fit state transition matrix acting as a globally linear approximation of the nonlinear system.

Taking Eqs. 3.4 and 3.5, and assuming validity in taking $\mathbf{y}$ as the original state vector, as previously mentioned, it can be approximated that $\mathbf{X'} - \mathbf{KX} \approx 0$, where the Frobenius norm of the left-hand side is minimized to obtain

$$\mathbf{K} = argmin_{\mathbf{A}} \|\mathbf{X'} - \mathbf{AX}\|_F \approx \mathbf{X'X}^{\dagger} \tag{3.6}$$

where $\mathbf{X}^{\dagger}$ is the pseudo-inverse. A convenient approach to this is by way of the SVD. The means by which the SVD extracts a system's dynamic modes have to do with its relationship to the correlation matrices, $\mathbf{XX}^*$ and $\mathbf{X}^*\mathbf{X}$. If it is said that a factorization exists such that $\mathbf{X} = \mathbf{U\Sigma V}$, where $\mathbf{U}$ and $\mathbf{V}$ are unitary matrices, then substitution reveals that $\mathbf{XX}^* = \mathbf{U}\ diag(\mathbf{\Sigma}^2, 0)\mathbf{U}^*$ and $\mathbf{X}^*\mathbf{X} = \mathbf{U\Sigma}^2\mathbf{V}^*$, where $(\ )^*$ is the complex conjugate transpose and is equal to the regular transpose when elements of the matrix are real numbers. Moving the conjugate transpose of the unitary matrices to the left-hand side reveals an eigendecomposition form wherein, e.g., for the former case, $\mathbf{U}$ contains the eigenvectors of $\mathbf{XX}^*$. Therefore, if the diagonal elements of $\mathbf{\Sigma}$ are arranged in descending magnitude, the columns of U are ordered in terms of how much correlation they capture in the columns of $\mathbf{X}$. The explanation in [14] also offers a geometric interpretation of the SVD as being a product of rotation matrices scaled by the singular values necessary to project data, $\mathbf{X}$, from the original coordinate system onto a frame wherein the bases of the column-space (i.e., y-components) are defined by $\mathbf{U}$ and row-space (i.e., x-components) are defined by $\mathbf{V}$. This is why $\mathbf{U}$ and $\mathbf{V}$ are to be unitary matrices, as unitary transformations are such that the inner product is preserved. Further, the Moore-Penrose pseudo-inverse can be applied to the aforementioned problem of solving for the $\mathbf{K}$ matrix in that the SVD factorization, $\mathbf{U\Sigma V}$, of $\mathbf{X}$ can be inverted individually, with $\mathbf{\Sigma}$ guaranteed to be a square matrix. It should be noted that $\mathbf{\Sigma}$ is square either coincidently, with zero-rows excluded (as when written in the 'economical' form), or when rows

beyond 1 to r are truncated as they correspond to negligible dynamic modes. In the lattermost case, the singular values on the latter rows may be significantly smaller in magnitude or even orders of magnitude as compared to the singular values in the initial rows.

Gavish and Donoho [143] present a method which can be used to calculate an optimal hard threshold for r. However, this value can also be determined via trial and error, to comply with a required truncation size, or by other means. Generally, truncation of the state dynamics matrix up to rank $r - 1$ is that which yields the best fit to data.

Once the data matrix $\mathbf{X}$ from Eq. 3.4 has been decomposed, the truncated Koopman matrix can be computed as

$$\widetilde{\mathbf{K}} = \widetilde{\mathbf{U}}^{*}\mathbf{X}'\widetilde{\mathbf{V}}\widetilde{\mathbf{\Sigma}}^{-1} \tag{3.7}$$

where $\widetilde{(\,)}$ denotes the truncated quantities. It is from this $\widetilde{\mathbf{K}}$ matrix that the state-space matrices, $\mathbf{A}$ and $\mathbf{B}$, of the surrogate model are extracted and used in the HAVOK algorithm (see Section 4.5). Eq. 3.7 arises from substituting the expansion $\mathbf{K} = \mathbf{X}'\widetilde{\mathbf{V}}\widetilde{\mathbf{\Sigma}}^{-1}\widetilde{\mathbf{U}}^{*}$ into $\widetilde{\mathbf{K}} = \widetilde{\mathbf{U}}^{*}\mathbf{K}\widetilde{\mathbf{U}}$, with $\widetilde{\mathbf{U}}$ representing the matrix of principal orthogonal decomposition modes; this establishes the relationship between the full and truncated state transition matrices. Thus Eq. 3.3 becomes practically obtainable as

$$\widetilde{\mathbf{x}}_{k+1} \approx \widetilde{\mathbf{K}}\widetilde{\mathbf{x}}_{k} \tag{3.8}$$

which is true in the space of principle orthogonal modes and reverted to the space of the original state vector by the projection $\mathbf{x} = \widetilde{\mathbf{U}}\widetilde{\mathbf{x}}$. This step is important to retain the physical meaning of the state variables in case they were formulated with such, which is generally the case when intending to subject the system to control action. Further analysis on the spectral analysis of DMD is available in [14].

3.3.1 Comparison with Other Methods

3.3.1.1 Comparison with Eigenvalue Realization Algorithm

The Eigensystem Realization Algorithm (ERA) is another technique that leverages the Hankel matrix. However, it is based exclusively on an arrangement of impulse responses, rather than concatenated raw data as in the case of the HAVOK algorithm. Depending on the nature of the system to be identified, this may not be possible. For example, the ERA is very useful when there exists the possibility of performing controlled experiments. An advantage of using the ERA is that one may capture a system's behavior using a minimal set of experimental data. The main

disadvantage is that lower frequency modes can be missed if lightly damped transients do not decay within the settling time of the impulse responses used to generate the data. At the expense of a larger Hankel matrix, the HAVOK algorithm is more robust in capturing complex behaviors including unknown disturbances and those which change over time. It is for these reasons that HAVOK was considered more suitable to identify the dynamics of a system under real-time operation. It is interesting to note that a property of the Hankel matrix is that it can be decomposed in terms of the product of controllability and observability matrices [144].

3.3.1.2 Comparison with Machine Learning Methods

Koopman operator theory and machine learning are both important tools for analyzing and modeling complex dynamical systems, but they approach the problem from different perspectives. Koopman operator theory is a mathematical framework for studying the behavior of nonlinear dynamical systems. The Koopman operator is a linear operator that acts on functions of the state variables of a system, and it provides a way to analyze the long-term behavior of the system. The Koopman operator can be used to compute observables and extract features from the state variables of a system, which can then be used to make predictions or control the system. Machine learning, on the other hand, is a set of techniques for building models from data. Machine learning algorithms are designed to learn patterns and relationships in data, and to use these patterns to make predictions or decisions. Machine learning is often used in applications where the system being modeled is complex and difficult to analyze using traditional techniques. While Koopman operator theory and machine learning have some similarities, they approach the problem of modeling complex dynamical systems from different perspectives. Koopman operator theory is more focused on the underlying mathematical structure of the system, while machine learning is more focused on learning patterns and relationships from data. In some cases, Koopman operator theory and machine learning can be used together to achieve better performance than either approach could achieve alone. The choice between Koopman operator theory and machine learning ultimately depends on the specific requirements of the application and the expertise of the practitioner.

CHAPTER 4

Superknock Prediction

4.1 Abstract

Super-knock is a phenomenon triggered by pre-ignition and has limited the design envelope of internal combustion engines in terms of power density. This poses a huge challenge for the automotive industry where engine sizes have been continuously decreasing due to the demand for weight savings and integration with electrified powertrains. Such downsized engines typically require increased boost pressure, availing conditions conducive to pre-ignition which in turn may trigger super-knock. Traditionally, this and other forms of knock have been managed by way of a 'detection and mitigation' approach in place of 'prediction and avoidance' due to an evolving understanding of corresponding combustion dynamics, as well as the incapability of emerging real-time computational methods to perform and actuate over the time-scale required. In this study, a data-driven algorithm is used to extract (and adapt) a globally linearized system representation using eigen-time series, isolating the system's dynamic modes to capture underlying effects leading to pre-ignition without the need for physics-based modeling. This approach is a unique application of 'Hankel Alternative View of Koopman' analysis for chaotic systems and can be executed onboard an engine control module supplying a buffer of recent to latest time-step data to predict an impending pre-ignition event. The proposed design does not require any change to existing sensors and actuators in the existing knock management system architecture, nor would it require any significant increase in computational capacity in terms of the associated engine control unit. A simulation was conducted with real super-knock data to nominally test applicability of the algorithm. From this training data set, the linearized dynamical system was able to predict pre-ignition approximately 2.27 seconds prior to the event, which is adequate to take mitigating action. Further validation runs covering low, medium, and high engine speeds within the envelope of low-speed pre-ignition generated similar results.

4.2 Introduction

Knock, in a spark-ignition internal combustion engine (ICE) is the condition resulting from improper air-fuel mixture or other combustion reactants unintentionally detonating due to any source excluding intentional spark-triggered flame propagation. The etymology of the word relates to the sound usually accompanying this condition, which may be the result of various direct or indirect mechanisms, for example, shock waves or detonation-induced vibrations in the cylinder wall [145]. Generally, classifications of knock may include heavy-knock, slight-knock, non-knock, deto-knock, and super-knock. The lattermost is often synonymous with, but technically a result of pre-ignition, which is most well-known to occur at low speed and high load conditions [146], [147], or during cold starts, and limits the downsizing of boosted engines [148], [149].

For efficiency and increased power, many modern engines use pressurized, 'charge air' to supply the intake manifold, in contrast to a naturally aspirated engine. This increased pressure is called boost pressure, which can be created by using a compressor, called a supercharger. When a supercharger is powered by a turbine, in turn, driven by exhaust gas to salvage excess kinetic energy from recirculated combustion products, it is then referred to as a turbocharger. Smaller engines, which are especially used in hybrid vehicles as secondary or shared-capacity propulsion typically require charge air to maintain adequate torque generation [150] and maximum power-to-weight ratio [151].

Consequentially, these smaller engines running at higher pressures are associated with increased sensitivity to pre-ignition. Pre-ignition as a chaotic event is characterized by this difficulty in prediction due to sensitivity to initial conditions [152], even though resulting from non-random underlying dynamical processes. Thus, it is in a mathematical, rather than colloquial, sense that abnormal combustion such as pre-ignition and super-knock are described as chaotic events. This is also in agreement with other literature [153], [154], and preserves the idea of combustion as a deterministic process upon which modeling efforts, such as [155], are based. Interestingly, the phase portrait of crank angle, piston velocity and cylinder pressure during super-knock would resemble the Rössler attractor – a classical chaotic system.

Ordinary knock has been described as quasi-periodic in nature [148]; pre-ignition, however, is sporadic, difficult to predict, very damaging, and tends to occur within certain transient conditions (e.g., low speed, engine warm-up). Also as opposed to ordinary knock, if pre-ignition could occur with any regularity whatsoever, then that entails the engine is already operating in a condition known to make it susceptible to pre-ignition and there is no need for prediction. Further, an

engine allowed to undergo a few occurrences of pre-ignition may potentially self-destruct anyway. For example, in another study [156] that investigated the relationship between pre-ignition and super-knock, only four instances of super-knock were achieved over 2000 crank cycles on a laboratory engine specifically tuned to solicit pre-ignition, with five other instances of pre-ignition which failed to produce super-knock. Furthermore, because the physics-based combustion dynamics of pre-ignition/super-knock is not fully understood [157], a reliable model to test a predictive algorithm does not exist for simulation, unless it is a computationally intensive 3D CFD model (and even then, experimental at best). This chapter demonstrates that there exist underlying dynamics at the root of pre-ignition/super-knock, rendering it predictable, as opposed to "random, abnormal combustion". Then, there should exist the possibility to extract features from measured data which can forewarn the phenomenon. This chapter shall present a data-driven algorithm that was successful in doing this on recorded vehicle data containing two super-knock events without the need to model combustion dynamics. The ability to predict and avoid even a single pre-ignition event in a real-world setting would be beneficial to the life of an engine and is the engineering problem being addressed herein.

Remark 10 *It is important to highlight that, unlike knock, pre-ignition and super-knock remains an unsolved problem in automotive research. The current development in prediction is limited to a few successful instances involving intensive 3D CFD modeling, such as [155], which are not developed for online implementation.*

Pre-ignition is a pre-requisite condition to super-knock, although the converse is not necessarily true [149] and may occur also in compression-ignition engines [158] and in those using alternative fuels, e.g., hydrogen [159], biofuel [160], [161] and in other, non-propulsive chemical processes [162]. As an unintended combustion event in the cylinder, pre-ignition results in a significant loss of energy. The associated increase in temperature tends to create initial conditions for autoignition over the following crank cycles, which is the specific mechanism for pre-ignition seeding super-knock. The off-design temporal characteristic of pre-ignition opposes the power-stroke in an ICE engine cycle, leading to high stresses and reduced efficiency. Specifically, valve timing (for evacuation and induction), fuel injection, and spark timing (for spark-ignition engines) are coordinated such that combustion occurs within a designated window of crank positions where the piston is near the top-dead-center (TDC) such that circular acceleration of the crank can be maintained. If [auto]ignition occurs inadvertently during the compression stroke, the force of combustion in that cylinder will oppose the crank's rotational momentum and power strokes of other cylinders in the firing sequence, subjecting the piston to extraordinary load. Such loads often result in a damaged piston head, damaged piston rings, damaged cylinder liner, bent connecting

rods, head gasket failure, and all the associated symptoms of these conditions (e.g., noise, vibration, harshness, blue or white smoke, burning oil and catastrophic engine failure). Figure 4.1 illustrates how the off-design temporal characteristic of pre-ignition opposes the power-stroke in an ICE engine cycle, leading to high stresses and reduced efficiency.

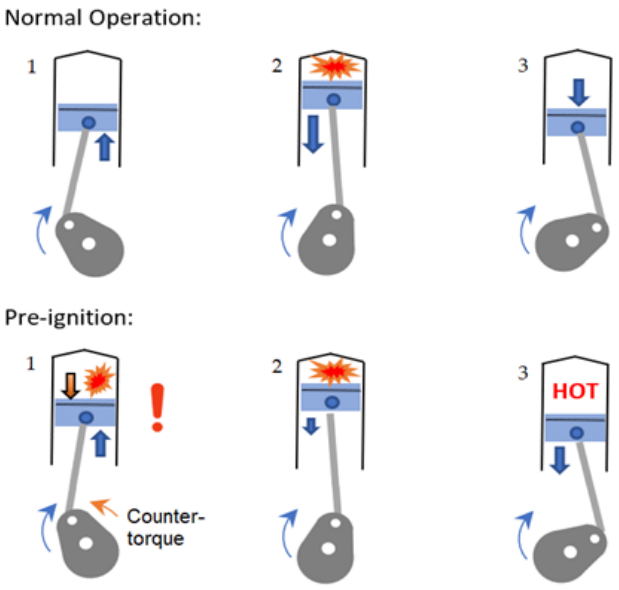

Fig. 4.1. Transverse cross-section of crankshaft and cylinder with piston sweeping through TDC.

In this chapter, the primary area of focus will be on super-knock, being the more significant form of knock in terms of the potential for damage and as a design limitation issue. The approach of this study is to bypass the need for a physics-based understanding of the underlying mechanisms, and instead relies on measurements of variables anyhow associated with generating effects leading up to the conditions where pre-ignition is likely, captured in data. The onset of a pre-ignition condition is presumed, in part, to be related to the cycle-to-cycle accumulation of heat, which upon an activation threshold ignites a residual oil droplet existing or splashed off the cylinder wall. Therefore, it is expected that cycle-to-cycle temperature or pressure would be an appropriate data set to consider in predicting pre-ignition and is supported by precedent [163]. As a numerical approach, a similar study [164] involved the demonstration of Fourier transform to detect patterns associated with knock; here, Koopman operator theory is applied to extract dynamic modes of the system, essentially as the solution to a correlation problem. Also analogous to this study is a process [165] similarly involving the estimation of system uncertainties and delays using advanced observer-based techniques in the processing of oxygen sensor data.

In terms of contributions, this study is a presentation of an approach to predict and avoid

super-knock, rather than to manage it after the fact, which has been an unsolved problem. This would serve to overcome the current downsizing limitation of ICE engines in hybrid electric vehicles, improve small engine longevity and improve noise, vibration & harshness (NVH). To the best of the authors' knowledge, this study is also the first application of Koopman operator theory to a problem of this nature. Further, the algorithm is sufficiently compact for real-time implementation on production vehicles.

The remainder of the chapter includes an overview of the general knock management system in terms of sensing, processing, and actuation. That is followed by some mathematical background on Koopman operator theory and associated predictive algorithm for application to the pre-ignition/super-knock problem. The section thereafter presents the utilized data and simulation results. Finally, some conclusions are drawn in terms of interpretation and future work.

4.3 General Knock Management Approach

With the advent and popularization of turbocharged engines, SAAB was the first automaker to implement knock management in 1982 via their 'automatic performance control' [166] electronic control unit (ECU), which adjusted the intake manifold pressure upon indication of excessive pressure from the knock sensor. This is a transducer that converts vibrational energy into an electric signal whose voltage output varies proportionally, or at least diffeomorphically to a force applied to it.

Figure 4.2 shows the general functional flow of a typical knock mitigation system, which can be preserved for knock avoidance as well. Typically, knock is flagged when at any point the magnitude of vibration exceeds a predetermined, calibrated threshold. Before the knock sensor output voltage can be used as a digital data value, it must be conditioned. Signal conditioning typically involves amplification (e.g., via an operational amplifier circuit, to increase the signal-to-noise ratio), filtered (using band-pass filtering to exclude engine noises resulting from frequencies not originating from the cylinder), and is then passed to an analog-to-digital converter.

The running vehicle and engine thereof onto which the knock sensor is mounted contain multiple sources of vibration (for example, road noise, serpentine and timing belts, AC compressor, coolant and fuel pumps, cam/crankshaft and valves, cabin audio, precipitation, suspension and chassis flexion, and so on) which may be detected by the knock sensor as false positives. In signal processing, the signal may then be calibrated by a transfer function to represent a peak cylinder

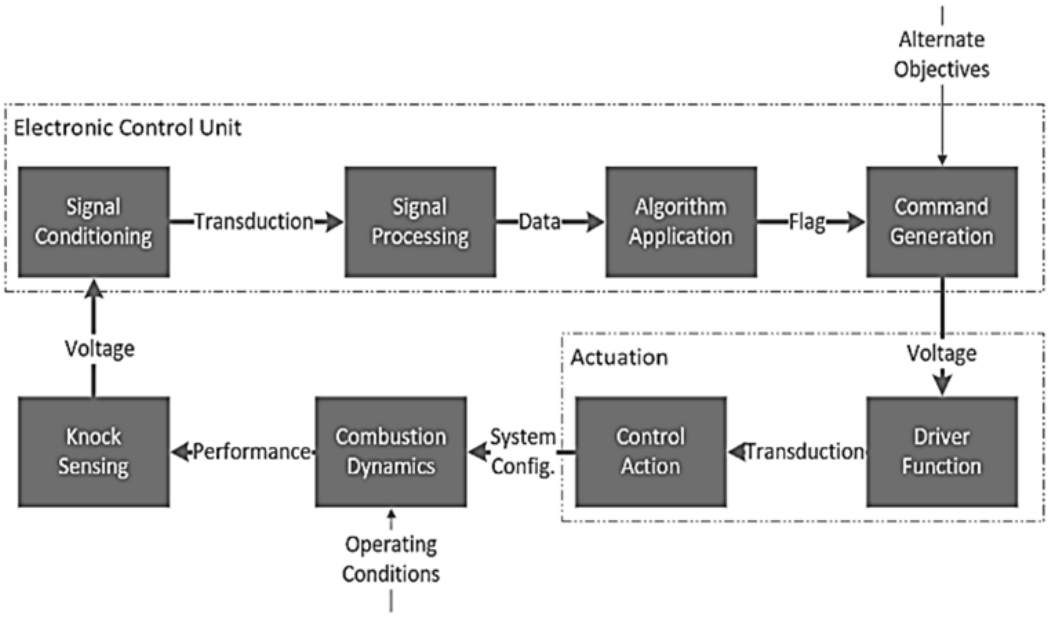

Fig. 4.2. Basic process for knock mitigation/avoidance.

pressure value, being largely proportional to the vibration detected, or to estimate other combustion parameters [167]. For this, a model must be formulated which is specific to the engine. The algorithm is typically a threshold comparison which the electronic control unit is programmed to compare against the knock sensor output to discern any type of knock event from normal operation. After the algorithm flags a knock event, a supervisory controller generates an actuator command. In practice, there are several actuations one may take to mitigate knock, including but not limited to the following:

- Decrease boost pressure via bleeding exhaust gas through the wastegate
- Decrease boost pressure via a reduction in throttle opening
- Enrich air-fuel-ratio (AFR) via an increased duration of the fuel injection pulse in direct-injection engines
- Enrich air-fuel-ratio via advancing the intake valve opening in port-injection engines
- Decrease piston-cylinder compression ratio if this feature is available
- Retard spark timing if the piston is close enough to TDC given the engine speed
- Inject fuel during the intake stroke to act as a coolant
- Cut fuel and spark in the expected cycle to avoid the issue altogether

- Modify exhaust gas recirculation; to suspend or increase may depend on the ambient humidity

Actuation of, e.g., the wastegate, can be an effective way to change upstream conditions to avoid pre-ignition once its occurrence is predicted. However, such actuators may have alternative objectives or competing effects, which necessitate a supervisory control loop for optimization or arbitration between them. For example, AFR is used not only for optimizing power and reducing fuel consumption, but also to manage emissions.

Following commitment to a course of action, low-level drivers transduce the command signal into the necessary physical response. This may be in the form of power electronics, pneumatics, solenoid hydraulics, etc. The control action is then carried out and the new system configuration modifies the combustion process, hopefully in a manner sufficiently favorable to preventing conditions where pre-ignition may occur while avoiding noticeably undesirable side-effects (in terms of performance, emissions, comfort, or reliability). The combustion dynamics are also dictated in part by operating conditions such as ambient conditions, speed, load, driver behavior, fuel type and quality, engine condition, and others, which the command generation process must sufficiently account for.

This study aims to extend the use of this pre-existing hardware and software system architecture to predict pre-ignition and super-knock. The adaptation of an algorithm originating from non-automotive applications towards a software solution for pre-ignition and super-knock is presented. Also, a framework wherein this solution can be implemented in an adaptive fashion is proposed. The scope at this level of technology readiness is limited to concept development using available data as a case study, with implementation and robustness analysis reserved as future exercises. The following section details an algorithm suitable for implementation in the 'Algorithm Application' block of the process shown in Figure 4.2, which would physically be expressed as an ECU software update. The knock sensor remains the key hardware component on which this approach relies.

4.4 Mathematical Background & Algorithm

In this study, pre-ignition is modeled as a chaotic event in a dynamical system, as explained in the Introduction. Chaos exhibits volatile and complex behaviors which are practically unpredictable given inexact measurements. However, such dynamics are theoretically deterministic due to the existence of governing principles. The trajectory that a system's state may take through a vector field formed by the set of solutions to the set of differential equations describing a given dynamical

system is highly sensitive to its initial conditions. Despite this, chaos is not truly random (unless it is, e.g., white noise), rather, it generally exhibits systemic and organized structures. In a physical system, these are generally associated with the underlying dynamics of disturbances and unmodelled elements of the system.

Takens embedding theorem shows that the full dynamics of a chaotic attractor can be reconstructed from the time-series of a single measurement, provided that the set of measurements is diffeomorphic to the original dynamics. An example of this is the reconstruction of an oscillator, such as the Lorenz system, in 3-dimensional space using measurements of oscillations along the x-axis only [14], [121]. From a geometric perspective then, one could qualitatively extract the overall dynamics by analyzing the topologies and organization of trajectories in phase-space. Similarly, using Koopman operator theory, one may find the emergence of approximately linear and nonlinear regions; the latter of which require large forcing terms to sustain the globally linear model. Other analyses used to characterize chaotic systems include delay embedding, singular & nonlinear Laplace spectrum analyses, and statistical approaches.

A brief mathematical background on Koopman Operator Theory is presented in the previous chapter, which also presents a brief mathematical background on Dynamic Mode Decomposition (DMD), which is a modern approach to solving for the Koopman operator from a data-driven perspective. The reader is advised to review that material before proceeding to the following section, and to [14] for more comprehensive details.

4.5 'Hankel Alternative View of Koopman' Analysis

An understanding of DMD is necessary to better understand the Hankel Alternative View of Koopman (HAVOK) [121], which relies on the same principles but yields an alternative perspective. An introduction to DMD is presented in Chapter 3 for convenience. If instead of composing the data matrix as in the typical form of Eq. 3.4, the data is arranged in the form of a Hankel matrix, as follows,

$$\mathbf{H} = \begin{bmatrix} \mathbf{x}(t_1) & \mathbf{x}(t_2) & \cdots & \mathbf{x}(t_p) \\ \mathbf{x}(t_2) & \mathbf{x}(t_3) & \cdots & \mathbf{x}(t_{p+1}) \\ \vdots & \vdots & \ddots & \vdots \\ \mathbf{x}(t_q) & \mathbf{x}(t_{q+1}) & \cdots & \mathbf{x}(t_m) \end{bmatrix} = \mathbf{U}\mathbf{\Sigma}\mathbf{V}^T$$
$$\approx \begin{bmatrix} \mathbf{x}(t_1) & \mathbf{K}\mathbf{x}(t_1) & \cdots & \mathbf{K}^{p-1}\mathbf{x}(t_1) \\ \mathbf{K}\mathbf{x}(t_1) & \mathbf{K}^2\mathbf{x}(t_1) & \cdots & \mathbf{K}^{p}\mathbf{x}(t_1) \\ \vdots & \vdots & \ddots & \vdots \\ \mathbf{K}^{q-1}\mathbf{x}(t_1) & \mathbf{K}^{q}\mathbf{x}(t_1) & \cdots & \mathbf{K}^{m-1}\mathbf{x}(t_1) \end{bmatrix} \tag{4.1}$$

One may obtain equations of motion arranged as,

$$\frac{d}{dt}\mathbf{v}(t) = \widetilde{\mathbf{K}}\mathbf{v}(t) \approx \mathbf{A}\mathbf{v}_{1:(r-1)}(t) + \mathbf{B}\mathbf{v}_r(t), \quad \widetilde{\mathbf{K}} = \begin{bmatrix} \mathbf{A}_{(r-1)\times(r-1)} & \mathbf{B}_{(r-1)\times 1} \\ \cdots \end{bmatrix} \tag{4.2}$$

The $\widetilde{\mathbf{K}}$ matrix is obtained from Eq. 3.7, following a further singular value decomposition of $\mathbf{V}^T$, from which the $\mathbf{A}$ and $\mathbf{B}$ matrices are extracted as shown in the second part of Eq. 4.2. The rows of $\widetilde{\mathbf{K}}$ beyond $r-1$ are disregarded due to the truncation, as they represent a "bad fit". Given that Eq. 4.2 represents a system that is not truly linear, the behavior of $\mathbf{v}_r$ serves as a corrective "forcing" entity that forces the linear model to behave like the actual system, lumping the effects of nonlinear dynamics. Eq. 4.2 is referred to herein as the surrogate model, where $\mathbf{v}$ contains the 1 to $r-1$ eigen-delay coordinates ($\mathbf{A}$ is the truncation of $\mathbf{H}$, from the SVD), and $\mathbf{v}_r$ (referred to herein as 'apparent forcing') is the next row; it represents the effective control input necessary to maintain Eq. 4.2 as true.

The interpretation of the r^{th} row of Eq. 4.2 is that a linear system (i.e., one with a constant state transition matrix, the columns of which project unit coordinate vectors of the original space into the output state) has a single fixed point at the origin (since a zero state yields a zero output under zero control input); however, a nonlinear system may have multiple fixed points, limit cycles, and other nonlinear spatial features. Thus, $\mathbf{v}_r$ is interpreted as the most significant [given $(\sigma_r \in \mathbf{\Sigma}) > \sigma_n, \forall\ n > r$] corrective "input" required to make this linear system behave like the observed [nonlinear] system, with chaotic behaviors being expressed as "bursts" ahead of the occurrence. This behavior is in agreement with the results shown in [121], which demonstrated predictive lobe switching observed in the Lorenz system using HAVOK.

The surrogate model arises from linear regression (e.g., using DMD) of the right-singular vectors, or $\mathbf{V}$ matrix, from the SVD factorization of the Hankel matrix. This $\mathbf{V}$ matrix represents a

time series (called the eigen-time series) which reconstructs the behavior (e.g., as delay coordinates) of the original dynamics, but without knowledge of the full data, given that the Hankel matrix was constructed using only a subset (e.g., $\mathbf{x} = f(a)$, an observable aspect of the dynamics such as fuel level) of the original state (e.g., a, b, c, a point in cartesian space such as position). If this subset data is a suitable measurable (or set thereof), the eigen-time series is indeed diffeomorphic to the original dynamics. Thus, linearization upon this embedded attractor will be easier. Also note from the second part of Eq. 4.1 that the significance of data in the form of a Hankel matrix is that it encompasses the idea of the Koopman operator given that every data point can be considered as an iterate of the Koopman operator applied to the first measurement, which in turn represents the general characteristic of chaotic systems as sensitive dependence on initial conditions. Note that p, q defines the desired aspect ratio of the Hankel matrix, which may be adjusted arbitrarily (although, the optimal truncated rank may change correspondingly). Figure 4.3 illustrates the generalized algorithm with the incorporation of a running buffer to retrain the model described in Eq. 4.2.

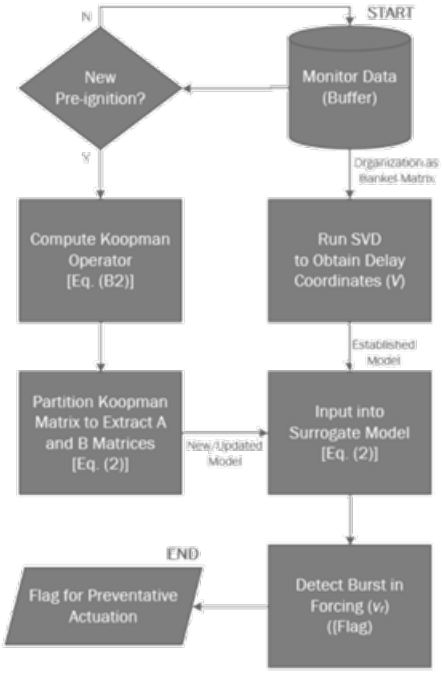

Fig. 4.3. Implementation of HAVOK algorithm.

This process can be incorporated into the 'Algorithm Application' block in the control system strategy shown in Figure 4.2, in place of the standard threshold comparison. After the measured data is arranged as a Hankel matrix and decomposed, the factors are truncated to preserve the significant $r - 1$ dynamic modes and assessed for best-fit. Depending on the nature of the system or from prior simulations, the r value may already be known so this assessment need not be

performed online.

The algorithm will be deemed successful if a flag can be inferred using apparent or non-apparent features embedded within the test data in advance of recorded pre-ignition events. Once the regression model of the system's delay embedding is developed and validated against the data, it can run online and be expected to capture most instances of pre-ignition.

Remark 11 *Eventually, the predictive quality of the model is expected to degrade over time due to the chaotic property of sensitivity to initial conditions, and the process should restart from Step 1 with a new model. Building this into the process, it is suggested to automatically retrain the model periodically through a running buffer wherein data leading to past escaped pre-ignition events are saved. The more novel conditions [e.g., low-speed pre-ignition (LSPI) in various ambient weather conditions, loads, oil qualities, etc.] leading to pre-ignition that are saved in the buffer, the more robust the algorithm should be against future pre-ignition events.*

4.6 Data & Simulation Results

The data available to test this algorithm on super-knock prediction is shown in Figure 4.4. It was collected from a 6-cylinder 3.5 L turbocharged gasoline direct-injection engine running 87 RON fuel, operating at an engine speed of approximately 1320 RPM during a cold start. The engine had a defect that made it more prone to pre-ignition. From it, the measurable used to construct the data matrix consisted of only the cycle-to-cycle peak cylinder pressure.

The collected data clearly shows each pressure cycle's conformance to the theoretical 4-stroke cycle. Pre-ignition occurs in cycles 149 and 355 with both events triggering super-knock. The crank cycle begins at -360° coincident with the intake stroke, followed by a rise in pressure due to compression after which the sharp rise in pressure near 0° corresponds to the work done by combustion. Pressure drops over the expansion stroke and then returns to 0 bar through the exhaust stroke.

Remark 12 *An alternative selection of the measurable may have been possible and should be guided by the information presented in the literature review. One study explored the combination of various parameters as nondimensional quantities to characterize the influence of fuel-oil film on pre-ignition [157]. Such type of efforts may be an option for a selection of measurable that yields maximum advance notice of pre-ignition over a wide variety of conditions. In this study,*

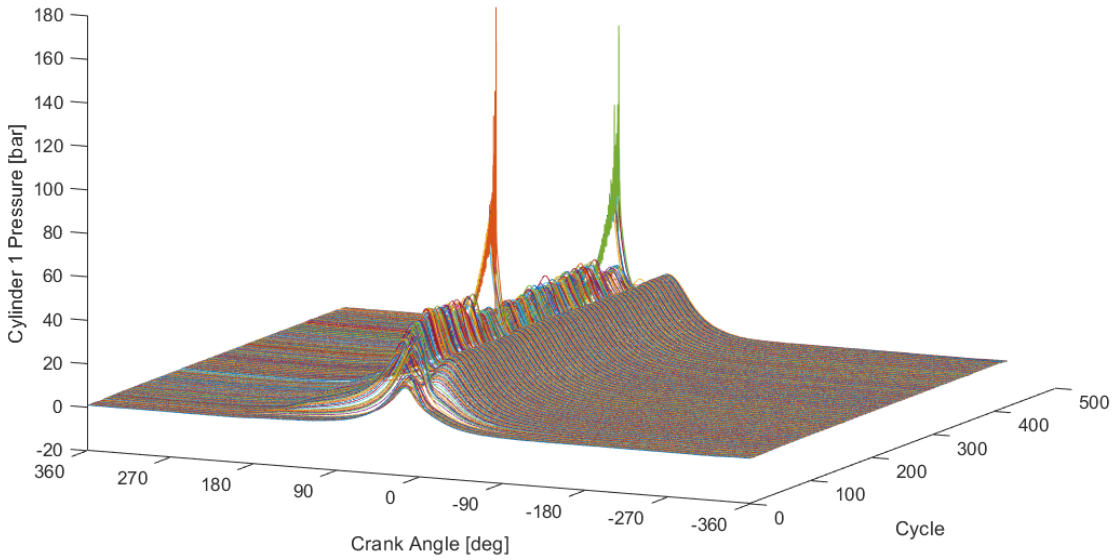

Fig. 4.4. Cylinder pressure test data with pre-ignition events, 1320 RPM.

peak pressure was sufficient to prove the concept for the conditions associated with available data. Another study [153] involved a similar theoretical approach using delay embeddings for advanced detection of pre-ignition employing statistical analysis of cycle-to-cycle pressure distributions. Other studies, such as [163], utilize the maximum amplitude of pressure oscillations or root-mean-square of pressure, which are suitable for ex post facto detection and not necessarily for prediction. In the context of the HAVOK approach, this is because such processing erases knowledge of cycle-to-cycle variabilities containing higher-order outputs of combustion. The SVD subprocess relies on the extraction of dynamic modes in order of correlation between eigen-delay coordinates and measured data, enabling the segregation of noise.

Using the data from Figure 4.4 data to construct the Hankel matrix and following the process, Figure 4.5 presents the output of the surrogate model, Eq. 4.2, along with the behavior of the apparent forcing term.

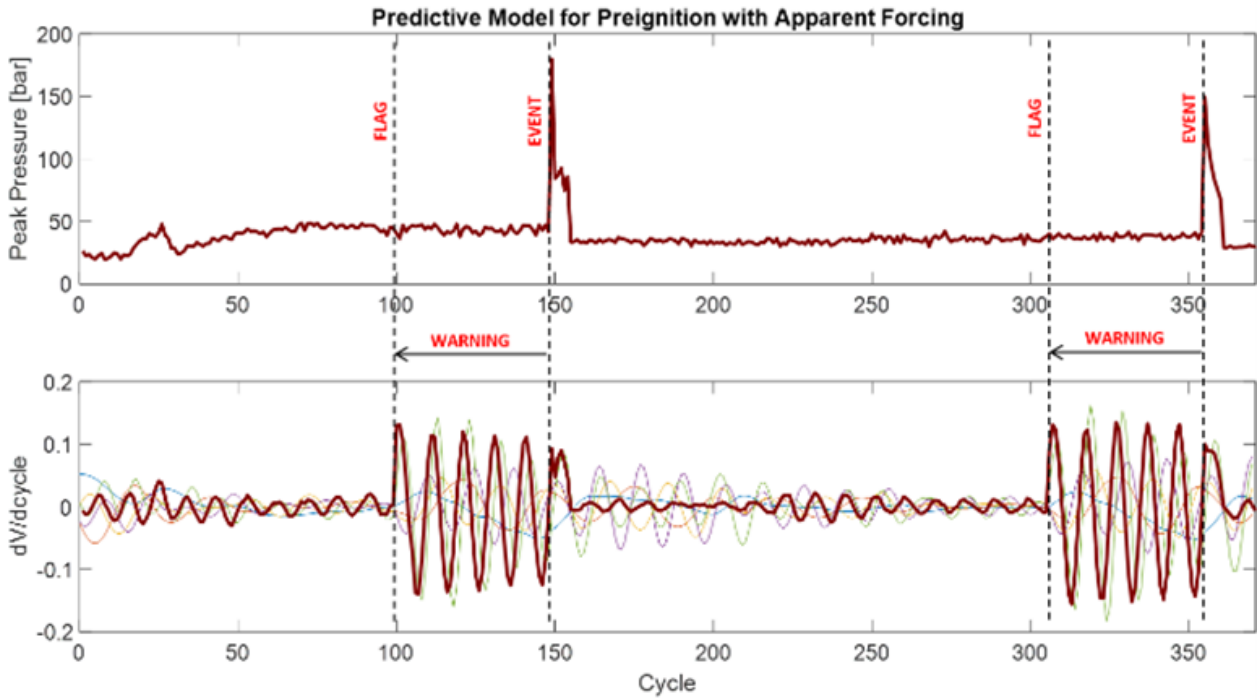

Fig. 4.5. Simulation results for HAVOK analysis applied to super-knock data.

The "flag" in this figure is defined to be the onset of excitation in the apparent forcing term. It refers to the instant a warning for the potential of the anticipated pre-ignition event can be generated, whereas "event" refers to the instant pre-ignition in fact occurs. Given that the engine was running at approximately 1320 RPM, both instances of pre-ignition are flagged over 2.27 seconds prior, upon which mitigating actuation can easily be applied to preemptively suppress the conditions in which the super-knock event is expected to occur. The associated reduced-order model came out to be of rank 10 (r = 11) with the following state-space matrices:

$$
\mathbf{A} = \begin{bmatrix}
1.0000 & -0.0065 & 0.0011 & 0.0034 & 0.0021 & -0.0042 & 0.0012 & \\
0.0035 & 0.9941 & 0.0610 & 0.0045 & -0.0625 & -0.0042 & 0.0411 & \\
0.0003 & -0.0615 & 0.9866 & -0.1227 & 0.0231 & 0.0659 & 0.0009 & \\
-0.0019 & 0.0038 & 0.1201 & 0.9751 & 0.1726 & -0.0032 & -0.0462 & \\
-0.0003 & 0.0603 & -0.0191 & -0.1689 & 0.9610 & -0.1894 & 0.0067 & \dots \\
0.0035 & 0.0009 & -0.0696 & -0.0023 & 0.1855 & 0.9422 & 0.2328 & \\
0.0005 & -0.0427 & 0.0017 & 0.0482 & -0.0095 & -0.2309 & 0.9207 & \\
0.0037 & 0.0003 & -0.0389 & -0.0010 & 0.0696 & 0.0019 & -0.2736 & \\
-0.0004 & 0.0327 & -0.0027 & -0.0289 & 0.0036 & 0.0829 & -0.0042 & \\
-0.0028 & -0.0002 & 0.0220 & 0.0004 & -0.0345 & 0.0000 & 0.0807 &
\end{bmatrix}
$$

$$
\begin{bmatrix}
-0.0041 & 0.0004 & 0.0034 \\
-0.0014 & -0.0342 & 0.0010 \\
0.0378 & 0.0013 & -0.0208 \\
-0.0032 & 0.0297 & 0.0015 \\
\dots \quad -0.0700 & 0.0016 & 0.0358 \\
0.0021 & -0.0830 & 0.0000 \\
0.2747 & 0.0001 & -0.0803 \\
0.8957 & -0.2817 & 0.0018 \\
0.2802 & 0.8673 & 0.3463 \\
0.0022 & -0.3453 & 0.8330
\end{bmatrix}
\approx
\begin{bmatrix}
1 & & & & & & & & & 0 \\
& 1 & & & & & & & & \\
& & 1 & -\frac{1}{8} & & & & & & \\
& & \frac{1}{8} & 1 & \frac{1}{6} & & & & & \\
& & & -\frac{1}{6} & 1 & -\frac{1}{5} & & & & \\
& & & & \frac{1}{5} & 1 & \frac{1}{4} & & & \\
& & & & & -\frac{1}{4} & 1 & \frac{2}{7} & & \\
& & & & & & -\frac{2}{7} & \frac{8}{9} & -\frac{2}{7} & \\
& & & & & & & \frac{2}{7} & \frac{7}{8} & \frac{1}{3} \\
0 & & & & & & & & -\frac{1}{3} & \frac{5}{6}
\end{bmatrix}
\tag{4.3}
$$

$$
\mathbf{B} = \begin{bmatrix} 0.0001 & -0.02760 & 0.00020 & 0.0226 & -0.0002 & -0.0603 & -0.0016 & \dots \\ \dots & -0.0286 & 0.0010 & -0.0060 \end{bmatrix}^T
$$

$$
\mathbf{C} = \mathbf{I}_{10}
$$

$$
\mathbf{D} = \mathbf{0}_{10\times 1}
$$

The **A** matrix in Eq. 4.3 is the approximated Koopman operator. It can be noted that the **A** matrix is approximately a skew-symmetric tridiagonal matrix. In accordance with spectral theory, this can be expected given the Koopman operator's function in executing a special orthogonal transformation. The fact that it is not exactly computed as such relates to the idea that regression was performed. As similarly highlighted in [117] where the same structural form availed, was interpreted therein to mean that system poles which happen to be slightly positive can be reasonably approximated to lie exactly on the imaginary axis. This model encompasses the dynamics of

combustion processes, which were not apparent enough for direct physics-based modeling, that led to the pre-ignition and super-knock shown in Figure 4.5.

Given a typical vehicle's CAN network having a message rate on the order of 1 millisecond, 2270 milliseconds are adequate to run through the steps of Figure 4.2 from sensing to actuation. This may represent a lower bound of advanced notice possible given that LSPI would otherwise be more likely to occur at lower engine speeds. The data used in the simulation was in terms of crank cycle. Thus, if the vehicle were idling, a flag similarly generated 50 cycles ahead of an expected event would correspond to 6 seconds. Although the underlying combustion dynamics might manifest differently across different speeds, it is still expected that the cycle-to-cycle peak pressure to capture the effect of in-cylinder boundary conditions upon the onset of pre-ignition. In the context of this case study, this relates to any detectable association since the dynamic mode extraction utilizes the correlation matrix within the singular value decomposition subprocess.

4.7 Validation of Predictive Capability

In the previous section, the HAVOK algorithm was applied to the entire dataset. Alternatively, only the first pre-ignition event can be used to construct the surrogate model and then used to predict the onset of the second pre-ignition event. In that case, the optimal truncation happens to yield rank 7 ($r = 8$), with the state state-space matrices and excitation in v_r as follows:

$$
\mathbf{A} = \begin{bmatrix}
0.9995 & -0.0090 & 0.0031 & 0.0035 & 0.0034 & -0.0042 & 0.0019 \\
0.0042 & 0.9957 & 0.0564 & 0.0056 & -0.0588 & -0.0037 & 0.0365 \\
0.0002 & -0.0569 & 0.9870 & -0.1318 & 0.0319 & 0.0558 & -0.0004 \\
-0.0026 & 0.0017 & 0.1276 & 0.9762 & 0.1527 & -0.0012 & -0.0541 \\
-0.0002 & 0.0531 & -0.0259 & -0.1458 & 0.9622 & -0.2098 & 0.0183 \\
0.0036 & 0.0008 & -0.0609 & 0.0000 & 0.2017 & 0.9425 & 0.2161 \\
0.0005 & -0.0391 & 0.0024 & 0.0568 & -0.0180 & -0.2117 & 0.9198
\end{bmatrix}
$$

$$
\approx \begin{bmatrix}
1 & & & & & & \\
& 1 & & & & & \\
& & 1 & -\frac{1}{8} & & & \\
& & \frac{1}{8} & 1 & \frac{1}{7} & & \\
& & & -\frac{1}{7} & 1 & -\frac{1}{5} & \\
& & & & \frac{1}{5} & 1 & \frac{2}{9} \\
& & & & & -\frac{1}{5} & 1
\end{bmatrix} \tag{4.4}
$$

$$
\mathbf{B} = [0.00490.0032 - 0.03610.00040.07410.0002 - 0.2914]^T
$$

$$
\mathbf{C} = \mathbf{I}_7
$$

$$
\mathbf{D} = \mathbf{0}_{7\times 1}
$$

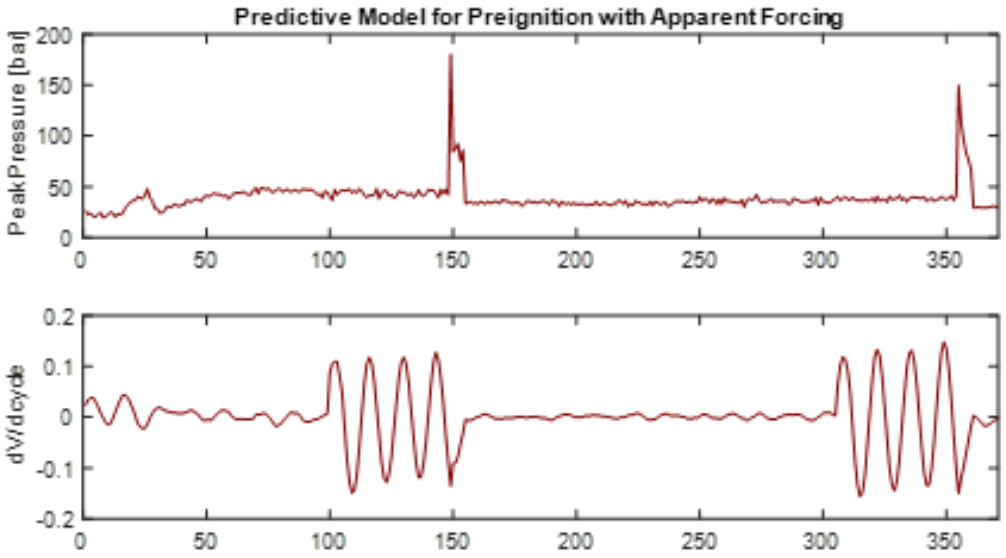

Fig. 4.6. Simulation results for HAVOK analysis applied to predict the second super-knock event.

The result in Figure 4.6 shows the same warning time for the second pre-ignition/super-knock event, even though the algorithm has no knowledge of it. This is interpreted to mean that the same or similar enough combustion dynamics were at play during both instances (i.e., both pre-ignition events occurred due to the same reasons). Finally, the form of Eq. 4.4 again yields the same structural properties as the prior results shown in Eq. 4.3, as expected.

Remark 13 *Signal-to-noise ratio is a key parameter for robustness and the Koopman approach resolves the measurement data into a distinct set of modes where relevant features become easily apparent, such that the boundary between that which truly affects the dynamics is more precisely discerned from that which is truly noise. A nominal surrogate model could be set as an initial calibration from a master dataset containing past pre-ignition events at various conditions. It could also be made adaptive by growing to include novel operating and environmental conditions from a running buffer (of knock-sensor data) to add cases where pre-ignition was not predicted. Thus, the possibility of false positives is minimized and diminish over time. The rank, r, of the Koopman matrix may come up different, yet will always be the global best fit, and therefore predict most super-knock events. Given that only a few pre-ignition events can cause a catastrophic failure of an engine, avoiding any pre-ignition at all is a valuable achievement.*

A sense of the time scales involved in performing the HAVOK computations in comparison with the processes being controlled is necessary for understanding the feasibility of in-vehicle implementation. The simulation environment of this desktop study consisted of a Dell Latitude 7424 with a 1.70 GHz Intel Core i5-8350U 4 Core processor and 16 GB RAM running Microsoft Windows 10. Using embedded timer functions, the duration of three key blocks of code were measured: T_1 being the extraction of 422 peak pressures from a total of 3,035,400 sampled pressure measurements over all the crank cycles in the available data; T_2 being the organization of the Hankel matrix, its decomposition using the singular value decomposition and organization of the surrogate model; and T_3 being the threshold comparison of the v_r values from the surrogate model. The total duration of these time segments, the computations of which would otherwise be performed on an engine control unit, came out to be 14.8 ms. In vehicular applications, the activity associated with T_1 is an analog process obtained from the knock sensor's conditioned output and is likely to be faster than the data extraction performed in the desktop simulation. The activity associated with T_2 comprises the main algorithmic processing and took merely 3.6 ms to compute in addition to the threshold comparison associated with T_3, which is what is traditionally done with knock sensor data currently. A CAN message can be transmitted in as little as 130 μs [168], with the added duration of final actuation ranging from null (no fire) to perhaps a few hundred milliseconds (e.g., opening the wastegate). Thus, even with added times for intermediate intra-ECU computation, the poten-

tial control response would very well be within the 2270 ms warning window generated in this study.

In terms of assessing the feasibility of in-vehicle implementation from the perspective of computational capacity, it is also necessary to note that necessary additions to an engine control module would be minimal. Beyond the threshold comparison already performed during knock-sensing, strategy code may additionally call for a function block to perform the singular value decomposition, which utilizes 605 bytes of code. Further additions would require a few lines of code to arrange stored data, invert a square matrix (of rank $\leq r$) and multiply four matrices (of length $\leq r$) in performing the required computations for Eq. 3.7. Therefore, the additional required code space would be under 1 kB in ROM, plus 1 byte per stored peak pressure data value in calibration space. Lastly, the surrogate model will take well under 100 bytes. Such capacity requirement would likely not justify any hardware upgrade and is relatively minor compared to typical software features emerging from engineering development today.

In terms of further experimental validation, additional data was obtained using the same engine over three relatively steady speeds averaging 1316 RPM (Figure 4.7), 1783 RPM (Figure 4.9) and 2036 RPM (Figure 4.11). These runs showed multiple instances of pre-ignition, all of which produced super-knock. The three speeds were selected to reasonably cover the design envelope within which LSPI is common and are classified as low, medium, and high, respectively. The calibrated cold-start idle speed for the engine used in this study is 1000 RPM. Above the selected high speed, the scenario evolves into medium-speed pre-ignition (MSPI). Further, LSPI is less likely to occur in a warmed-up engine. The mechanism for this, as described in the literature review, may relate to oil residue on the cylinder wall. Thermal expansion of the piston and cylinder after warm-up may tighten the interfacing tolerance, decreasing the likelihood of such residue to manifest. Older engines with worn-out piston rings are thus more susceptible to LSPI during cold-start. Following the same steps from Figure 4.3, validation results for these three additional cases are given below in Figures 4.8, 4.10 and 4.12. For all cases, the **A** and **B** matrices were computed based on the first pre-ignition event as training data. The remaining data, converted into delay coordinates, used the same surrogate state-space model for observation of bursts in the apparent forcing term.

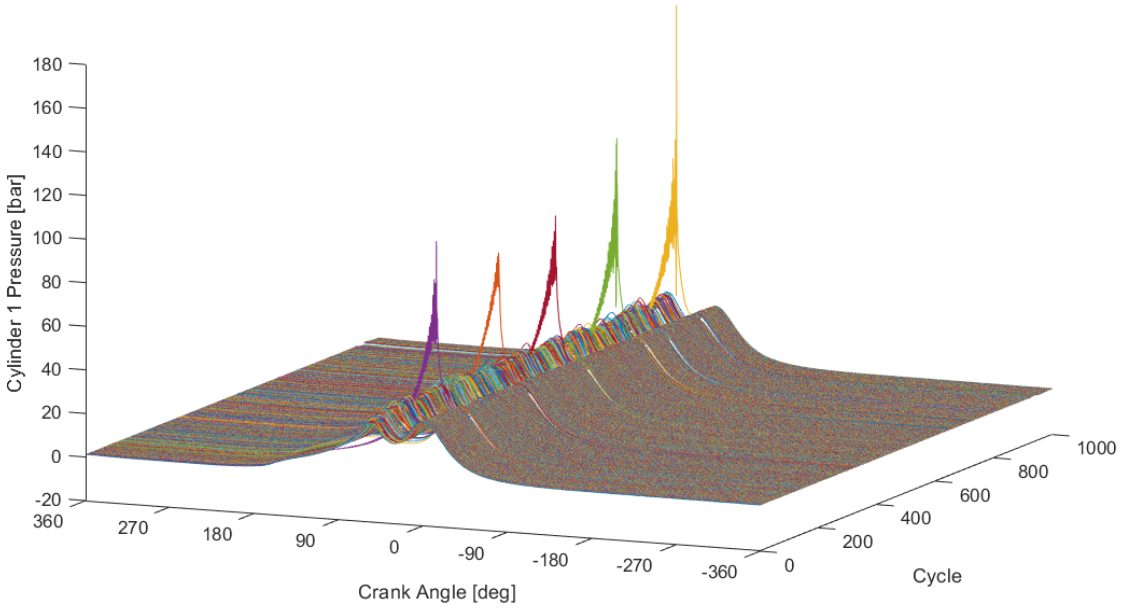

Fig. 4.7. Cylinder pressure test data with pre-ignition events, 1316 RPM.

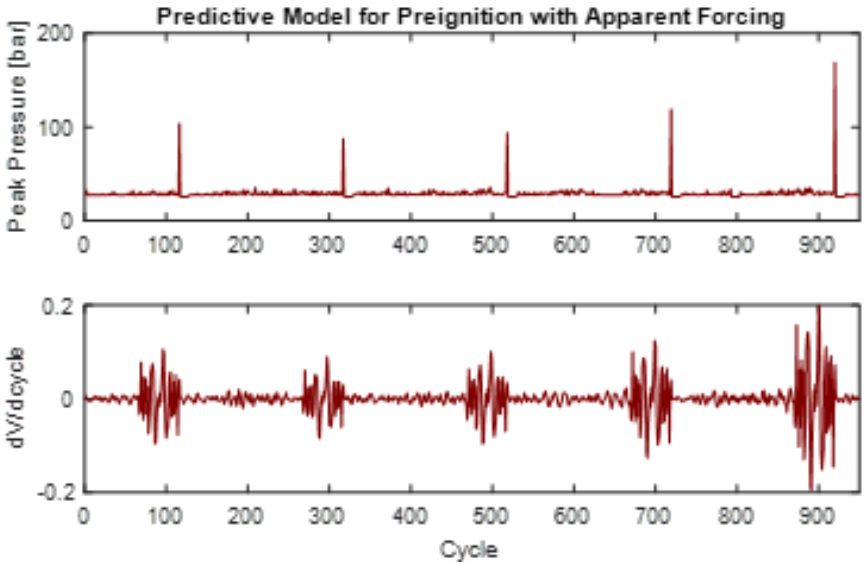

Fig. 4.8. Prediction results using HAVOK, 1316 RPM.

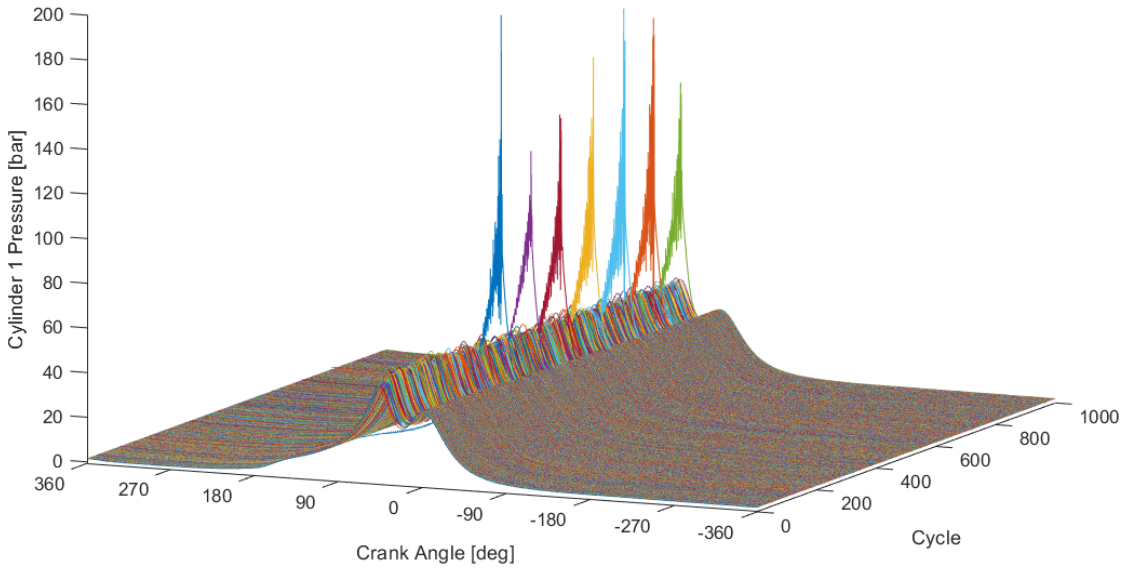

Fig. 4.9. Cylinder pressure test data with pre-ignition events, 1783 RPM.

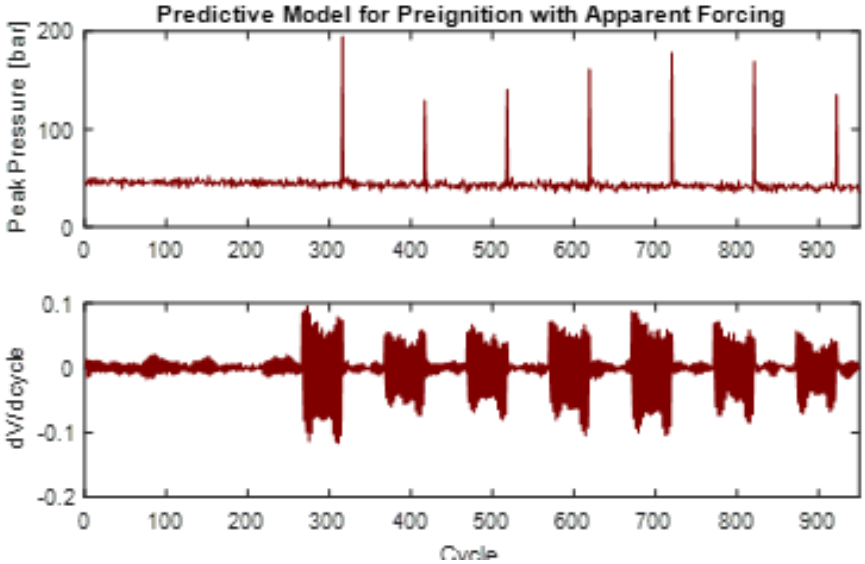

Fig. 4.10. Prediction results using HAVOK, 1783 RPM.

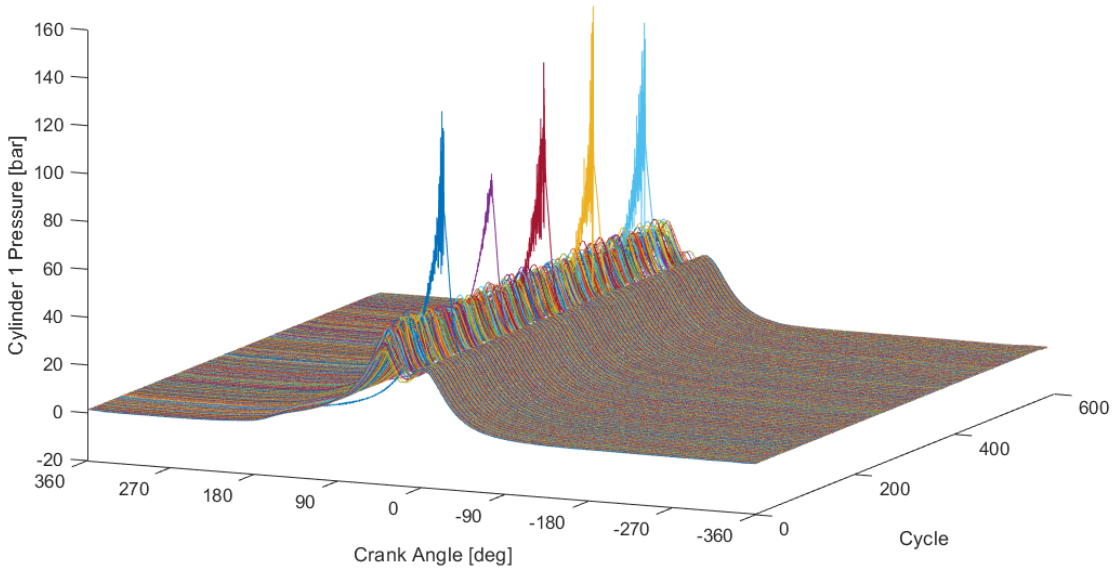

Fig. 4.11. Cylinder pressure test data with pre-ignition events, 2036 RPM.

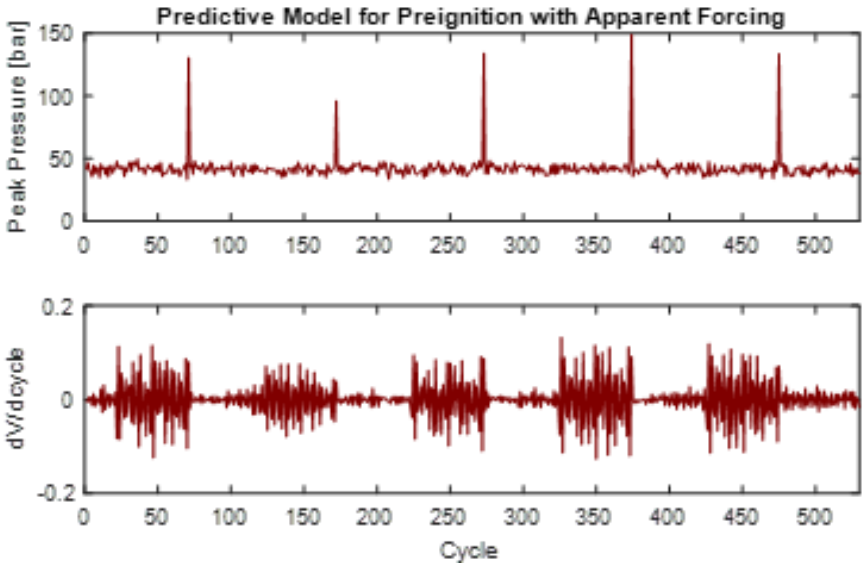

Fig. 4.12. Prediction results using HAVOK, 2036 RPM.

With the bursting threshold taken as 0.02, a prediction flag was established around 49 cycles prior to pre-ignition in all cases. This corresponds to 2.3 s, 1.7 s and 1.4 s for the three speed cases, respectively. These are again sufficient durations to allow for mitigating actuation.

4.8 Conclusions

The proposed technique involved the construction of a linear representation of the system solely using peak pressure data as the input, from which an apparent nonlinear forcing term was extracted. In all cases, the apparent forcing term exhibited excitation approximately 50 crank cycles before the pre-ignition/super-knock events occurred. This number may be different for environmental and operating conditions differing from test conditions. However, the data used in this study included 19 instances of pre-ignition and super-knock from over 2850 cycles at various speeds within the envelope where LSPI can be expected. Further, the proposed algorithm is designed to be implemented in an adaptive fashion where the surrogate model can be updated to include new pre-ignition data. Advance notice for pre-ignition prior to its occurrence on the order achieved in this study is sufficient to preemptively take mitigating action (e.g., opening the wastegate), up to and including disablement of fuel and spark to the affected cylinder in the anticipated cycle. Further, the necessity for a data-driven approach is justified due to the facts that:

- The combustion dynamics are unknown
- There currently exist no feasible physics-based models
- Behavioral models are over-simplified and void of underlying dynamical behaviors necessary for prediction
- The difference in timescales of measurements that alert us to an upcoming super-knock event compared to that on which the event itself manifests and lasts are so large that the signal-to-noise ratio is too low

The state dynamics matrix attained from the Koopman operator of eigen-time series data was of size 7×7, which is much smaller than the many series of calibration maps already handled by a modern engine controller, which tend to rely on semi-physics-based models with empirical corrective factors determined from engine sweep calibration. Implementation of a trained model, up to the point developed herein, would be especially useful in critical operating regions susceptible to super-knock (e.g., low speed, high-load, cold start). The algorithm is well suited for self-tuning, building upon re-evaluation of the surrogate model from buffered

data, and so may learn and avoid new conditions resulting in pre-ignition. It seems that the right-singular vectors have a predictive property due to the effective compression of observed dynamics onto a smaller time scale, which is why the size of the Hankel matrix is also effectively a tuning parameter, ensuring that any repeatable pattern in the data will be detected there first.

By its nature, pre-ignition occurs sporadically. It typically seeds super-knock which dissipates over the following few crank cycles, returning the engine to nominal operation. If adverse conditions persist pre-ignition may recur until a favorable steady-state condition is attained (e.g., engine warm-up). Thus, it is not likely to see too many occurrences in data collected over a relatively short time span. Future studies may involve a study of predictive performance with respect to the accumulation of engine damage from pre-ignition up to the point of failure. One could also apply HAVOK to predict other types of instabilities in other engine variants operating in specific dynamical contexts (e.g., thrust variation in gas turbine engines, or current ripple in electric motors).

Further work may include the determination of a standardized nondimensional parameter that more optimally captures the effects of conditions leading up to pre-ignition than peak pressure over a large variety of conditions. Self-recalibration may be innate to this technique so long as the buffer is stored in memory, and the surrogate reevaluated upon every failed prediction. If proven successful in real-world driving conditions, it would be a significant advancement in the field of engine controllability and a solution to a major limitation in the design envelope of hybrid electric vehicles and small engines.

CHAPTER 5

Tethered Subsatellite Deployment

5.1 Abstract

Compact tether-based actuation is a suitable approach for the deployment of femto/picosatellite bodies from CubeSats using ultrasmall electrodynamic tethers for fuel-free propulsion and deorbiting. Despite the advantages of tethered satellite systems, control technologies for these have yet to mature in several domains including robustness to structural faults and unmodeled dynamics. A proposed solution for the identification of disturbances to tethered satellite dynamics is to use a data-driven algorithm to learn the system's behavior over previous orbits and then provide an estimated prediction for the evolution of system states. To achieve the goal of state prediction via a globally linearized system model, this chapter employs the Koopman operator constructed from observed dynamics to extrapolate future motion of a tethered subsatellite subject to unknown disturbances while being deployed from its mothership. Numerical simulations of the constructed model versus the nonlinear model of the tethered satellite system demonstrate the effective prediction capabilities of the proposed Koopman operator-based numerical algorithm for the general flight characteristics many orbits into the future.

5.2 Introduction

Tethered satellite systems (TSS) have found various applications ranging from tethered propulsion, which offers the potential for significantly cheaper space operations by way of fuel-free solutions to boosting and deorbiting, to attitude stabilization and orbital flight control [169]. Conventional satellites often include redundant control actuators, such as oblique reaction wheels in their attitude control systems. Consequently, failure of a primary control actuator does not lead to the loss of satellite controllability. On the other hand, having such reaction wheel-based actuators introduces a coupling between the degrees-of-freedom affecting the satellite attitude dynamics [8]. Furthermore, the undesirable economic tradeoff to such control redundancy is the loss of valuable

payload capacity and increased weight.

In tethered propulsion, in contrast to thruster/wheel-based satellite actuation technologies, the flow of electric current through a conductive-electrodynamic tether (EDT) induces a Lorentz force acting against the ambient magnetic field which accelerates or decelerates the TSS (see Fig. 5.1 for the mechanism of TSS-deployment into the orbit). In other words, the Lorentz force generates either propulsive or braking effects, depending on the EDT current direction. Such compact tether-based actuation, which relies on the exchange of momentum with the planet's magnetosphere, is especially suitable for deployment of pico-/femto-satellite bodies from CubeSats using ultra-small electrodynamic tethers [170]. The tethered satellite technology further enables applications such as deorbiting, detumbling and underactuated control of damaged/decommissioned satellites, which have been contributing to the growing problem of unmanaged space debris [171].

In addition to EDTs, there are other factors affecting the motion of the general TSS. In particular, the difference in altitude between the subsatellite and its mothership results in differential aerodynamic drag due to the gradient in atmospheric density, gravity gradient torque, and pitch motion. The pitch motion itself is caused by the masses of the tethered satellite and its mothership at different orbital radii, being constrained to move with the same orbital velocities [172]. In addition to this differential aerodynamic drag force, the large inertial distribution along the radial axis of tethered satellites implies a greater sensitivity, in comparison with conventional satellites, to J_2 perturbations [173]. The superposition of these effects along with space weather factors such as solar radiation pressure, geomagnetic storms, and solar/lunar tidal effects on the atmosphere lead to heightened sensitivities in the operational performance of a TSS. Therefore, the accumulated effect of incremental disturbances over relatively long tethers necessitates the identification of the TSS dynamics subject to environmental disturbances. Identification of the TSS dynamics, in turn, enables the design of reliable motion control and prediction algorithms for the TSS.

Many control laws and fault detection schemes for the TSS are formulated using physics-based approaches. Rawashdeh & Lumpp [174], Varma [175] and others have created physics-based models of conventional miniature satellites subject to environmental forces including aerodynamic drag and gravity gradient assuming constant parameters. Furthermore, Yu et al. [176] have derived equations of motion describing the TSS motion as chaotic behavior resulting from atmospheric drag and the Earth's oblateness. In a related work, He & Ge [177] provided an in-depth derivation of a free-beam model for flexible satellites including those with large solar panels. They state that with higher-order frequency modes often being neglected, reduced models adapted for control can result

in spill-over instability under certain conditions. For example, they show that a Lyapunov-based control law eliminates an approximately 3.5 meter vibration in two 10 meter solar panels over 50 seconds. Furthermore, a spacecraft is subject to all sorts of potentially unmodeled disturbances including but not limited to time-varying gravitational magnitude and direction, atmospheric swelling, solar flaring, momentum exchange from micro-debris impacts, thruster misalignment, and sensor resolution issues. These effects will only become more pronounced as the trend moves towards miniature satellites (such as, Micro/Nano/Pico/Femto-Can/CubeSats). Physics-based modeling, which explicitly consider all these unknown disturbances, for the purposes of control and fault detection in highly sensitive spacecraft operations, is an almost intractable task.

Over the last decade there has been an increased interest in online model adaptation and automated calibration algorithms for autonomous vehicle systems as an alternative to physics-based approaches. Accordingly, the goal of TSS dynamics identification under unknown disturbances can be accomplished by analyzing available real-time flight data and subsequent construction of models from which future trajectories can be extrapolated. Without prior knowledge of the exact TSS dynamical model, variability, volatility and nonlinearities, this estimation task is understandably very difficult to accomplish, often requiring simplifications [178]. Moreover, identifying these unknown dynamics during the sensitive operation of TSS tether deployment (see Fig. 5.1) is of crucial importance as post-deployment oscillations might yield tether forces beyond the expected strength and subsequent failure of the deployment operation. Indeed, such post-deployment oscillations were among the main causes of the failure of the 1996 TSS-1R demonstrator mission [179].

Previous research on the TSS deployment problem using tension control has highlighted the criticality of adequate modeling. One approach has been to use a qualitative lumped disturbance model, as Wen et al. [180] did to demonstrate the performance of an optimal feedback controller. Similarly, Wang et al. [181] constructed an open-loop tether tension control law using particle swarm optimization and compared its performance with proportional-derivative and sliding mode controllers subjected to uncertainties and perturbations. Others have focused on the system identification aspect and sought to create higher fidelity physics-based models. For example, Yu & Dai [43] established an approach to identify tether dynamics from a structural perspective and showed how deployment performance is affected not only by operational, but also mechanical and material properties of the tether. Williams [182] identified tether dynamics including models for tether shape, vibrations, drag and electrodynamic forces using Chebyshev polynomials. State estimation of TSS has also been performed using genetic algorithms [183] and Kalman filters [184], [185]. Among space systems applications, Koopman operator-based methods have only

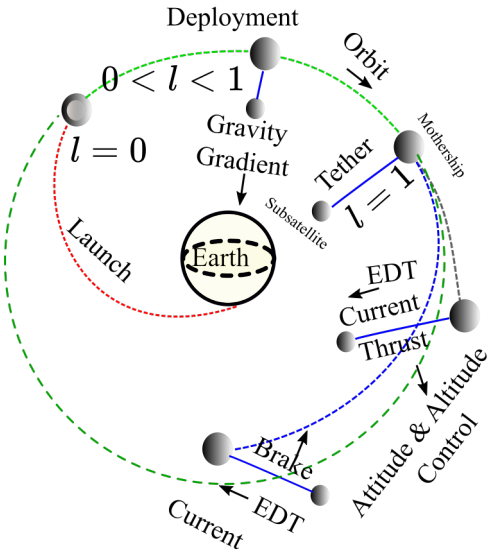

Fig. 5.1. Deployment of a TSS into the orbit.

very recently been employed in the context of rocket engines [48], [63], landing [76], attitude control [30], and the orbital flight of monolithic spacecraft [36], [50].

The present work seeks to address the problem of identifying spacecraft dynamics under environmental disturbances from a data-driven perspective in a non-conventional satellite configuration undergoing a specific maneuver, namely, deployment of a subsatellite via a single tether. Although disturbance observer-based techniques are widely used for estimating unknown disturbances acting on nonlinear control systems [186], these techniques rely on the knowledge of the exact underlying dynamical model. On the other hand, the time-varying nature of nonhomogeneity in the flight environment of TSSs requires an adaptive, real-time approach for system identification, which would result in improved predictions of future trajectories. Specifically, in low Earth orbit (LEO), where a tethered satellite is most effective if deploying a conductive tether, planetary oblateness introduces a gravitational perturbation 430 times greater than that of J_3 effects, and the nominal solar radiation perturbation has an order of magnitude of $10^{-6} m/s^2$ [187]. Further, LEO coincides with the Appleton–Barnett layer, or "F layer" of the ionosphere, a region with the greatest electron density. Thus, an EDT in LEO would be most effective. Atmospheric and electron density in the F layer varies in relation to lunar position and solar activity, with segmentation into two distinct sub-layers occurring diurnally [188].

5.2.1 Background on Global Linearization Techniques

Real systems can be represented by dynamical models of varying levels of fidelity, including nonlinear systems. These may include processes which act over a wide range of timescales, necessitating a trade-off between fidelity and computational efficiency. Further, nonlinear dynamics may demonstrate chaotic behaviors such as bifurcation and sensitivity to initial conditions, which are not observable in systems with linear dynamics. Thus, when not inherently linear (a rare case), conventional linearization of nonlinear dynamics typically involves negligence or approximations of higher order dynamics, state-input dependence, and disturbances.

Conventional methods of linearization include approximating a system's behavior at a particular state, usually an equilibrium or an operating point. Such linear models are typically obtained by way of small perturbation theory which utilizes small angle approximations and vanishing terms containing products of differentials, or the use of a truncated series expansion about the desired point. Decoupling of nonlinear terms or affine control inputs by these means can also be enabled through increasing the order of differential equations describing the system. However, the model is then only or approximately valid at or near the point of linearization, respectively, and increased in sensitivity through noise amplification. The neglected dynamics are left to be taken as disturbance, along with all other unknown or unmodeled processes. In the LEO environment, the occurrence and magnitude of geomagnetic storms are unpredictable [189]. Also, the local density of rarefied gasses are functions of chaotic meteorological processes, yielding drag as a time-varying force [190]. If a deterministic model otherwise existed, it could be linearized along a reference trajectory and gain scheduling implemented. However, an adaptive and computationally more efficient approach would be to learn the system's empirical behavior in real-time, accounting for all influences. This approach is utilized in this research. Such a reduced-order non-physics-based model in a globally linear form could readily take advantage of state-space control techniques.

To address the limitations of conventional linearization, there has been much research into the area of global linearization. One such technique is that of changing state variables. As detailed by Jordan & Nowacki [5], this can be accomplished using either the General or Heuristic methods to find a system of linear equations in an intermediate variable which is itself a function of the original state variable. In the Heuristic method, one equates the nonlinear equation to the general state space equation in controller canonical-like Frobenius form and unknowns are selected to comply with the Routh-Hurwitz stability criteria. Disadvantages of this approach is that a stable solution may not be easy to find, and it is computationally complex for automation. In the General method, the approach is a matter of collecting like terms containing state variables from the expanded nonlinear equation and grouping them into convenient definitions for intermediate

variables. However, such linearized system of equations may still be time varying and do not necessarily isolate the effect of state from control inputs. Thus, the result is not generally in true state space form, which is problematic for the implementation of some control methods and analyses.

Additional classifications of global linearization methods exist for affine and bilinear systems including state linearization, feedback linearization and restricted feedback linearization. Čelikovský [7] derived a formal definition in which global linearizability may be achievable by these means via a change of state variables. However, he also provided examples of systems that do not fulfill the criteria yet are linearizable within some range, at some point(s), at all but some point(s), or at "every point locally". However, guarantees of smoothness and continuity from formal proofs are sometimes unachievable, especially in the case of empirical system descriptions, when there is noise and disturbance, or where there are limitations in understanding of the physical processes involved.

Other global linearization methods involve alternative ways of representing nonlinear system descriptions to forms which may be linear (with decoupled input/output, endogenous feedback and disturbance) including as difference fields, 1-forms, Kähler differentials, Carleman linearization, generalized transfer functions, using output feedback, and as time-delay systems [9]. These methods are least common and continue to be studied as open areas of research in the field of pure mathematics. Alternatively, there exists a class of global linearization methods relating to regression methods, among which include those based on the Koopman operator [117].

Operator theory is the study of linear operators on function spaces, alternative to geometric or stochastic frameworks. The Koopman approach to operator theory distinguishes itself through its goal in determining coordinate changes required to represent nonlinear dynamics in a linear space through the construction of required bases from measurement data [14]. This high dimensional space is framed upon a coordinate system consisting of up to infinite orthonormal bases in suitable function spaces rather than unit vectors, wherein the properties of spatial completeness are preserved [97]. The result is a state transition matrix mapping the propagation of a system's set of measurable quantities in a best-fit manner over the entire domain. Hence, this transformation matrix is denoted as the Koopman operator. This approach to linearized system identification has found applications in data-driven modeling of complex systems ranging from fluid dynamics [191]–[193] to neuroscience [117] and power grids [194]. The interested reader is referred to the work in [121] for a detailed treatment of Koopman operator theory.

In the context of model predictive controllers (MPCs), the linear predictors obtained from

the Koopman operator-based approach exhibit a performance superior to conventional linear predictors such as those relying on the so-called Carleman linearization or local linearization techniques. Additionally, the numerical schemes for constructing these linear predictors is totally data-driven and simple to compute, where the underlying computation boils down to a proper nonlinear transformation of the data and a subsequent linear least squares problem in the lifted space readily solvable for large data sets [195].

Contributions of the chapter. The Koopman operator, particularly in its numerical approach as with Dynamic Mode Decomposition (DMD) [13] has the intrinsic property of learning unmodeled dynamics, computational efficiency, and has been useful to solve a breadth of engineering problems. To exploit these opportunities further, this approach has been selected for investigation in the context of TSS systems. More broadly, this research is undertaken as a means to expand the literature of advanced system identification into the area of space systems engineering, where dynamics modeling is imperative. In this chapter, a linear global state-transition matrix is found for the TSS dynamics, which is a linear approximation of the Koopman operator of the TSS. This TSS Koopman operator incorporates proper functions of the online data obtained from angular positions and tether length measurements from the TSS. Subsequently, using the incoming stream of TSS data, the Koopman operator, which is approximated using the DMD algorithm, provides a reduced-order and globally linearized representation of an otherwise nonlinear dynamical system that includes the effect of unmodeled processes affecting the behavior of the TSS. Thus, the proposed Koopman operator-based algorithm is suitable for data-driven modeling of the behavior of TSSs subject to unknown disturbances. Simulations of the constructed Koopman operator-based linear dynamics versus the true nonlinear model of the tethered satellite system demonstrate the predictive capabilities of the proposed Koopman operator-based numerical algorithm for the general flight characteristics including many orbits into the future. Further, the TSS being simulated is modeled after the University of Michigan's Miniature Tether Electrodynamics Experiment (MiTEE), which is a 3U CubeSat equipped to deploy a femto-satellite housing an electron collector/emitter to actuate current within the connecting EDT [196].

The rest of this chapter is organized as follows. In the following, a brief review of the dynamics of tethered satellite systems while being deployed into circular orbit is provided. Then, a data-driven Koopman operator-based numerical algorithm is presented for estimating the unknown disturbances acting on a given TSS. This is followed by a presentation of simulation results and effectiveness of the proposed approach. Finally, this chapter concludes with further remarks and future research directions.

5.3 Tethered Satellite Dynamics

In this work, the maneuver of tethered subsatellite deployment from its mothership is considered. The control-oriented dynamic model appearing in the TSS literature [180], [197] is adopted, which describes the deployment and retrieval behavior of this system as illustrated in Fig. 5.1. The interested readers are referred to Williams [182] for a full physics-based model of TSS dynamics.

For presenting the control-oriented model of the TSS dynamics, an Earth-centered Inertial (ECI) coordinate frame is considered. The ECI frame is fixated on the celestial body, Earth, about which the satellite is orbiting. Moreover, a Local-Vertical-Local-Horizon (LVLH) body-fixed frame on the satellite itself can be considered. The LVLH frame is centered on the mothership and is convenient for attitude analysis. Having fixed these coordinate systems, the equations of motion,

$$\begin{aligned} \ddot{\theta} - 2\left(\dot{\theta} - 1\right)\left(\dot{\varphi} tan\varphi - \frac{\dot{\xi}}{\xi}\right) + 3 sin\theta cos\theta = 0, \\ \ddot{\varphi} + \frac{2\dot{\xi}}{\xi}\dot{\varphi} + \left[\left(\dot{\theta} - 1\right)^2 + 3\cos^2\theta\right] sin\varphi cos\varphi = 0, \\ \ddot{\xi} - \xi\left[\dot{\varphi}^2 + \left(\dot{\theta} - 1\right)^2 \cos^2\varphi + 3\cos^2\varphi\cos^2\theta - 1\right] = -u, \end{aligned} \tag{5.1}$$

model the behavior of the subsatellite's attitude and position with respect to the mothership in the LVLH frame depicted in Fig. 5.2. This TSS model, Eq. 5.1, was taken from Wen et al. [180], and is also common in the TSS literature [198]; originally adapted from Stuiver [199]. Here, the angle θ denotes the pitch angle, which is the angle between the tether projection on the orbital plane and the local vertical, or nadir, the angle φ denotes the roll angle about the axis defining the local horizon and is thus the out-of-plane rotation of the TSS, and ξ is the nondimensionalized tether length, $\xi = l_t/l_c$, where l_t is the tether length at time t and l_c is the characteristic length, taken to be the maximum tether length. In Eq. 5.1, $u = \frac{T}{m\Omega^2 l_c} > 0$ is the nondimensionalized control input, where T denotes the tension force of the tether. The in- and out-of-plane vibrations are dynamically coupled. The right-hand side of Eq. 5.1 can be nondimensionalized using the generalized [external] forces in the first two equations of motion.

The equations of motion in Eq. 5.1 are expressed in terms of nondimensionalized time, which is scaled by Ω^{-1}. The parameter $\Omega = \sqrt{\mu/r_o^3} = 1.133 \times 10^{-3}\ rad/s$ is the mean orbital angular velocity, where $\mu = 3.986005 \times 10^{14}\ m^3/s^2$ is the gravitational parameter for the Earth and $r_o = (6371 + 400)\ km$ is the Earth's radius plus flight altitude considered in this study. Other relevant values following the MiTEE design includes the maximum tether length of $l_c = 50\ m$, mothership mass of $M = 3.3\ kg$, and subsatellite mass of $m = 100\ g$. The mothership and its

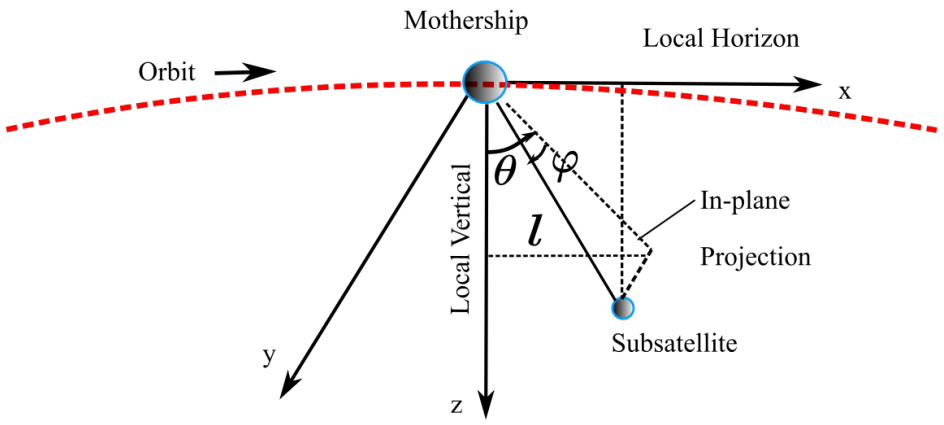

Fig. 5.2. Geometry of the orbital motion of a TSS.

subsatellite are assumed to be point masses (M and m, respectively), in accordance with the vast majority of the TSS literature (see, e.g., [200], [201]). This assumption results in decoupling the attitude control of the individual satellites from the problem, which is independent of the specific exercise of TSS configuration. Also, attitude control of the subsatellite may not be relevant depending on the mission specifics (e.g., the electron collector of the MiTEE's EDT). It is important to note that the out-of-plane rotation occurs at the TSS barycenter, which is approximately coincident with the mothership's center of mass given that $M \gg m$, and that the mass of the tether is negligible compared to m. As a result, the rotation about the axis collinear with the tether can be ignored. Finally, it is assumed that the tether is always taut, such that there is no slack or bending, which may introduce infinite degrees of freedom into the problem. These are very common simplifications in the TSS literature [180], [198], [199], whereas the true center of mass exists at the system's barycenter. The dynamical model given in Eq. 5.1 is in accordance with the assumption of a circular orbit about a spherical geoid with uniform mass distribution. Thus, planetary oblateness and J_2 perturbations are neglected. However, these effects are indirectly incorporated through the exogenous disturbance model.

Remark 14 *As it can be seen from Eq. 5.1, the TSS is an underactuated control system since there are three degrees-of-freedom and only one control input. Contingency for underactuation is an important topic by itself since there have been numerous tumbling satellites causing mission failures, dangerous space debris, and recent development of international legislation that mandate deorbiting expended satellites [202].*

In the dynamical system given by Eq. 5.1, the tether itself is always assumed to be straight. This condition is ensured by constraining the controller in a way that ensures there is always a

positive, nonzero tension in the tether, which is physically true even in the case of zero applied force due to the gravity gradient torque on the TSS. This gravity torque is generated by the subsatellite while being situated at a lower altitude and constrained to move with the same velocity as the mothership. Otherwise, the subsatellite would be required to move at a higher velocity to maintain a circular orbit. This fact also reveals that the applied control tension should be a braking force; or else, there may be slack introduced in the tether that leads to flexibility and tugging, entailing infinite degrees of freedom. However, by imposing the inequality constraint $\dot{\xi} > 0$, one can easily avoid slack. Furthermore, it is possible to consider disturbance effects such as elasticity by adding a lumped disturbance term to the nominal control input acting on the TSS dynamics in Eq. 5.1. The interested reader is referred to Wen et al. [180] and Yu & Dai [43] for further details.

5.4 Koopman Operator-based Approximations of TSS Nonlinear Dynamics

This section provides a brief overview of Koopman operator theory fundamentals in the context of the TSS dynamics. Consider the TSS nonlinear dynamical system given by Eq. 5.1 and define the state vector $\mathbf{x} = [\theta, \varphi, \xi, \dot{\theta}, \dot{\varphi}, \dot{\xi}]^T \in \mathcal{X}$, where the state space $\mathcal{X} \subset R^6$ is an open and connected set. Hence, the state vector $\mathbf{x}$ includes the TSS pitch and roll angles, normalized tether length, and their corresponding rates of change, respectively. The Koopman operator, denoted by $\mathcal{K}$, for the TSS dynamics given by Eq. 5.1 advances 'measurement functions' of the state of the TSS with the flow of the dynamics. Indeed, one can consider candidate output functions of the state, $\mathbf{g}(\mathbf{x}_k)$, which are known as the 'observables' of the nonlinear TSS dynamics in Eq. 5.1 and belong to the function space $\mathcal{G}(\mathcal{X})$. If the flow of the TSS dynamics in Eq. 5.1 is given by the mapping $\mathbf{F} : \mathcal{X} \rightarrow \mathcal{X}$, the evolution of the TSS states is governed by

$$\mathbf{x}_{k+1} = \mathbf{F}(\mathbf{x}_k), \tag{5.2}$$

where $\mathbf{x}_k = \mathbf{x}(t_k)$. Therefore, the Koopman operator $\mathcal{K} : \mathcal{G}(\mathcal{X}) \rightarrow \mathcal{G}(\mathcal{X})$, advances a given observable function $\mathbf{g}(\ )$ along the flow of the dynamics in Eq. 5.2 as

$$\mathcal{K}(\mathbf{g}) = \mathbf{g} \circ \mathbf{F}. \tag{5.3}$$

The observables may be the states themselves (such as, $\dot{\theta}$), and/or powers (such as, $\dot{\theta^2}$), trigonometric functions (such as, $sin(\theta)$), or other nonlinear combinations thereof (such as, $\dot{\theta}\sin(\theta)$) of the states of the TSS. These nonlinear observable functions of the TSS states can be concatenated

as

$$\mathbf{y}_k = \mathbf{g}(\mathbf{x}_k) = [\mathbf{g}_1(\mathbf{x}_k), \mathbf{g}_2(\mathbf{x}_k), \ldots, \mathbf{g}_p(\mathbf{x}_k)]^T, \tag{5.4}$$

to form a vector of observables. Computing a closed-form expression for the flow map $\mathbf{F}(\ )$ is a nontrivial task in many dynamical systems. Rather, Koopman operator theory seeks to find a collection of observable functions $\mathbf{g} : \mathcal{X} \rightarrow R$ that in composition with the flow map $\mathbf{F}(\ )$ result in linear dynamics in the space of those functions $\mathcal{G}(\mathcal{X})$, such that $\mathcal{K}(\mathbf{g}) = \lambda\mathbf{g}$. Such functions are called the eigenfunctions of the Koopman operator $\mathcal{K}$. In other words, if $\mathbf{g}^* \in \mathcal{G}(\mathcal{X})$ is an eigenfunction associated with the Koopman operator of Eq. 5.2, it follows that

$$\mathbf{g}^*(\mathbf{x}_{k+1}) = \mathcal{K}(\mathbf{g}^*)(\mathbf{x}_k) = \lambda\mathbf{g}^*(\mathbf{x}_k), \tag{5.5}$$

where λ is the eigenvalue associated with the eigenfunction $\mathbf{g}^*$. For a vector of Koopman eigenfunctions $\mathbf{g}_i^*, 1 \leq i \leq p$, such as the one in Eq. 5.4, it follows that

$$\mathbf{y}_{k+1} = (\mathcal{K}\mathbf{g})(\mathbf{x}_k) = \mathbf{\Lambda}\mathbf{g}(\mathbf{x}_k), \tag{5.6}$$

where $\mathbf{\Lambda} = diag\{\lambda_1, \cdots, \lambda_p\}$ is the diagonal matrix containing the eigenvalues of the Koopman operator eigenfunctions. Hence, if one can compute an approximation of $\mathcal{K}$ associated with the TSS dynamics along with proper Koopman eigenfunctions, then the TSS states can be easily predicted using the identified Koopman operator.

In the next section, a data-driven scheme is presented, called the dynamic mode decomposition (DMD) method, for approximating the Koopman operator of the TSS dynamics.

5.4.1 Dynamic Mode Decomposition

The DMD method, formalized by Schmid [13], approximates dynamic modes of the Koopman operator in a data-driven manner, resolving the system's state dynamics. Indeed, the DMD algorithm computes, from experimental data, the eigenvalues and eigenvectors (low-dimensional modes) of a linear model that approximates the underlying dynamics. One interesting feature of this data-driven method is that the DMD approximation is valid even if the dynamics are nonlinear [121]. Here, an overview of the DMD algorithm is provided in the context of the TSS dynamics. A detailed treatment of the DMD algorithm can be found in Tu et al. [203].

A sequential set of data vectors $\{\mathbf{x}_0, \cdots, \mathbf{x}_m\}$ is sampled during the operation of the TSS. These

data vectors are the "snapshots" of the state of the TSS dynamics in Eq. 5.1 that are sampled from the continuous TSS evolution $\mathbf{x}(t)$, where $\mathbf{x}_k = \mathbf{x}(k\ \Delta t)$ where a fixed sampling rate Δt is assumed. When DMD is applied to data generated by the TSS nonlinear dynamics in Eq. 5.1, the DMD algorithm yields a best fit linear operator $\mathbf{A}$ that approximately advances the state of the TSS dynamics $\mathbf{x}$ in R^6 according to the linear dynamical system

$$\mathbf{x}_{k+1} = \mathbf{A}\mathbf{x}_k, \tag{5.7}$$

To obtain the operator $\mathbf{A}$ for the TSS dynamics, the snapshots of measurable quantities $\{\mathbf{x}_0, \cdots, \mathbf{x}_m\}$ are arranged into two data matrices

$$\begin{aligned} \mathbf{X} &= [\mathbf{x}_0, \cdots, \mathbf{x}_{m-1}], \\ \mathbf{X}' &= [\mathbf{x}_1, \cdots, \mathbf{x}_m]\,. \end{aligned} \tag{5.8}$$

The best fit linear operator $\mathbf{A}$, which is obtained by the DMD algorithm, is the solution to the optimization problem

$$\mathbf{A} = \ argmin_{\mathbf{A}}\ ||\ \mathbf{X}' - \mathbf{A}\mathbf{X}\ ||_F, \tag{5.9}$$

where $||\cdot\ ||_F$ denotes the Frobenius norm. It is remarked that Eq. 5.4 describes the general case of selecting observables, if a catalog of functions of the states were incorporated into the data matrices, the algorithm would then be referred to as Extended DMD.

Solving the optimization problem in Eq. 5.9 involves employing Singular Value Decomposition (SVD) whose outputs can be arranged to determine the dominant Koopman eigenvalues of the system, thus enabling a lower-order linear approximation of the Koopman operator. Since the SVD is derived from the correlation matrix, the singular values extracted thereby are conveniently arranged by decreasing magnitudes of dynamic mode, allowing for truncation. The details on solving the optimization problem in Eq. 5.9 using SVD algorithm can be found in [203].

In summary, the end-result of the DMD algorithm for the dynamics is a best-fit state transition matrix acting as a globally linear approximation of the nonlinear system. The obtained DMD-based Koopman operator can then be used to propagate the desired states of the system to a future instant in time and thus providing a prediction of the evolution of the underlying dynamical system. Fig. 5.3 provides a schematic of the DMD-based Koopman operator approximation for the TSS dynamics. In the next section, this identification algorithm is applied to a TSS maneuver where the TSS subsatellite is being deployed into a circular orbit while there is a time-varying disturbance to the tension control input.

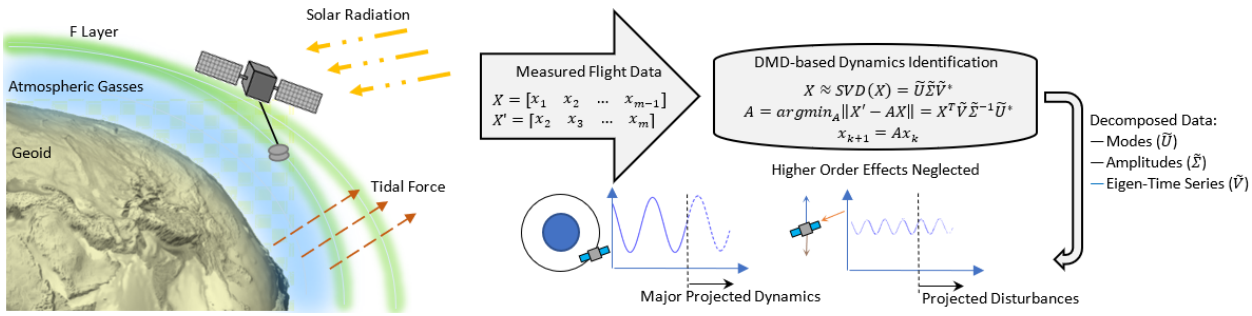

Fig. 5.3. Sources of variabilities in TSS flight environment & DMD process.

Remark 15 *It is assumed that there is no knowledge of the underlying TSS dynamics in Eq. 5.1. Rather, an approximation of these nonlinear dynamics is obtained using the stream of data* $\{x_0, \cdots, x_m\}$ *and the solution to the optimization problem in Eq. 5.9. See Fig. 5.3 for a schematic of the DMD-based Koopman operator approximation for the TSS dynamics.*

5.4.2 Dynamic Mode Decomposition with Control

Dynamic mode decomposition with control (DMDc) is a variant of DMD that resolves the **A** and **B** state space matrices separately. This approach allows for extraction of the open loop dynamics independent of the control actions applied. The modification required herein is to replace the data matrix from Eq. 5.8 with an input matrix that includes both the data and control inputs. The SVD is then performed on this input matrix and the resulting unitary matrices have corresponding state and control portions. Taking the state portion only, and an SVD of the time-shifted data matrix from Eq. 5.8, the optimization of Eq. 5.9 is again achieved through the projection of the data matrix onto the unitary matrices and scaled by singular values generated by the SVD.

Specifically, the estimated Koopman operator is constructed as a product of the time-shifted data matrix and the singular value decomposition of the data matrix, as shown in Eq. 2.13. In DMDc, the procedure is as follows: let $\mathbf{U}$, $\mathbf{\Sigma}$ and $\mathbf{V}$ be the SVD factors of the combined data matrix, $\mathbf{\Psi}$, where $\mathbf{\Psi} = [\mathbf{X}, \mathbf{Y}]^T$ and $\mathbf{Y}$ is the matrix of sampled control actions; and let $\mathbf{U}_o$, $\mathbf{\Sigma}_o$ and $\mathbf{V}_o$ be the SVD factors of the time-shifted data matrix, $\mathbf{X}'$. Then,

$$\begin{aligned} A &= \mathbf{U_0}^T X' \mathbf{\Sigma}^{-1} \mathbf{U}_1^T \mathbf{U_0}, \\ B &= [0\,0\,1\,0\,0\,0]^T \end{aligned} \tag{5.10}$$

where the input matrix, **B**, is structured as such in this case due to it being known that the sampled control action only came from the third state equation. $\mathbf{U}_1$ is the state portion of **U**. Note that one may continue to use economical forms of the SVD factors. Further details and examples of the DMDc algorithm are provided by Proctor et al. [18].

5.4.3 TSS Dynamics Identification During Subsatellite Deployment

In this section, the DMD-based identification algorithm is applied to a TSS maneuver where the TSS subsatellite is being deployed into a circular orbit. During the deployment operation, the subsatellite starts lowering to a desired altitude vertically below the mothership. Most of the useful mission activities start after complete deployment of the subsatellite.

Here, it is assumed that there is no knowledge of the underlying TSS dynamics in Eq. 5.1. Rather, during the early stages of tether deployment, the tether length is being controlled via a proportional-derivative control scheme of the form

$$u_n = K_p \left(\xi - \xi^d \right) + K_d \dot{\xi}, \tag{5.11}$$

where ξ^d is the desired tether length. Furthermore, it is assumed that there is an unknown time-varying disturbance in the tension force, which gets added to the control input. In other words, the disturbance force affects the dynamics of the TSS as

$$u = u_n + u_d, \tag{5.12}$$

where u_d is the tension disturbance, which can lump the effects of atmospheric, geomagnetic, or J_2 perturbations. Following Wen et al. [180], the following disturbance model is used for the simulation studies undertaken herein.

$$u_d = 0.01 \frac{m_n}{m_p} \left(sin\left(100t\right) + sin\left(0.01t\right) \right). \tag{5.13}$$

Remark 16 *All reference to nonlinear TSS dynamics herein refers to the TSS equations of motion used for simulation represented by Eq. 5.1, where u is taken from Eq. 5.12. This set of equations comprises the exogenous model, which is unknown to the learning algorithm.*

In Eq. 5.13, m_p denotes the subsatellite mass, which is within ±5% of the subsatellite nominal value $m = m_n$. It is assumed that the mothership is negligibly affected by perturbations due to its much greater inertia. Furthermore, the subsatellite, due to its lower altitude is immersed more in

Earth's atmosphere and experiences the drag effects more than the mothership. The proportional and derivative gains in the control law given by Eq. 5.11 are chosen such that the nondimensional tension control input is constrained between $u_{min} = 0.01$ and $u_{max} = 2u_s$, with $u_s = 3$ being the nominal static force, in consistence with Wen et al. [180] and representing a reasonable upper bound acting as a limiting factor in TSS missions, as with the failure of the aforementioned TSS-1R mission [179]. The lower bound is set to a practical minimum yet positive finite value. Indeed, any occurrence of negative tension implies slack in the tether that corresponds to introducing infinite degrees of freedom and tugging. Thus, the control action in the current context represents a continuous yet modulated braking during the subsatellite deployment.

In the deployment of a subsatellite, Banium & Kumar [197] proposed a practically suitable reference trajectory for optimal control. The trajectory follows an exponential decay in rate of deployment, leveling off upon approach to the target length, and consists of a tunable first-order time constant, p, as given in the following equation.

$$l(t) = l_o + l_c(1 - e^{-t/p}) \tag{5.14}$$

Here, l_o and l_c are the initial and maximum tether lengths, respectively.

5.5 Simulation Results

For demonstration, Fig. 5.4 illustrates a baseline result showing unforced deployment, comparing the original nonlinear dynamics with introduced disturbances and linearized dynamics obtained via DMD. Fig. 5.5 presents the results of simulation where tension as a braking force was applied upon the tether as a control input using a simple proportional–derivative (PD) controller with both gains set to 100. In both cases, the deployment of the tether follows a reference trajectory defined by Eq. 5.14 using a time constant of 0.1. The PD controller gains were selected to yield an appropriate magnitude and range for control input of 1 to 100 μN, comparable to an alternative propulsion system for small satellites [204]. The tension control result in Fig. 5.6 did indeed meet this requirement. The true [dimensionalized] tension force of the tether can be recovered by multiplying the values of this control input by $m\Omega^2 l_c$.

Fig. 5.5 shows the performance of the DMD/DMDc model estimation compared to the nonlinear dynamics. Following the convention of Eq. 5.9, the state vector is organized as $\mathbf{x} = [\theta, \varphi, \xi, \dot{\theta}, \dot{\varphi}, \dot{\xi}]^T$ which includes the TSS pitch and roll angles, as well as the normalized tether length, and their corresponding rates of change. The initial roll angle was non-zero due to

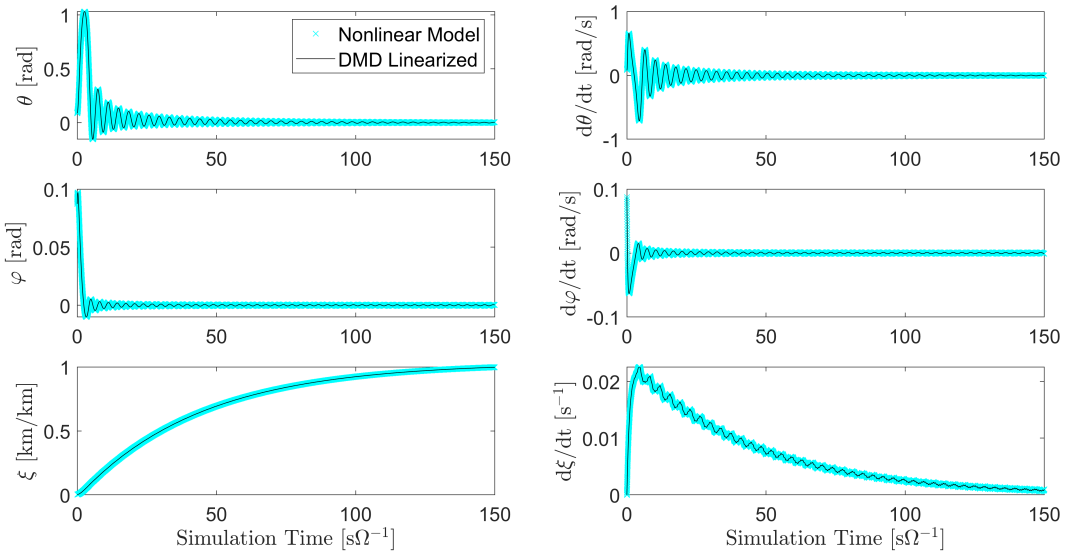

Fig. 5.4. Simulation comparing nonlinear vs. globally linearized model: unforced dynamics.

start-up errors and disturbances. Initial tether length is taken to be 1 cm and terminating at the deployed normalized length of $\xi = 1$, that is, 100%, which in this study was taken to be 50 m. Thus, there is no desired state or reference trajectory imposed on the pitch and roll angles, nor on their rates. This is because the scope of this study was on the deployment maneuver, and the TSS, as configured, is underactuated to perform such angular control.

Figs. 5.4 and 5.5 illustrate the progression of the state variables (solid black) over the course of the subsatellite deployment. Superimposed thereon (dotted blue) is the output of the linearized model constructed using DMD/DMDc. The necessity of a controlled deployment is evident in Fig. 5.4 in that the tether length stops increasing abruptly. In practice, this is undesirable due to several reasons including the possibility of impulsive forces exceeding the tether strength and elasticity in the tether causing recoil which introduces slack and tugging dynamics not modeled in Eq. 5.1. Note that in the case of controlled deployment, the linearized model includes closed-loop feedback, as the effects of control action have been absorbed into the data matrices of Eq. 5.8. Table 5.1 details the minute deviations in the graphed results, which are not discernable visually. These errors particularly tended to occur during the transient phases of the deployment maneuver and are inconsequential.

Eq. 5.15 provides the result of state transition matrix for the lumped system as derived via DMD, and Eq. 5.16 provides the result of the DMDc algorithm which decomposes it to the natural and forced components in terms of the state-space **A** and **B** matrices, respectively.

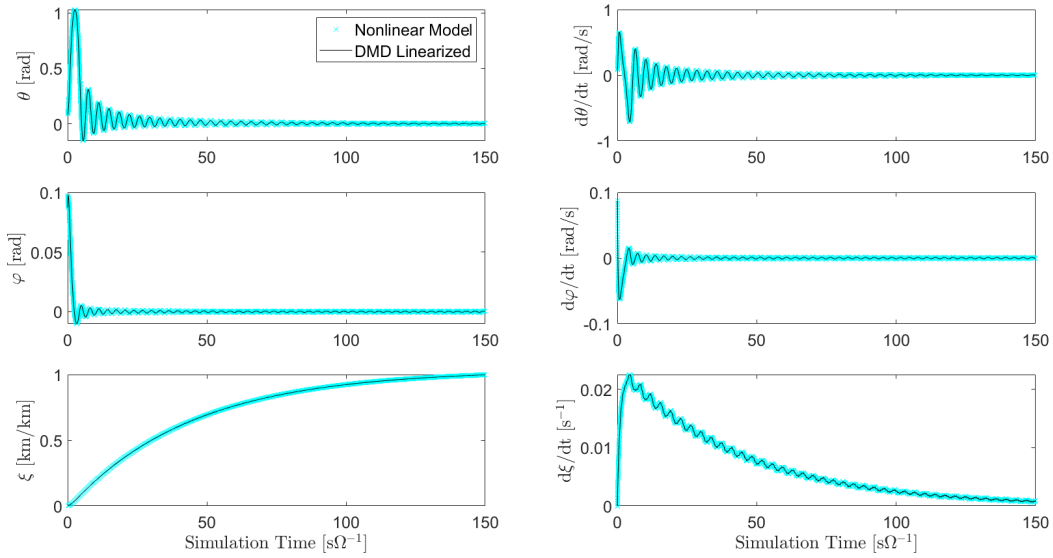

Fig. 5.5. Simulation comparing nonlinear vs. globally linearized model: controlled deployment.

Table 5.1. Maximum state errors between nonlinear dynamics and globally linearized model.

State Error	Uncontrolled DMD	Controlled DMD [$\times 10^{-3}$]	Controlled DMDc	Units
$\mid \delta\theta \mid$	0.0371	0.0430	0.0021	rad
$\mid \delta\varphi \mid$	0.0001	0.0041	0.0100	rad
$\mid \delta\xi \mid$	0.0252	0.0005	0.0762	-
$\mid \delta\dot{\theta} \mid$	0.0398	0.8177	0.0024	rad/s
$\mid \delta\dot{\varphi} \mid$	0.0005	8.5000	0.0151	rad/s
$\mid \delta\dot{\xi} \mid$	0.0081	0.0728	0.0076	s^{-1}

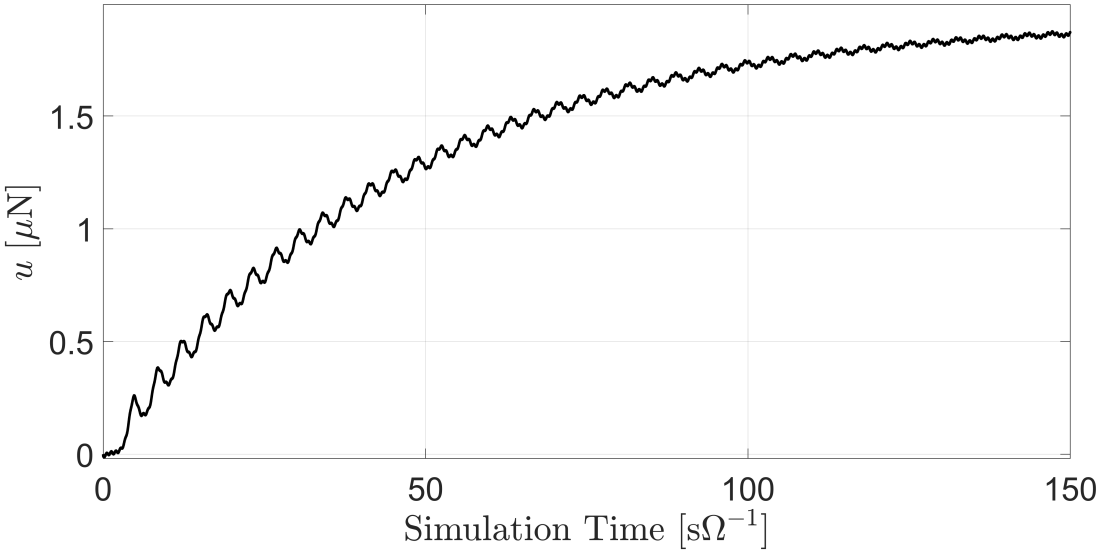

Fig. 5.6. Simulation results showing control input associated with controlled deployment.

$$\mathbf{A} = \begin{pmatrix} 1 & 0.0004 & 0 & 0.01 & -0.0002 & 0.0002 \\ 0 & 0.9999 & 0 & 0 & 0.0099 & 0 \\ 0 & 0 & 1 & 0 & 0 & 0.01 \\ -0.0085 & 0.0852 & -0.0002 & 0.9962 & -0.0402 & 0.0443 \\ 0 & -0.0262 & 0 & 0.0001 & 0.9784 & -0.0001 \\ 0 & 0.0017 & 0 & 0 & 0.0008 & 0.9996 \end{pmatrix} \tag{5.15}$$

$$\mathbf{A} = \begin{pmatrix} 1 & -0.0003 & 0 & 0.0061 & -0.0079 & 0 \\ -0.0001 & 1 & -0.01 & -0.0004 & -0.0001 & -0.0008 \\ 0.0277 & 0.0062 & 0.9979 & 0.1183 & 0.0344 & -0.0218 \\ -0.0002 & 0 & -0.0005 & 0.999 & 0.001 & 0.0166 \\ -0.0011 & 0 & 0 & -0.0031 & 0.9989 & 0.012 \\ -0.0004 & 0 & 0 & -0.0115 & -0.0097 & 0.9759 \end{pmatrix}, \quad \mathbf{B} = \begin{pmatrix} 0 \\ 0 \\ 1 \\ 0 \\ 0 \\ 0 \end{pmatrix} \tag{5.16}$$

There is excellent agreement between the exogenous and DMD-linearized models. Discrepancies in the angular overshoots are less than one degree for the worst case. Overall, the frequency and magnitudes of all state variables are appropriately captured. As shown in Fig. 5.5, the subsatellite deployments along the nadir. Short-period oscillations are attributed to the

disturbance model, and as is evident from the figure, are totally captured in the linear model as well. The tether deployment rate is expected to increase monotonically in free deployment, which is indeed the nominal case. However, it is important to note that the behavior shown in Fig. 5.4 includes the effects of simulated disturbance affecting tether tension, superimposed sinusoidally, as described in Eq. 5.13. The otherwise desired constraints on tether tension continue to hold, such as positive and non-zero. Moreover, the controllability matrix derived from Eq. 5.16 is of full rank. Although beyond the scope of the current chapter, such identified dynamics of the TSS can be used in more advanced control algorithms such as model predictive controllers.

To provide a quantitative measure of the training data needed to acquire an accurate state dynamics matrix, Fig. 5.7 depicts the convergence of learning error against the simulation time. The error matrix denoted by δA is the maximum difference between the current learned state dynamics matrix and the terminal learned state dynamics matrix, namely, the final state dynamics matrix that is computed from the Koopman operator-based identification algorithm in the final step of the numerical simulation. In the final step of the simulation, the terminal state dynamics matrix is computed by incorporating the total available data at the time of full deployment, which corresponds to $m = 15001$ state measurements. Fig. 5.7 shows both the Frobenius norm of the error matrix as well as the absolute value of its greatest element. The change in Frobenius norm beyond 141 $s\Omega^{-1}$ is less than 1% (within the first 35 hours of flight time), which corresponds to $m = 14101$ state measurements under the selected controller gains. However, the absolute change in matrix values diminishes to be on the order of 10^{-3} beyond 65.3 $s\Omega^{-1}$ (equivalent to the 16 hours of flight time), which corresponds to $m = 6531$ state measurements. Consequently, by half of the mission time, the tether is only ~80% deployed under the selected reference trajectory. Yet, the learned state matrix has converged to a very close vicinity of the terminal state dynamics matrix.

5.6 Conclusion and Further Remarks

With conventional linearization techniques in spacecraft dynamics, a limitation is imposed on the robustness of forecasting motion under the influence of unknown and unmodeled effects. Thus, the exercise of dynamics modeling constitutes an engineering judgment on how much sacrifice in fidelity can be tolerated within an acceptable level of risk – an envelope that should be minimized. In this research, an established model for TSS deployment was taken and superimposed with disturbances, all unknown to a Koopman operator-based learning algorithm. The aim of this study has been to apply an emergent system identification technique from outside of the space systems field, namely, dynamic mode decomposition and to develop a more practical

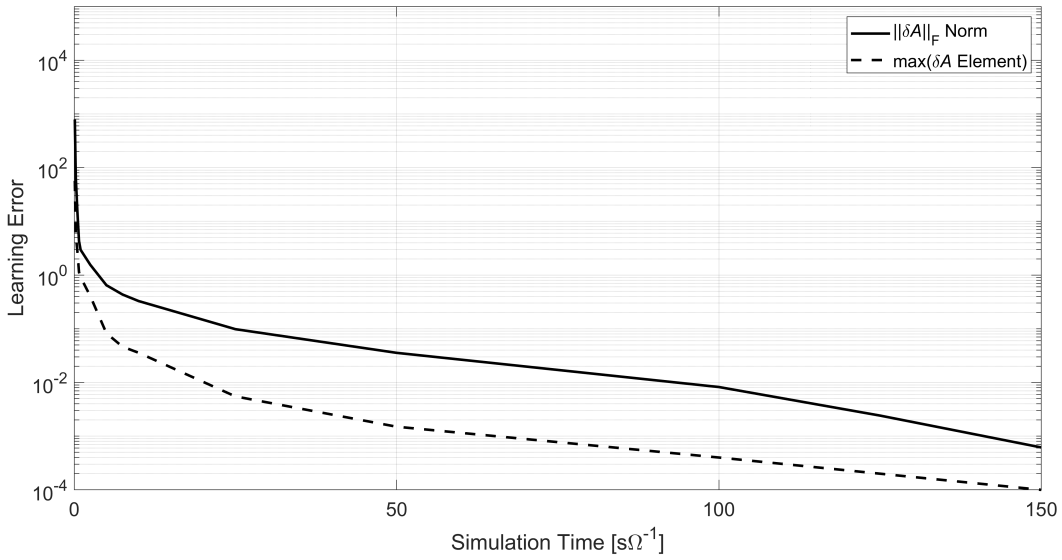

Fig. 5.7. Convergence in learning error of state dynamics matrix.

model that can capture unmodeled effects. Furthermore, the proposed Koopman operator-based methodology is a computationally efficient approach that can be implemented in real-time and will be amenable to state-space control synthesis techniques (the focus of this chapter has been on system identification though). In essence, a TSS exhibiting nonlinear behavior was analyzed from which measured data was used to construct a globally linear dynamical model. It is also worth reiterating that a useful application of the approach presented herein is to easily assess in real-time, the controllability of the system (mission operability), given its operating environment. The dynamic modes identified included those of the system's nominal motion, as well as of external disturbances and control. Moreover, the resultant model is globally linear, which is not achievable with traditional perturbation or truncated series-based linearization techniques at fixed operating points. The DMDc algorithm produced an **A** matrix which extracted the unforced state dynamics of the deploying TSS, while the **A** matrix output from the DMD algorithm was that of the closed-loop system. Both models captured the behavior of the nonlinear dynamics with disturbances. Comparison of both linearized models against the exogenous (nonlinear) dynamics yielded excellent agreement. These system identification approaches applied to the TSS deployment maneuver or similar space system problem are the first known to the authors rooted in Koopman operator theory.

The TSS deployment behavior as simulated by the DMD linearized model can be used to optimally tune control action or be used in alternate robust controller designs requiring a linear state-space representation of the system dynamics, including in the formation of a model and

prediction horizon for model predictive control. Further, if the source of nonlinearity acting upon nominally linear unforced dynamics is the disturbance, then the disturbance model can be extracted by taking the difference between the nominal and globally linearized models. Potential future research involves combining model-based and data-driven observers. For example, in Bruder et al. [80] an Extended DMD algorithm was used to estimate the loads of objects being lifted by a soft robotic arm by means of a model predictive controller. One can potentially use such a combined model-based and data-driven approach also in space systems applications to estimate underactuated states (e.g., in attitude control), linearize affine systems (e.g., in solar sailing), or optimize mission-specific parameters (e.g., in imaging). DMD enables the possibility of further analyses of complex spacecraft dynamics problems, especially TSSs which are especially sensitive to disturbances and control, increasing overall mission reliability of space systems applications.

CHAPTER 6

Conclusions & Further Research

Emergent techniques of determining the Koopman operator have become a contender for the identification of dynamical systems of any complexity in a way that is computationally superior to machine learning methods. Moreover, the HAVOK approach offers predictive properties for systems that are highly nonlinear and even chaotic in nature, thereby becoming invaluable for applicability to a host of unsolved problems in vehicle systems and controls.

This dissertation examined vehicular applications of Koopman operator theory in the recent literature and extended contributions to the field using the case studies of predicting superknock and pre-ignition in an internal combustion engine, and in tethered subsatellite deployment subjected to unmodelable environmental effects. Firstly, it was shown that the evolutionary manifestations of Koopman operator theory have emerged in recent years and the extent to which they have been applied to vehicular applications continues to grow. Consequently, it was established that this research area is unique in its own right and highly undersaturated. Next, the case study of pre-ignition and superknock prediction was presented wherein the HAVOK algorithm was framed such that it could be implemented as a real-time, computationally efficient operation to improve the safety, efficiency, reliability and harshness of a conventional internal combustion engine in the automotive context (with equal relevance to aerospace, marine, rail, mine, construction, robotic, and other applications). The framework developed can be used as an engineering guide to do similar with other engine features. Finally, the case study of a deployment operation in a tethered satellite system was presented. Here, the general theme was the learning of complex environmental effects to which the system may be highly sensitive. The result was an accurate capturement of dynamics and the generation of linearized equations of motion without the need to understand underlying physical processes. This concept can also be extended to other problems, such as predictive battery pre-cooling in electrical vehicles, and docking of spacecraft.

6.1 Future Research Directions

This section highlights some candidate systems upon which demonstration of this research was considered, but have not yet developed to a sufficient degree for publication. These ideas are works in progress and may be completed in the near future at the RMI Laboratory.

6.1.1 Adaptive Control of Peristaltic Locomotion in Unknown Environments

Figure 6.1 is an example of a vehicle that employs underactuated peristaltic motion to traverse soft terrain in the emulation of a worm [135]. System identification techniques such as those proposed herein could be used to learn the characteristics of its environment in real-time and auto-tune its control algorithm accordingly. For example, the adaptation of its peristaltic wave can optimize its speed in surface or sub-surface operation and in varying mediums (e.g., snow, mud, water, oil, etc.). A learning window can be hard coded to run nominal data through the DMD algorithm. After that, the duration it takes for the robot to travel a fixed distance over several test terrains can be measured to confirm any improvement in the performance of a linear model-based controller.

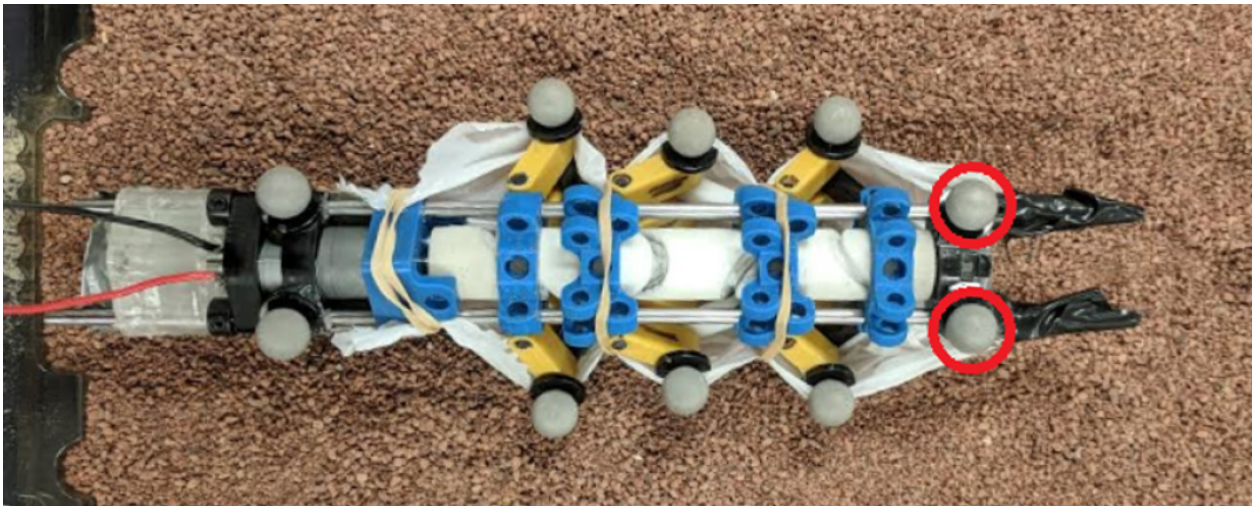

Fig. 6.1. Peristaltic robot developed at the RMI Laboratory at the University of Michigan - Dearborn

6.1.2 An Empiric Approach to Seismic Hazard Prediction for Railway and Mine Safety

Rail transport continues to be amongst the most economical and environmentally friendly means of transferring passengers and freight across long distances. Among safety issues, high-speed rail is particularly susceptible to seismic hazards, with several catastrophes littered throughout

recent history. While not all earthquakes cause train derailments, they potentially confound further dangerous and costly situations such as damage to railway infrastructure (including safety mechanisms and health monitoring systems), the propensity of human error, and a decline in ridership confidence, among others. Currently, there are limited technologies in place to warn of impending seismic hazards for railway operations comprised of networked seismic sensors (land- or sea-based) along railway tracks or near known seismic hotspots. However, these systems are reactionary and are limited by the geological literature not yet producing a reliable algorithm for earthquake prediction.

Although the forecasting of earthquakes remains an open challenge, the proposed technique is solidly grounded in the science of data-driven capturement of dynamical processes. The only assumption enabling this is that deterministic physical processes should indeed exist to cause the target events, no matter the complexity; i.e., the target events are not purely random phenomena in the statistical sense. This assumption is justified through at least one means of earthquake genesis, namely, Rayleigh-Taylor instability which occurs when magma rises from the mantle and pushes into the overlying Earth's crust [205]. The instability can cause cracking and deformation of the crust, leading to the buildup of tectonic stress that is released as an earthquake when the stress exceeds the strength of the crust. This mechanism has been proposed as a possible explanation for the generation of shallow earthquakes in volcanic regions and has been observed in laboratory simulations. Crack propagation through the crust further follows its own set of deterministic physical principles. Given this assumption of earthquake processes being deterministic, and not random in the mathematical sense, it follows that the HAVOK algorithm may be suitable to learn a linear model given enough data.

The Global Seismic Activity Level (GSAL) is the daily combined magnitude of global seismic activity and is updated live on the internet [206]. After digitizing 10 years of this data from 2010 to 2020 and processing it through the HAVOK algorithm, the result is given in Fig. 6.2.

The top portion of the figure shows the daily combined Richter scale magnitude, M_c, with days registered as ≥ 6 (classified as High) highlighted in red. The bottom graph shows the apparent forcing required to make the data fit a globally linearized linear model of rank 20 (this can be used as a tuning variable). Although a detailed analysis is this data is yet to be performed in terms of statistical significance, it seems that some significant earthquakes were indeed predictable within a few days of their manifestation. However, most were not predictable. Thus, some more work needs to be done to work with the data from a proper perspective. It is also theorized that more reliable predictions may be possible from data collected at a specific site, ideally over a suspected

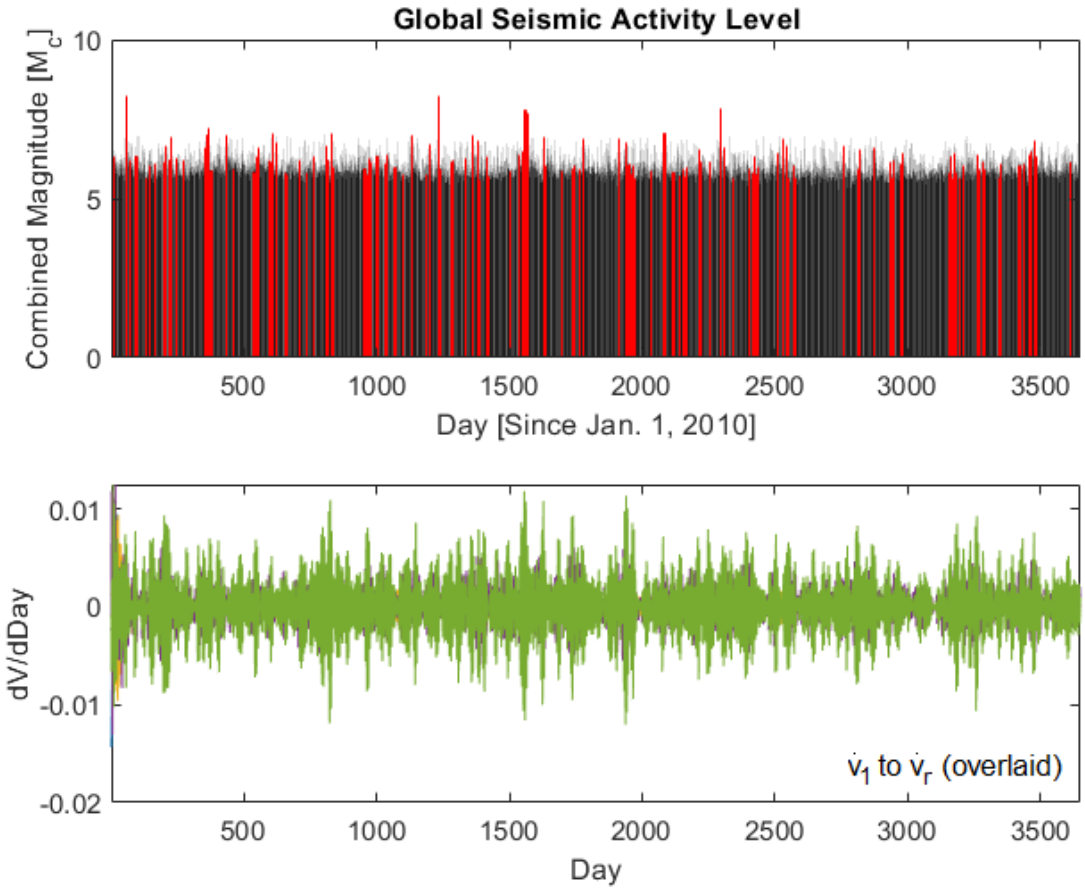

Fig. 6.2. Global seismic activity level from 2010 to 2020 with HAVOK apparent forcing

tectonic hot spot or an active volcano. Such may fall within the scope of railway safety since most of the world's high-speed and bullet trains exist in the Ring of Fire nations (e.g., Japan)

When replicating this approach for coal mine data from the UCI Machine Learning Repository [207], a much stronger predictive result was obtained and is shown in Fig. 6.3.
However, it may be that the algorithm has caught on to shift schedules and recurrent blasting operations. Even if that is the case, it helps to realize the potential recconnance value of this approach to learning troop movements and logistic patterns beyond boarders or near a theatre of armed conflict. Nonetheless, this area of research may soon prove successful.

6.1.3 Other Future Work

Future work in addition to the aforementioned (and what has already been mentioned throughout Chapter 2) may include efforts in the realm of preventative maintenance, anticipated user behavior,

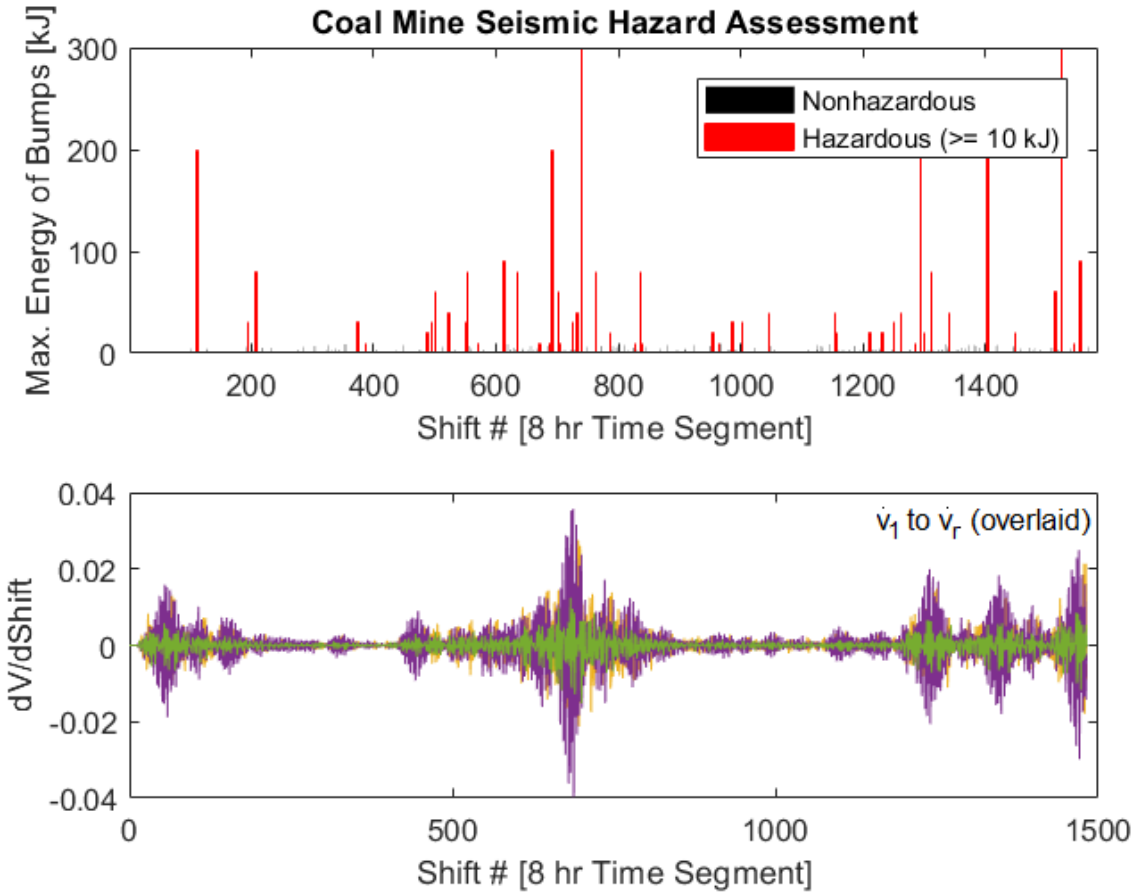

Fig. 6.3. Coal mine seismic hazard assessment with HAVOK apparent forcing

performance & reliability, manufacturability & operation management, automated calibration or gain scheduling of virtually any powertrain feature, and much more.

Koopman operator theory is a powerful mathematical framework that has a proven potential to revolutionize the design and control of complex systems, including vehicular applications, as demonstrated in this dissertation. Koopman operator theory is concerned with the analysis and modeling of dynamic systems using a novel approach based on the observation of the evolution of functions rather than states. Thus, the application of Koopman operator theory to vehicular applications has significant potential to improve system modeling, enhance control, enable autonomous vehicle control, and reduce development time and costs. As such, it is an exciting area of research with significant potential for real-world impact.

BIBLIOGRAPHY

[1] Merriam-Webster, *Vehicle*, in *Merriam-Webster.com dictionary*, Available: https://www.merriam-webster.com/dictionary/vehicle (visited on 11/14/2022).

[2] K. Kumar, *Fundamentals of Avionics Systems*. Ryerson University Press, 2014.

[3] W. Manzoor, "A comparative study of formation control at the Earth-Moon L2 libration point," M.S. thesis, Ryerson University, Toronto, ON, 2011.

[4] J. Stewart, D. K. Clegg, and S. Watson, *Calculus: early transcendentals*. Cengage Learning, 2020.

[5] A. J. Jordan and J. P. Nowacki, "Global linearization of non-linear state equations," *International Journal of Applied Electromagnetics and Mechanics*, vol. 19, no. 1-4, pp. 637–642, 2004.

[6] P. Myszkowski, "The change of state variables in global linearization of non-linear state equation," in *International Symposium on Parallel Computing in Electrical Engineering (PARELEC'06)*, IEEE, 2006, pp. 454–460.

[7] S. Čělikovský, "Global linearization of nonlinear systems - A survey," *Banach Center Publications*, vol. 32, no. 1, pp. 123–137, 1995.

[8] A. Frias, "Modeling and control of spacecraft systems with coupled orbital and attitude dynamics," Ryerson University, Toronto, ON, 2012.

[9] J. Belikov, A. Kaldmäe, and Ü. Kotta, "Global linearization approach to nonlinear control systems: A brief tutorial overview," *Proceedings of the Estonian Academy of Sciences*, vol. 66, no. 3, 2017.

[10] S. L. Brunton, B. W. Brunton, J. L. Proctor, and J. N. Kutz, "Koopman invariant subspaces and finite linear representations of nonlinear dynamical systems for control," *PloS one*, vol. 11, no. 2, e0150171, 2016.

[11] B. O. Koopman, "Hamiltonian systems and transformation in Hilbert space," *Proceedings of the National Academy of Sciences of the United States of America*, vol. 17, no. 5, pp. 315–318, 1931.

[12] I. Mezić, "Analysis of fluid flows via spectral properties of the Koopman operator," *Annual Review of Fluid Mechanics*, vol. 45, no. 1, pp. 357–378, 2013.

[13] P. J. Schmid, "Dynamic mode decomposition of numerical and experimental data," *Journal of Fluid Mechanics*, vol. 656, pp. 5–28, 2010.

[14] S. L. Brunton and J. N. Kutz, *Data-driven science and engineering: Machine learning, dynamical systems, and control.* Cambridge University Press, 2019.

[15] Y. Susuki, I. Mezić, F. Raak, and T. Hikihara, "Applied Koopman operator theory for power systems technology: Nonlinear theory and its applications," *Institute of Electronics, Information and Communication Engineers*, vol. 7, no. 4, pp. 430–459, 2016.

[16] H. Arbabi, *Introduction to koopman operator theory of dynamical systems.* 2018.

[17] A. Bruce, V. Zeidan, and D. Bernstein, "What is the koopman operator? a simplified treatment for discrete-time systems," in *2019 American Control Conference (ACC)*, IEEE, 2019, pp. 1912–1917.

[18] J. L. Proctor, S. L. Brunton, and J. N. Kutz, "Dynamic mode decomposition with control," *SIAM Journal on Applied Dynamical Systems*, vol. 15, no. 1, pp. 142–161, 2016.

[19] D. Bruder, B. Gillespie, C. D. Remy, and R. Vasudevan, "Modeling and control of soft robots using the koopman operator and model predictive control," in *2019 Robotics: Science and Systems*, 2019.

[20] J. L. Schmid Peter J.; Sesterhenn, "Dynamic mode decomposition of numerical and experimental data," in *Bulletin of the American Physical Society*, ser. 61st APS meeting, vol. 61, San Antonio, 2008, p. 208.

[21] I. Mezić, *On the geometrical and statistical properties of dynamical systems: Theory and applications*. California Institute of Technology, 1994.

[22] I. Mezić, "Spectral properties of dynamical systems, model reduction and decompositions," *Nonlinear Dynamics*, vol. 41, pp. 309–325, 2005.

[23] I. Mezić and A. Banaszuk, "Comparison of systems with complex behavior," *Physica D: Nonlinear Phenomena*, vol. 197, no. 1-2, pp. 101–133, 2004.

[24] K. K. Chen, J. H. Tu, and C. W. Rowley, "Variants of dynamic mode decomposition: Boundary condition, koopman, and fourier analyses," *Journal of nonlinear science*, vol. 22, no. 6, pp. 887–915, 2012.

[25] M. Budišić, R. Mohr, and I. Mezić, "Applied Koopmanism," *Chaos: An Interdisciplinary Journal of Nonlinear Science*, vol. 22, no. 4, p. 047 510, 2012.

[26] P. J. Schmid, "Dynamic mode decomposition and its variants," *Annual Review of Fluid Mechanics*, vol. 54, pp. 225–254, 2022.

[27] I. Mezić, "Analysis of fluid flows via spectral properties of the Koopman operator," *Annual Review of Fluid Mechanics*, vol. 45, pp. 357–378, 2013.

[28] K. Balakrishnan and D. Upadhyay, "Stochastic adversarial Koopman model for dynamical systems," *arXiv preprint arXiv:2109.05095*, 2021.

[29] M. J. Colbrook, L. J. Ayton, and M. Szőke, "Residual dynamic mode decomposition: Robust and verified Koopmanism," *arXiv preprint arXiv:2205.09779*, 2022.

[30] T. Chen and J. Shan, "Koopman-operator-based attitude dynamics and control on SO(3)," *Journal of Guidance, Control, and Dynamics*, vol. 43, no. 11, pp. 2112–2126, 2020.

[31] V. Cibulka, T. Haniš, M. Korda, and M. Hromčıćk, "Model predictive control of a vehicle using Koopman operator," *IFAC-PapersOnLine*, vol. 53, no. 2, pp. 4228–4233, 2020.

[32] A. Leonard, J. Rogers, and A. Gerlach, "Koopman operator approach to airdrop mission planning under uncertainty," *Journal of Guidance, Control, and Dynamics*, vol. 42, no. 11, pp. 2382–2398, 2019.

[33] G. Gutow and J. D. Rogers, "Koopman operator method for chance-constrained motion primitive planning," *IEEE Robotics and Automation Letters*, vol. 5, no. 2, pp. 1572–1578, 2020.

[34] J. Meyers, A. Leonard, J. Rogers, and A. Gerlach, "Koopman operator approach to optimal control selection under uncertainty," in *Proc. 2019 IEEE American Control Conference (ACC)*, IEEE, Jul. 2019, pp. 2964–2971.

[35] S. Sinha, U. Vaidya, and R. Rajaram, "Operator theoretic framework for optimal placement of sensors and actuators for control of nonequilibrium dynamics," *Journal of Mathematical Analysis and Applications*, vol. 440, no. 2, pp. 750–772, 2016.

[36] S. Servadio, D. Arnas, and R. Linares, "Dynamics near the three-body libration points via Koopman operator theory," *Journal of Guidance, Control, and Dynamics*, vol. 45, no. 10, pp. 1800–1814, 2022.

[37] T. Salam, V. Edwards, and M. A. Hsieh, "Learning and leveraging features in flow-like environments to improve situational awareness," *IEEE Robotics and Automation Letters*, vol. 7, no. 2, pp. 2071–2078, 2022.

[38] D. Arnas, "Solving perturbed dynamic systems using Schur decomposition," *Journal of Guidance, Control, and Dynamics*, pp. 1–18, 2022.

[39] G. Mamakoukas, M. L. Castano, X. Tan, and T. D. Murphey, "Derivative-based Koopman operators for real-time control of robotic systems," English, *IEEE transactions on robotics*, vol. 37, no. 6, pp. 2173–2192, 2021.

[40] V. Zinage and E. Bakolas, "Far-field minimum-fuel spacecraft rendezvous using Koopman operator and l2/l1 optimization," in *2021 American Control Conference (ACC)*, IEEE, 2021, pp. 2992–2997.

[41] A. Sinha and Y. Wang, "Koopman operator–based knowledge-guided reinforcement learning for safe human–robot interaction," *Frontiers in Robotics and AI*, vol. 9, 2022.

[42] F. E. Sotiropoulos and H. H. Asada, "Dynamic modeling of bucket-soil interactions using Koopman-DFL lifting linearization for model predictive contouring control of autonomous excavators," *IEEE Robotics and Automation Letters*, vol. 7, no. 1, pp. 151–158, 2021.

[43] B. Yu and P. Dai, "Deployment dynamics of a tape-shaped tethered satellite," *Journal of Aerospace Engineering*, vol. 35, no. 4, 2022.

[44] G. Mamakoukas, S. Di Cairano, and A. P. Vinod, "Robust model predictive control with data-driven Koopman operators," in *2022 American Control Conference*, Mitsubishi Electric Research Laboratories, 2022, pp. 3885–3892.

[45] X. Zhang, W. Pan, R. Scattolini, S. Yu, and X. Xu, "Robust tube-based model predictive control with Koopman operators," *Automatica*, vol. 137, p. 110 114, 2022.

[46] A. M. Avila, "Applications of Koopman operator theory to highway traffic dynamics," M.S. thesis, University of California, Santa Barbara, 2017.

[47] J. Hogg, M. Fonoberova, and I. Mezić, "Exponentially decaying modes and long-term prediction of sea ice concentration using Koopman mode decomposition," *Scientific reports*, vol. 10, no. 1, pp. 1–15, 2020.

[48] M. H. Canham, "On flexible tubes conveying a moving fluid: Variational dynamics and spectral analysis," M.S. thesis, University of Alberta, Edmonton, AL, 2017.

[49] S. Servadio, R. Armellin, and R. Linares, "A Koopman-operator control optimization for relative motion in space," *arXiv preprint arXiv:2207.07079*, 2022.

[50] C. Hofmann, S. Servadio, R. Linares, F. Topputo, *et al.*, "Advances in Koopman operator theory for optimal control problems in space flight," in *2022 AAS/AIAA Astrodynamics Specialist Conference*, 2022, pp. 1–13.

[51] E. Qian, B. Kramer, B. Peherstorfer, and K. Willcox, "Lift & learn: Physics-informed machine learning for large-scale nonlinear dynamical systems," *Physica D: Nonlinear Phenomena*, vol. 406, p. 132 401, 2020.

[52] S. A. Renganathan, Y. Liu, and D. N. Mavris, "Koopman-based approach to nonintrusive projection-based reduced-order modeling with black-box high-fidelity models," *AIAA Journal*, vol. 56, no. 10, pp. 4087–4111, 2018.

[53] S. E. Otto, "Advances in data-driven modeling and sensing for high-dimensional nonlinear systems," Ph.D. dissertation, Princeton University, 2022.

[54] I. Cohen, T. Berkov, and G. Gilboa, "Total-variation mode decomposition," in *International Conference on Scale Space and Variational Methods in Computer Vision*, Springer, 2021, pp. 52–64.

[55] Z. Wu, S. L. Brunton, and S. Revzen, "Challenges in dynamic mode decomposition," *Journal of the Royal Society Interface*, vol. 18, no. 185, p. 20 210 686, 2021.

[56] E. Ling, L. Zheng, L. J. Ratliff, and S. Coogan, "Koopman operator applications in signalized traffic systems," *IEEE Transactions on Intelligent Transportation Systems*, 2020.

[57] E. Ling, L. Ratliff, and S. Coogan, "Koopman operator approach for instability detection and mitigation in signalized traffic," in *2018 21st International Conference on Intelligent Transportation Systems (ITSC)*, IEEE, 2018, pp. 1297–1302.

[58] A. M. Boudali, P. J. Sinclair, R. Smith, and I. R. Manchester, "Human locomotion analysis: Identifying a dynamic mapping between upper and lower limb joints using the Koopman operator," in *2017 39th Annual International Conference of the IEEE Engineering in Medicine and Biology Society (EMBC)*, IEEE, 2017, pp. 1889–1892.

[59] S. Hanke, S. Peitz, O. Wallscheid, S. Klus, J. Böcker, and M. Dellnitz, "Koopman operator-based finite-control-set model predictive control for electrical drives," *arXiv preprint arXiv:1804.00854*, 2018.

[60] S. Le Clainche, D. Rodriguez, V. Theofilis, and J. Soria, "Flow around a hemisphere-cylinder at high angle of attack and low reynolds number. Part II: POD and DMD applied to reduced domains," *Aerospace Science and Technology*, vol. 44, pp. 88–100, 2015.

[61] S. Vasisht and M. Mesbahi, "Data-guided aerial tracking," *Journal of Guidance, Control, and Dynamics*, vol. 43, no. 8, pp. 1540–1549, 2020.

[62] C. L. Journell, R. M. Gejji, I. V. Walters, A. I. Lemcherfi, C. D. Slabaugh, and J. B. Stout, "High-speed diagnostics in a natural gas–air rotating detonation engine," *Journal of Propulsion and Power*, vol. 36, no. 4, pp. 498–507, 2020.

[63] H. T. Luong, Y. Wang, H.-G. Sung, and C. H. Sohn, "A comparative study of dynamic mode decomposition methods for mode identification in a cryogenic swirl injector," *Journal of Sound and Vibration*, vol. 503, p. 116 108, 2021.

[64] R. Larusson, N. Andersson, L.-E. Eriksson, and J. Östlund, "Comparison of eigenmode extraction techniques for separated nozzle flows," in *50th AIAA/ASME/SAE/ASEE Joint Propulsion Conference*, 2014, p. 4003.

[65] A. M. Avila, M. Fonoberova, J. P. Hespanha, *et al.*, "Game balancing using Koopman-based learning," in *2021 American Control Conference (ACC)*, IEEE, 2021, pp. 710–717.

[66] W. A. Manzoor, S. Rawashdeh, and A. Mohammadi, "Koopman operator-based data-driven identification of tethered subsatellite deployment dynamics," *Journal of Aerospace Engineer*, 2022, Submitted.

[67] X. Zhu, C. Ding, L. Jia, and Y. Feng, "Koopman operator based model predictive control for trajectory tracking of an omnidirectional mobile manipulator," English, *Measurement and control (London)*, 2022.

[68] T. A. Berrueta, I. Abraham, and T. Murphey, *Experimental applications of the koopman operator in active learning for control*. Springer, 2020, pp. 421–450.

[69] V. Cibulka, T. Haniš, and M. Hromčıćk, "Data-driven identification of vehicle dynamics using Koopman operator," *2019 22nd International Conference on Process Control (PC19)*, pp. 167–172, 2019.

[70] M. Švec, Š. Ileš, and J. Matuško, "Model predictive control of vehicle dynamics based on the Koopman operator with extended dynamic mode decomposition," in *2021 22nd IEEE International Conference on Industrial Technology*, IEEE, vol. 1, 2021, pp. 68–73.

[71] P. Mi, Q. Wu, and Y. Wang, "Suboptimal control law for a near-space hypersonic vehicle based on Koopman operator and algebraic Riccati equation," *Proceedings of the Institution of Mechanical Engineers, Part G: Journal of Aerospace Engineering*, p. 09 544 100 211 045 594, 2022.

[72] M. Švec, Š. Ileš, and J. Matuško, "Predictive approach to torque vectoring based on the Koopman operator," in *2021 European Control Conference (ECC)*, IEEE, 2021, pp. 1341–1346.

[73] S. Zinage, S. Jadhav, Y. Zhou, I. Bilionis, and P. Meckl, "Data driven modeling of turbocharger turbine using Koopman operator," *arXiv preprint arXiv:2204.10421*, 2022.

[74] J. Buzhardt and P. Tallapragada, "A Koopman operator approach for the vertical stabilization of an off-road vehicle," *Modelling, Estimation and Control Conference*, Apr. 2022.

[75] D. Lehmberg, F. Dietrich, and G. Köster, "Modeling Melburnians—using the Koopman operator to gain insight into crowd dynamics," *Transportation Research Part C: Emerging Technologies*, vol. 133, p. 103 437, 2021.

[76] S. Bhandari, "Landing a spaceship with Koopman operator theory and model predictive control," M.S. thesis, Technical University of Munich, Munich, BY, 2021.

[77] M. Li and L. Jiang, "Deep learning nonlinear multiscale dynamic problems using Koopman operator," *Journal of Computational Physics*, vol. 446, p. 110 660, 2021.

[78] M. O. Williams, M. S. Hemati, S. T. Dawson, I. G. Kevrekidis, and C. W. Rowley, "Extending data-driven Koopman analysis to actuated systems," *IFAC-PapersOnLine*, vol. 49, no. 18, pp. 704–709, 2016.

[79] H. M. Calderón, I. Hammoud, T. Oehlschlägel, H. Werner, and R. Kennel, "Data-driven model predictive current control for synchronous machines: A Koopman operator approach," in *2022 International Symposium on Power Electronics, Electrical Drives, Automation and Motion (SPEEDAM)*, IEEE, 2022, pp. 942–947.

[80] D. Bruder, X. Fu, R. B. Gillespie, C. D. Remy, and R. Vasudevan, "Koopman-based control of a soft continuum manipulator under variable loading conditions," *IEEE Robotics and Automation Letters*, vol. 6, no. 4, pp. 6852–6859, 2021.

[81] L. Shi and K. Karydis, "Enhancement for robustness of Koopman operator-based data-driven mobile robotic systems," in *2021 IEEE International Conference on Robotics and Automation (ICRA)*, IEEE, 2021, pp. 2503–2510.

[82] B. Chen, Z. Huang, R. Zhang, *et al.*, "Data-driven Koopman model predictive control for optimal operation of high-speed trains," *IEEE Access*, vol. 9, pp. 82 233–82 248, 2021.

[83] M. O. Williams, I. G. Kevrekidis, and C. W. Rowley, "A data–driven approximation of the Koopman operator: Extending dynamic mode decomposition," *Journal of Nonlinear Science*, vol. 25, no. 6, pp. 1307–1346, 2015.

[84] J. Moyalan, Y. Chen, and U. Vaidya, "Navigation with probabilistic safety constraints: Convex formulation," *arXiv preprint arXiv:2203.12520*, 2022.

[85] A. Broad, I. Abraham, T. Murphey, and B. Argall, "Data-driven Koopman operators for model-based shared control of human-machine systems," *The International Journal of Robotics Research*, vol. 39, no. 9, pp. 1178–1195, 2020.

[86] A. Broad, T. Murphey, and B. Argall, "Learning models for shared control of human-machine systems with unknown dynamics," *arXiv preprint arXiv:1808.08268*, 2018.

[87] S. Pan, "Robust and interpretable learning for operator-theoretic modeling of non-linear dynamics," Ph.D. dissertation, University of Michigan, 2021.

[88] W. Guo, H. Cao, S. Zhao, M. Li, B. Yi, and X. Song, "A data-driven model-based shared control strategy considering drivers' adaptive behavior in driver-automation interaction," *Proceedings of the Institution of Mechanical Engineers, Part D: Journal of Automobile Engineering*, p. 09 544 070 221 104 888, 2022.

[89] C. Folkestad, D. Pastor, and J. W. Burdick, "Episodic Koopman learning of nonlinear robot dynamics with application to fast multirotor landing," in *2020 IEEE International Conference on Robotics and Automation (ICRA)*, IEEE, 2020, pp. 9216–9222.

[90] C. Folkestad, Y. Chen, A. D. Ames, and J. W. Burdick, "Data-driven safety-critical control: Synthesizing control barrier functions with Koopman operators," *IEEE Control Systems Letters*, vol. 5, no. 6, pp. 2012–2017, 2020.

[91] W. Jin, Z. Wang, Z. Yang, and S. Mou, "Pontryagin differentiable programming: An end-to-end learning and control framework," *Advances in Neural Information Processing Systems*, vol. 33, pp. 7979–7992, 2020.

[92] J. Sullivan, "Application of data-driven modal decomposition techniques to the non-stationary case of scramjet unstart," M.S. thesis, The Ohio State University, 2021.

[93] H. Arbabi and I. Mezic, "Ergodic theory, dynamic mode decomposition, and computation of spectral properties of the Koopman operator," *SIAM Journal on Applied Dynamical Systems*, vol. 16, no. 4, pp. 2096–2126, 2017.

[94] N. Ali, B. Viggiano, M. Tutkun, and R. B. Cal, "Forecasting the evolution of chaotic dynamics of two-phase slug flow regime," *Journal of Petroleum Science and Engineering*, vol. 205, p. 108 904, 2021.

[95] D. A. Haggerty, M. J. Banks, P. C. Curtis, I. Mezić, and E. W. Hawkes, "Modeling, reduction, and control of a helically actuated inertial soft robotic arm via the Koopman operator," *arXiv preprint arXiv:2011.07939*, 2020.

[96] Z. Ma, G. Wang, T. Cui, and Y. Zheng, "Interpretation of intermittent combustion oscillations by a new linearization procedure," *Journal of Propulsion and Power*, vol. 38, no. 2, pp. 190–199, 2022.

[97] W. A. Manzoor, S. Rawashdeh, and A. Mohammadi, "Real-time prediction of pre-ignition and super-knock in internal combustion engines," *SAE Int. J. Engines*, vol. 16, no. 3, 2023.

[98] S. Le Clainche, R. Moreno-Ramos, P. Taylor, and J. M. Vega, "New robust method to study flight flutter testing," *Journal of Aircraft*, vol. 56, no. 1, pp. 336–343, 2019.

[99] M. L. Castaño, A. Hess, G. Mamakoukas, T. Gao, T. Murphey, and X. Tan, "Control-oriented modeling of soft robotic swimmer with Koopman operators," in *2020 IEEE/ASME International Conference on Advanced Intelligent Mechatronics (AIM)*, IEEE, 2020, pp. 1679–1685.

[100] P. J. Baddoo, B. Herrmann, B. J. McKeon, J. N. Kutz, and S. L. Brunton, "Physics-informed dynamic mode decomposition (piDMD)," *arXiv preprint arXiv:2112.04307*, 2021.

[101] C. Folkestad and J. W. Burdick, "Koopman NMPC: Koopman-based learning and nonlinear model predictive control of control-affine systems," in *2021 IEEE International Conference on Robotics and Automation*, IEEE, 2021, pp. 7350–7356.

[102] Y. Xiao, "DDK: A deep Koopman approach for dynamics modeling and trajectory tracking of autonomous vehicles," *arXiv preprint arXiv:2110.14700*, 2021.

[103] Y. Xiao, X. Zhang, X. Xu, X. Liu, and J. Liu, "Deep neural networks with Koopman operators for modeling and control of autonomous vehicles," *IEEE Transactions on Intelligent Vehicles*, 2022.

[104] R. Wang, Y. Han, and U. Vaidya, "Deep Koopman data-driven control framework for autonomous racing," in *Proc. Int. Conf. Robot. Autom.(ICRA) Workshop Opportunities Challenges Auton. Racing*, 2021, pp. 1–6.

[105] Y. Han, W. Hao, and U. Vaidya, "Deep learning of Koopman representation for control," in *2020 59th IEEE Conference on Decision and Control (CDC)*, IEEE, 2020, pp. 1890–1895.

[106] Y. Wang, Y. Yang, Y. Pu, and C. Manzie, "Data-driven predictive tracking control based on Koopman operators," *arXiv preprint arXiv:2208.12000*, 2022.

[107] C. Bakker, A. Bhattacharya, S. Chatterjee, C. J. Perkins, and M. R. Oster, "Learning Koopman representations for hybrid systems," *arXiv preprint arXiv:2006.12427*, 2020.

[108] J. Zhan, Z. Ma, and L. Zhang, "Data-driven modeling and distributed predictive control of mixed vehicle platoons," *IEEE Transactions on Intelligent Vehicles*, 2022.

[109] A. Maksakov and S. Palis, "Koopman-based optimal control of boost dc-dc converter," in *2020 IEEE Problems of Automated Electrodrive. Theory and Practice (PAEP)*, IEEE, 2020, pp. 1–4.

[110] V. Zinage and E. Bakolas, "Neural Koopman Lyapunov control," *arXiv preprint arXiv:2201.05098*, 2022.

[111] Y. Xiao, X. Xu, and Q. Lin, "Cknet: A convolutional neural network based on Koopman operator for modeling latent dynamics from pixels," *arXiv preprint arXiv:2102.10205*, 2021.

[112] S. B. Leask, "Dynamical feature extraction of atomization phenomena using deep Koopman analysis," Ph.D. dissertation, University of California, Irvine, 2021.

[113] K. Bieker, S. Peitz, S. L. Brunton, J. N. Kutz, and M. Dellnitz, "Deep model predictive flow control with limited sensor data and online learning," *Theoretical and computational fluid dynamics*, vol. 34, no. 4, pp. 577–591, 2020.

[114] L. Songy, J. Wangy, and J. Xuz, "A data-efficient reinforcement learning method based on local Koopman operators," in *20th IEEE International Conference on Machine Learning and Applications*, IEEE, 2021, pp. 515–520.

[115] A. M. Girgis, H. Seo, J. Park, M. Bennis, and J. Choi, "Split learning meets Koopman theory for wireless remote monitoring and prediction," in *2021 IEEE 32nd Annual International Symposium on Personal, Indoor and Mobile Radio Communications (PIMRC)*, IEEE, 2021, pp. 1191–1196.

[116] T. Goyal, S. Hussain, E. Martinez-Marroquin, N. A. Brown, and P. K. Jamwal, "Impedance control of a wrist rehabilitation robot based on autodidact stiffness learning," *IEEE Transactions on Medical Robotics and Bionics*, vol. 4, no. 3, pp. 796–806, 2022.

[117] B. Brunton, L. Johnson, J. Ojemann, and J. Kutz, "Extracting spatial–temporal coherent patterns in large-scale neural recordings using dynamic mode decomposition," *Journal of Neuroscience Methods*, vol. 258, pp. 1–15, 2016.

[118] H. Matpan, "Data driven model discovery and control of longitudinal missile dynamics," M.S. thesis, Middle East Technical University, 2021.

[119] L. Yingzhao and C. Jones, "On Gaussian process based Koopman operators," *Ifac Papersonline*, vol. 53, no. CONF, pp. 52–58, 2020.

[120] M. L. Bujorianu, R. Wisniewski, and E. Boulougouris, "Stochastic safety for random dynamical systems," in *2021 American Control Conference (ACC)*, IEEE, 2021, pp. 1340–1345.

[121] S. L. Brunton, B. W. Brunton, J. L. Proctor, E. Kaiser, and J. N. Kutz, "Chaos as an intermittently forced linear system," *Nature Communications*, vol. 8, no. 1, pp. 1–9, 2017.

[122] W. A. Manzoor, S. Rawashdeh, and A. Mohammadi, "Koopman operator-based data-driven identification of tethered subsatellite deployment dynamics," *ASCE Journal of Aerospace Engineering*, 2023, Accepted, in print.

[123] J. Meyers, J. Rogers, and A. Gerlach, "Koopman operator method for solution of generalized aggregate data inverse problems," *Journal of Computational Physics*, vol. 428, p. 110 082, 2021.

[124] W. A. Manzoor, S. Rawashdeh, and A. Mohammadi, "Real-time prediction of pre-ignition and super-knock in internal combustion engines," *SAE International Journal Engines*, vol. 16, no. 3, 2023.

[125] S. Gupta, D. Shen, D. Karbowski, and A. Rousseau, "Koopman model predictive control for eco-driving of automated vehicles," in *2022 American Control Conference (ACC)*, IEEE, 2022, pp. 2443–2448.

[126] D. Shen, J. Han, D. Karbowski, and A. Rousseau, "Data-driven design of model predictive control for powertrain-aware eco-driving considering nonlinearities using Koopman analysis," *IFAC-PapersOnLine*, vol. 55, no. 24, pp. 117–122, 2022.

[127] M. E. Marco, J. A. de la Riva, C. B. Sopena, and J. C. S. Cortes, "A data-driven methodology applied to X-in-the-loop environments for electric vehicle development," in *2021 IEEE Vehicle Power and Propulsion Conference (VPPC)*, IEEE, 2021, pp. 1–5.

[128] B. B. Kanbur, V. Kumtepeli, and F. Duan, "Thermal performance prediction of the battery surface via dynamic mode decomposition," *Energy*, vol. 201, p. 117 642, 2020.

[129] H. Moreno and A. Schaum, "Low-order electrochemical state estimation for Li-Ion batteries," *Algorithms*, vol. 16, no. 2, p. 73, 2023.

[130] A. Narasingam and J. S.-I. Kwon, "Application of Koopman operator for model-based control of fracture propagation and proppant transport in hydraulic fracturing operation," *Journal of Process Control*, vol. 91, pp. 25–36, 2020.

[131] H. Klie and H. Florez, "Data-driven discovery of unconventional shale reservoir dynamics," in *SPE Reservoir Simulation Conference*, OnePetro, 2019.

[132] A. Narasingam, "Operator theoretic model predictive control of moving boundary dynamical systems: Application to hydraulic fracturing," Ph.D. dissertation, Texas A&M University, 2020.

[133] A. Bao, E. Gildin, A. Narasingam, and J. S. Kwon, "Data-driven model reduction for coupled flow and geomechanics based on DMD methods," *Fluids*, vol. 4, no. 3, p. 138, 2019.

[134] A. M. Avila and I. Mezić, "Data-driven analysis and forecasting of highway traffic dynamics," *Nature Communications*, vol. 11, no. 1, p. 2090, 2020.

[135] S. Scheraga, A. Mohammadi, T. Kim, and S. Baek, "Design of an underactuated peristaltic robot on soft terrain," in *2020 IEEE/RSJ International Conference on Intelligent Robots and Systems (IROS)*, IEEE, 2020, pp. 6419–6426.

[136] E. Nekouei, M. Pirani, H. Sandberg, and K. H. Johansson, "A randomized filtering strategy against inference attacks on active steering control systems," *IEEE Transactions on Information Forensics and Security*, vol. 17, pp. 16–27, 2021.

[137] A. Mohammadi, H. Malik, and M. Abbaszadeh, "Generation of wheel lockup attacks on nonlinear dynamics of vehicle traction," in *2022 American Control Conference (ACC)*, IEEE, 2022, pp. 1994–1999.

[138] M. Taheri, K. Khorasani, N. Meskin, and I. Shames, "Data-driven Koopman operator based cyber-attacks for nonlinear control affine cyber-physical systems," in *2022 IEEE 61st Conference on Decision and Control (CDC)*, IEEE, 2022, pp. 6769–6775.

[139] E. A. Pool, J. F. Kooij, and D. M. Gavrila, "Context-based cyclist path prediction using recurrent neural networks," in *2019 IEEE Intelligent Vehicles Symposium*, IEEE, 2019, pp. 824–830.

[140] C. Schöller, V. Aravantinos, F. Lay, and A. Knoll, "What the constant velocity model can teach us about pedestrian motion prediction," *IEEE Robotics and Automation Letters*, vol. 5, no. 2, pp. 1696–1703, 2020.

[141] S. Kumar, A. Mohammadi, D. Quintero, S. Rezazadeh, N. Gans, and R. D. Gregg, "Extremum seeking control for model-free auto-tuning of powered prosthetic legs," *IEEE Transactions on Control Systems Technology*, vol. 28, no. 6, pp. 2120–2135, 2020.

[142] F. Aprigliano, S. Micera, and V. Monaco, "Pre-impact detection algorithm to identify tripping events using wearable sensors," *Sensors*, vol. 19, no. 17, p. 3713, 2019.

[143] M. Gavish and D. Donoho, "The optimal hard threshold for singular values is 4/ý3," *IEEE Transactions on Information Theory*, vol. 60, no. 8, pp. 5040–5053, 2014.

[144] L. Lessard, *Lecture notes advanced control systems, lecture 15: Balanced realization*, Oct. 2022.

[145] Y. Qi, Y. Wang, Y. Li, J. Wang, X. He, and Z. Wang, "Auto-ignition characteristics of end-gas in a rapid compression machine under super-knock conditions," *Combustion and Flame*, vol. 205, pp. 378–388, 2019.

[146] X. Luo, H. Teng, T. Hu, R. Miao, and L. Cao, "An experimental investigation on low speed pre-ignition in a highly boosted gasoline direct injection engine," *SAE International Journal of Engines*, vol. 8, no. 2, pp. 520–528, 2015.

[147] M. Dalla Nora and H. Zhao, "High load performance and combustion analysis of a four-valve direct injection gasoline engine running in the two-stroke cycle," *Applied Energy*, vol. 159, pp. 117–131, 2015.

[148] J.-M. Zaccardi and D. Escudié, "Overview of the main mechanisms triggering low-speed pre-ignition in spark-ignition engines," *International Journal of Engine Research*, vol. 16, no. 2, pp. 152–165, 2015.

[149] L. Ruichen, X. Boyan, Q. Yunliang, and X. Weiyang, "Numerical analysis of low speed pre-ignition and knock process in downsized turbocharged direct injection engines with ethanol-gasoline blends," *International Journal of Automotive Technology*, vol. 21, pp. 13–22, 2020.

[150] M. Amann, D. Mehta, and T. Alger, "Engine operating condition and gasoline fuel composition effects on low-speed pre-ignition in high-performance spark ignited gasoline engines," *SAE International Journal of Engines*, vol. 4, no. 1, pp. 274–285, 2011.

[151] W. Zhang, T. Wu, L. Dong, and W. Hao, "Analysis and detection methodology of knock phenomenon in gasoline engines based on cylinder pressure sensors," in *Proceedings of the 19th Asia Pacific Automotive Engineering Conference & SAE-China Congress 2017: Selected Papers*, Springer, 2019, pp. 359–373.

[152] K. T. Alligood, T. D. Sauer, and J. A. Yorke, *Chaos: An introduction to dynamical systems*. Springer, 1997.

[153] B. Kaul, C. Finney, R. Stiffler, and J. Drallmeier, "Advanced intra-cycle detection of pre-ignition events through phase-space transforms of cylinder pressure data," *SAE [Technical Papers]*, vol. 2020, no. 01, 2020.

[154] H. Xu, X. Ni, X. Su, *et al.*, "Experimental and numerical investigation on effects of pre-ignition positions on knock intensity of hydrogen fuel," *International Journal of Hydrogen Energy*, vol. 46, no. 52, pp. 26 631–26 645, 2021.

[155] N. Peters, B. Kerschgens, and G. Paczko, "Super-knock prediction using a refined theory of turbulence," *SAE International Journal of Engines*, vol. 6, no. 2, pp. 953–967, 2013.

[156] Z. Wang, H. Liu, T. Song, *et al.*, "Relationship between super-knock and pre-ignition," *International Journal of Engine Research*, vol. 16, no. 2, pp. 166–180, 2015.

[157] H. Kubach, A. Weidenlener, J. Pfeil, *et al.*, "Investigations on the influence of fuel oil film interaction on pre-ignition events in highly boosted di gasoline engines," SAE Technical Paper, Tech. Rep., 2018.

[158] K. P. Grogan and M. Ihme, "A new ignition time model applied to super knock," *Proceedings of the Combustion Institute*, vol. 37, no. 3, pp. 3487–3494, 2019.

[159] M. Sadiq Al-Baghdadi, "Development of a pre-ignition submodel for hydrogen engines," *Proceedings of the Institution of Mechanical Engineers, Part D: Journal of Automobile Engineering*, vol. 219, no. 10, pp. 1203–1212, 2005.

[160] O. Budak, F. Hoppe, B. Heuser, S. Pischinger, U. Burke, and A. Heufer, "Hot surface pre-ignition in direct-injection spark-ignition engines: Investigations with tailor-made fuels from biomass," *International Journal of Engine Research*, vol. 19, no. 1, pp. 45–54, 2018.

[161] M. Radwan, S. M. Elfeky, and O. S. M. Abu-Elyazeed, "An investigation on abnormal combustion, emissions and performance of novel jojoba bio-gasoline and its blends with gasoline in a spark-ignition engine," SAE Technical Paper, Tech. Rep., 2012.

[162] K. Thyagarajan and K. Bhaskaran, "Effect of argon dilution on the pre-ignition oxidation kinetics of benzene," *International journal of energy research*, vol. 15, no. 3, pp. 235–248, 1991.

[163] G. Panzani, G. Pozzato, S. M. Savaresi, J. Rösgren, and C. H. Onder, "Engine knock detection: An eigenpressure approach," *IFAC-PapersOnLine*, vol. 52, no. 5, pp. 267–272, 2019.

[164] K. Akimoto, H. Komatsu, and A. Kurauchi, "Development of pattern recognition knock detection system using short-time fourier transform," *IFAC Proceedings Volumes*, vol. 46, no. 21, pp. 366–371, 2013.

[165] H.-M. Wu and R. Tafreshi, "Observer-based internal model air–fuel ratio control of lean-burn si engines," *IFAC Journal of Systems and Control*, vol. 9, p. 100 065, 2019.

[166] K. Jack, "Turbocharger with a brain," Jul. 1982, Popular Science.

[167] J. Chauvin, O. Grondin, E. Nguyen, and F. Guillemin, "Real-time combustion parameters estimation for hcci-diesel engine based on knock sensor measurement," *IFAC Proceedings Volumes*, vol. 41, no. 2, pp. 8501–8507, 2008.

[168] K. Tindell, A. Burns, and A. J. Wellings, "Calculating controller area network (can) message response times," *Control engineering practice*, vol. 3, no. 8, pp. 1163–1169, 1995.

[169] V. Jain, L. Murugathasan, G. Bindra U.and Li, *et al.*, "CubeSats can serve multiple stakeholders too: Use of the DESCENT mission to develop national and international collaboration," in *Proc. of Guidance, Navigation and Control*, ASTRO 2018, Quebec City, QC: CASI, 2018.

[170] I. Bell, J. McTernan, B. Gilchrist, and S. Bilen, "Investigating miniature electrodynamic tethers and interaction with the low earth orbit plasma," in *AIAA Space 2013 Conference and Exposition*, AIAA, 2013, p. 5391.

[171] S. Nishida, S. Kawamoto, Y. Okawa, F. Terui, and S. Shoji Kitamura, "Space debris removal system using a small satellite," *Acta Astronautica*, vol. 65, no. 1-2, pp. 95–102, 2009.

[172] M. Dobrowolny and N. H. Stone, "A technical overview of TSS-1: The first tethered-satellite system mission," *Il Nuovo Cimento C*, vol. 17, no. 1, pp. 1–12, 1994.

[173] B. S. Yu and D. P. Jin, "Deployment and retrieval of tethered satellite system under J_2 perturbation and heating effect," *Acta Astronautica*, vol. 67, no. 7-8, pp. 845–853, 2010.

[174] S. A. Rawashdeh and J. E. Lumpp, "Aerodynamic stability for CubeSats at ISS orbit," *Journal of Small Satellites*, vol. 2, no. 1, pp. 85–104, 2013.

[175] S. Varma, "Control of satellites using environmental forces: Aerodynamics drag / solar radiation pressure," Ryerson University, Toronto, ON, 2011.

[176] B. Yu, S. Xu, and D. Jin, "Chaos in a tethered satellite system induced by atmospheric drag and Earth's oblateness," *Nonlinear Dynamics*, vol. 101, no. 2, pp. 1233–1244, 2020.

[177] W. He and S. S. Ge, "Dynamic modeling and vibration control of a flexible satellite," *IEEE Transactions on Aerospace and Electronic Systems*, vol. 51, no. 2, pp. 1422–1431, 2015.

[178] A. Schutte and B. Dooley, "Constrained motion of tethered satellites," *Journal of Aerospace Engineering*, vol. 18, no. 4, 2005.

[179] N. Stone and C. Bonifazi, "The TSS-1R mission: Overview and scientific context," *eophysical Research Letters*, vol. 25, no. 4, pp. 409–412, 1998.

[180] H. Wen, D. P. Jin, and H. Y. Hu, "Optimal feedback control of the deployment of a tethered subsatellite subject to perturbations," *Nonlinear Dynamics*, vol. 51, no. 4, pp. 501–514, 2008.

[181] C. Wang, P. Wang, A. Li, and Y. Guo, "Deployment of tethered satellites in low-eccentricity orbits using adaptive sliding mode control," *Journal of Aerospace Engineering*, vol. 30, no. 6, p. 04 017 077, 2017.

[182] P. Williams, "Deployment/retrieval optimization for flexible tethered satellite systems," *Nonlinear Dynamics*, vol. 52, no. 1, pp. 159–179, 2008.

[183] T. Lovell, "Application of genetic algorithms to state estimation of tethered systems," *Computer methods in applied mechanics and engineering*, vol. 192, no. 15, pp. 1799–1819, 2003.

[184] D. Cicci, E. Volovecky, and C. Qualls, "Identification of a tethered satellite using a Kalman filter," *Advances in the Astronautical Sciences*, vol. 119, no. 15, pp. 983–998, 2005.

[185] E. Volovecky, "Identification of a tethered satellite using an extended Kalman filter," M.S. thesis, Auburn University, Auburn, AL, 2007.

[186] A. Mohammadi, H. J. Marquez, and M. Tavakoli, "Nonlinear disturbance observers: Design and applications to Euler-Lagrange systems," *IEEE Control Systems Magazine*, vol. 37, no. 4, pp. 50–72, 2017.

[187] J. Gonzalez, "Spacecraft formation control: Adaptive PID-extended memory recurrent neural network controller," California State University, Long Beach, CA, 2018.

[188] D. F. Martyn, "The normal F region of the ionosphere," *Proceedings of the Institute of Radio Engineers*, vol. 47, no. 2, pp. 147–155, 1959.

[189] A. V. Dmitriev, A. V. Suvorova, M. V. Klimenko, *et al.*, "Predictable and unpredictable ionospheric disturbances during St. Patrick's Day magnetic storms of 2013 and 2015 and on 8–9 march 2008," *Journal of Geophysical Research: Space Physics*, vol. 122, no. 2, pp. 2398–2423, 2017.

[190] J. A. M. McDonnell, P. R. Ratcliff, and I. Collier, "Atmospheric drag modelling for orbital micro-debris at LEO altitudes," *Advances in Space Research*, vol. 17, no. 12, pp. 183–188, 1996.

[191] P. Schmid, D. Violato, and F. Scarano, "Decomposition of time-resolved tomographic PIV," *Experiments in Fluids*, vol. 52, no. 6, pp. 1567–1579, 2012.

[192] B. Zang, U. Vevek, and T. New, "Some insights into the screech tone of under-expanded supersonic jets using dynamic mode decomposition," *Journal of Aerospace Engineering*, vol. 34, no. 4, 2021.

[193] X. Zhu, C. Hu, X. Yang, and Z. Du, "Dynamic mode decomposition analysis of the unsteady flow in a centrifugal compressor volute," *Journal of Aerospace Engineering*, vol. 32, no. 1, 2019.

[194] S. Sinha, S. Nandanoori, and E. Yeung, "Data driven online learning of power system dynamics," in *IEEE Power & Energy Society General Meeting*, IEEE, Aug. 2020, pp. 1–5.

[195] M. Korda and I. Mezić, "Linear predictors for nonlinear dynamical systems: Koopman operator meets model predictive control," *Automatica*, vol. 93, pp. 149–160, 2018.

[196] B. Bronner and D. Trung, *Developing the miniature tether electrodynamics experiment: Completion of key milestones and future work*, University of Michigan, Ann Arbor, MI, 2015.

[197] P. Banium and V. Kumar, "Optimal control of the shuttle-tethered-subsatellite system," *Acta Astronautica*, vol. 7, no. 12, pp. 1333–1348, 1980.

[198] H. Gläßel, F. Zimmermann, S. Brückner, U. M. Schöttle, and S. Rudolph, "Adaptive neural control of the deployment procedure for tether-assisted re-entry," *Aerospace Science and Technology*, vol. 8, no. 1, pp. 73–81, 2004.

[199] W. Stuiver, "Dynamics and configuration control of two-body satellite systems," *AIAA Journal of Spacecraft and Rockets*, vol. 11, no. 8, pp. 545–546, 1974.

[200] K. Kumar, "Review on dynamics and control of nonelectrodynamic tethered satellite systems," *Journal of spacecraft and rockets*, vol. 43, no. 4, pp. 705–720, 2006.

[201] Godard, K. Kumar, and B. Tan, "Fault-tolerant stabilization of a tethered satellite system using offset control," *Journal of Spacecraft and Rockets*, vol. 45, no. 5, pp. 1070–1084, 2008.

[202] UNOOSA, *Inter-agency space debris coordination committee space debris mitigation guidelines*, United Nations Office of Outer Space Affairs, United Nations, 2007, p. 9.

[203] J. Tu, C. Rowley, D. Luchtenberg, S. Brunton, and J. Kutz, "On dynamic mode decomposition: Theory and applications," *Journal of Computational Dynamics*, vol. 1, no. 2, pp. 391–421, 2014.

[204] L. Boccaletto and L. d'Agostino, "Design and testing of a micro-Newton thrust stand for FEEP," in *36th AIAA/ASME/SAE/ASEE Joint Propulsion Conference and Exhibit*, AIAA/ASME/SAE/ASEE, 2000, p. 3268.

[205] T. V. Gerya and D. A. Yuen, "Rayleigh–taylor instabilities from hydration and melting propel 'cold plumes' at subduction zones," *Earth and Planetary Science Letters*, vol. 212, no. 1-2, pp. 47–62, 2003.

[206] T. Pfeiffer, *Global seismic activity level (GSAL)*, Available: https://www.allquakes.com/earthquakes/global-seismic-activity-level.html, Volcano Discovery, 2023.

[207] M. Sikora and L. Wrobel, "Application of rule induction algorithms for analysis of data collected by seismic hazard monitoring systems in coal mines," *Archives of Mining Sciences*, vol. 55, no. 1, pp. 91–114, 2010.